Design and Control of High Temperature PEM Fuel Cell System

Andreasen, Søren Juhl

Publication date:
2009

Document Version
Publisher's PDF, also known as Version of record

Design and Control of High Temperature PEM Fuel Cell System

Søren Juhl Andreasen

Department of Energy Technology

Aalborg University

A dissertation submitted for the degree of

Philosophiæ Doctor (Ph.D.)

2009 November

Aalborg University
Department of Energy Technology
Pontoppidanstræde 101
DK-9220 Aalborg East
Denmark

Printed in Aalborg, Denmark by Uniprint

ISBN : 87-89179-78-1

Acknowledgements

This dissertation is written under the innovation consortium entitled *Fuel Cell Shaft Power Pack* (FCSPP), supported by the Danish Government and numerous Danish companies and institutions. My research was carried out under the supervision of Professor Søren Knudsen Kær from the Department of Energy Technology, Aalborg University. First of all, I am grateful to him for both his professional support, honest opinions and for giving me the freedom to chose my own path through the research presented in this dissertation. I would also like to express my appreciation to my colleagues Erik Schaltz and Mads Pagh Nielsen for their comments and inputs to new problems and ideas. To Jan Christiansen, Mads Lund and Walter Neumayr I would like to extend my gratitude for their constructive ideas and high quality performance when constructing components and complex laboratory setups never seen before. And most of all I would like to thank my family. The confidence and encouragement I receive from them every day makes any technical problems endurable.

Aalborg, August 2009

Søren Juhl Andreasen

Abstract

Efficient fuel cell systems have started to appear in many different commercial applications and large scale production facilities are already operating to supply fuel cells to support an ever growing market. Fuel cells are typically considered to replace lead-acid batteries in applications where electrical power is needed, because of the improved power and energy density and the removal of long charging hours.

The primary focus of this dissertation is the use of high temperature polymer electrolyte membrane (HTPEM) fuel cells that operate at elevated temperatures (above 100^oC) compared to conventional PEM fuel cells, that use liquid water as a proton conductor and thus operate at temperatures below 100^oC. The HTPEM fuel cell membrane in focus in this work is the BASF Celtec-P polybenzimidazole (PBI) membrane that uses phosphoric acid as a proton conductor. The absence of water in the fuel cells enables the use of designing cathode air cooled stacks greatly simplifying the fuel cell system and lowering the parasitic losses. Furthermore, the fuel impurity tolerance is significantly improved because of the higher temperatures, and much higher concentrations of CO can be endured without performance or life time losses.

In order to evaluate the performance of using HTPEM fuel cells for electricity production in electrical applications, a 400 W fuel cell system is initially designed using a cathode air cooled 30 cell HTPEM stack. The stack runs on pure hydrogen in a dead-end anode configuration at a pressure of 0.2 bar with a combined PI and feedforward air flow control strategy. Some of the problems involved in using fuel cells running at high temperatures is longer start-up times, therefore different heating strategies are examined in order to minimize the heating time for systems with critical demands for this. A 1kW fuel cell stack with optimized flow plates was heated in $\approx$5 minutes using

the introduction of an electrical air pre-heater.

Using pure hydrogen in compressed form is problematic due to the very small density of hydrogen, even at high pressures. Hydrogen is a very energy efficient gas, but large investments are required for a full production and distribution system before the fuel is available for general purpose use in consumer applications. Using liquid renewable fuels that can be produced and transported using existing techniques is beneficial if the fuel cell systems are adapted. Converting a liquid renewable fuel such as methanol in a chemical reactor, a reformer system, can provide the high temperature PEM fuel cells with a hydrogen rich gas that efficiently produces electricity and heat at similar efficiencies as with pure hydrogen. The systems retain their small and simple configuration, because the high quality waste heat of the fuel cells can be used to support the steam reforming process and the heat and evaporation of the liquid methanol/water mixture. If efficient heat integration is manageable, similar performance to hydrogen based systems can be expected.

In many applications benefits can be gained from operating fuel cells together with batteries. In automotive applications and small utility vehicles large power peaks are experienced for accelerations. Very large and expensive fuel cell systems are needed in order to supply these peak powers, which do not occur that often during a normal driving cycle. The combination of batteries and super capacitors together with fuel cells can improve the system performance, lifetime and cost. Simple systems can be designed where the fuel cells and batteries are directly connected, but the introduction of power electronics can increase the degrees of freedom for the system when determining control strategy.

The high temperature PEM fuel cell is a promising alternative for converting renewable fuels into electricity and heat in it's simplicity in systems design and reliability during operation.

Dansk resumé

Effektive brændselscellesystemer bliver brugt i forskellige kommercielle applikationer, og storskala produktionsfaciliteter forsyner allerede det voksende marked med brændselsceller. Brugen af brændselsceller overvejes typisk som erstatning for blysyrebatterier i applikationer, hvor der er brug for elektrisk effekt pga. den forbedrede effekt- og energidensitet, og fordi lange opladningstider undgås.

I denne afhandling fokuseres der primært på brugen af højtemperatur PEM (HTPEM) brændselsceller, som opererer ved forhøjede temperaturer (over 100^oC) sammenlignet med konventionelle PEM brændselsceller, der bruger flydende vand som protonleder og derfor arbejder ved temperaturer under 100^oC. HTPEM brændselscellemembranen, der benyttes i dette arbejde, er en BASF Celtec-P polybenzimidazol (PBI) membran som bruger fosforsyre som protonleder. Fraværet af vand i brændselscellerne tillader brugen af katodeluftkølede stakke hvilket i høj grad simplificerer brændselscellesystemet og mindsker de parasitiske tab. Ydermere er tolerancen for urenheder i brændslet væsentlig forbedret pga. de højere temperaturer, og meget højere CO-koncentration kan tolereres uden performance- eller levetidsnedsættelse.

For at kunne evaluere performance ved brugen af HTPEM brændselsceller til elproduktion i elektriske applikationer, er et 400 W brændselscellesystem begyndelsesvis designet ved brug af en 30 celle katodeluftkølet HTPEM stak. Stakken bruger ren brint i en dead-end anode konfiguration ved et tryk på 0.2 bar med en kombineret PI og feedforward luftflowreguleringsstrategi. Nogle af problemerne forbundet med at benytte brændselsceller, der har høje arbejdstemperaturer, er længere opstartstider, og derfor afprøves forskellige opvarmningsstrategier for at minimere opvarmningstiden for systemer, der har kritiske krav hertil. En 1 kW brændselscellestak med optimerede flowplader kan

opvarmes på ca. 5 minutter ved brug af en elektrisk luftforvarmer.

Brugen af ren brint som komprimeret gas er problematisk pga. den meget lave densitet af brint selv ved høje tryk. Brint er en gas med en meget høj brændværdi, men der er behov for store investeringer til både produktions- og distributionssystemer før brændstoffet er til rådighed til forbrugerapplikationer. Benyttelsen af flydende, fornybare brændstoffer, der kan produceres og transporteres ved brug af eksisterende teknikker er fordelagtig, hvis brændselscellesystemerne kan tilpasses. Konverteringen af et flydende, fornybart brændstof som f.eks. metanol i en kemisk reaktor, et reformersystem, kan forsyne højtemperatur PEM brændselsceller med en brintholdig gas, der effektivt producerer elektricitet og varme ved virkningsgrader lignende dem for et system, der bruger rent brint. Systemet bibeholder et lille og simpelt design, da højkvalitetsrestvarmen fra brændselscellerne kan bruges til at forsyne dampreformeringsprocessen og opvarme og fordampe den flydende blanding af metanol og vand. Hvis det er muligt at implementere en effektiv varmeintegration, kan der opnås samme performance som i et brintbaseret system.

I mange applikationer kan fordele opnås ved at bruge brændselsceller sammen med batterier. I bilapplikationer og ved mindre elektriske køretøjer opleves store power peaks under accelerationer. Der er behov for meget store og dyre brændselscellesystemer for at levere disse peak-effekter, som ikke er hyppige under normale kørselsmønstre. Kombinationen af batterier og superkapacitorer sammen med brændselsceller kan forbedre systemperformance, levetid og kostpris. Simple systemer kan designes, hvor brændselsceller og batterier er direkte forbundet, men introduktionen af effektelektronik kan forbedre frihedsgraderne for systemet når der vælges styrestrategier.

Højtemperatur PEM brændselscellen er et lovende alternativ til konverting af fornybare brændstoffer til elektricitet og varme pga. simpliciteten i systemdesignet og pålideligheden under drift.

Notation List

A	Atom index
$\hat{A}_j$	Atom balance of the A'th atom
A_{MEA}	Fuel cell membrane active area
F	Faraday's constant [C/mol]
G	Gibbs free energy [J]
i	Current density [A/cm^2] / Species index
I_{FC}	Fuel cell current [A]
j	Atom index
$K_{estimator}$	Methanol fuel flow estimation constant
L	Lagrange partial differential
$\dot{m}_{H_2}$	Mass flow of hydrogen [kg/s]
$\dot{n}_{Burner,H_2}$	Molar flow of hydrogen to burner [mol/s]
N	Number of species
n_{cells}	Number of cells in stack
$\dot{n}_{CH_3OH}$	Molar flow of methanol [mol/s]
$\dot{n}_{FC,H_2}$	Molar flow of hydrogen to fuel cell stack [mol/s]
$\dot{n}_{H_2O}$	Molar flow of water [mol/s]
p	Pressure [bar]
p^0	Atmospheric pressure [bar]
P_{Blower}	Cathode blower power [W]
P_{H_2}	Partial pressure of hydrogen [Pa]
P_{H_2O}	Partial pressure of water [Pa]
P_{O_2}	Partial pressure of oxygen [Pa]
$\dot{q}_{CH_3OH}$	Volumetric flow of methanol [m^3/s]
R	Gas constant [J/(K·mol)]
T	Temperature [K/^{o}C]
U^0	Reaction electromotive force [V]
U_{FC}	Fuel cell voltage [V]
U_{OCV}	Open circuit voltage [V]
x_{H_2}	Molar fraction of hydrogen [-]
X_i	Molar fraction of i'th specie
η_A	Fuel cell anode overpotential [V]
η_C	Fuel cell cathode overpotential [V]
η_{conc}	Fuel cell concentration losses [V]
η_Ω	Fuel cell ohmic losses [V]
η_{system}	Fuel cell system efficiency [-]
λ_{H_2}	Fuel cell anode stoichiometry [-]
λ_i	Langrange multiplier of the i'th specie
λ_j	Langrange multiplier of the j'th atom
ρ_{CH_3OH}	Density of methanol [kg/m^3]

AC	Alternating current
ATR	Autothermal reforming
BEV	Battery electric vehicle
BPP	Bipolar plate
CL	Catalyst layer
DC	Direct current
DMFC	Direct methanol fuel cell
EIS	Electrochemical Impedance Spectroscopy
EMF	Electromotive force
EUDC	Extra-urban driving cycle
FCEV	Fuel cell electric vehicle
FCHEV	Fuel cell hybrid electric vehicle
FCSPP	Fuel Cell Shaft Power Pack
GDL	Gas diffusion layer
HHV	Lower heating value
HTPEM	High temperature polymer electrolyte membrane
ICE	Internal combustion engine
IPCC	Intergovernmental Panel on Climate Change
LHV	Lower heating value
LSM	Lanthanum strontium manganese
LTPEM	Low temperature polymer electrolyte membrane
MEA	Membrane electrode assembly
MFC	Mass flow controller
PBI	Polybenzimidazole
PEM	Polymer electrolyte membrane
PMSM	Permanent magnet synchronous motor
POX	Partial oxidation
PTFE	Polytetrafluoroethylene
SC	Steam-to-carbon ratio
SOC	State-of-charge
SR	Steam reforming
SOFC	Solid oxide fuel cell
WGS	Water-gas-shift
YSZ	Yttria-stabilized zirconia

Contents

List of Figures

List of Tables

1

Introduction

1.1 Fuel Cell Shaft Power Pack research project

The work presented here is part of the research project *Fuel Cell Shaft Power Pack* (FCSPP), which involves multiple partners from both the industry and academia. 3 Ph.d. students have been employed for research within the technical fields of designing a fuel cell shaft power pack, and resources have also been allocated to evaluate the potential business strategies and commercial challenges involved with introducing new technology products into a changing and evolving commercial market. The companies involved in the project are outlined below:

- Aalborg University (2 Academic Ph.D. students)
- Copenhagen Business School
- Cykellet/DSR Scandinavia
- Danish Technological Institute (1 Industrial Ph.D. student)
- Dantherm A/S
- EGJ Udvikling
- Falsled Højtryk
- GMR Maskiner A/S
- Hydrogen Innovation & Research Center
- H2 Logic Aps.
- KK-Electronic A/S
- Migatronic A/S
- Parker Hannifin DK
- Serenergy A/S
- Trans-Lift
- Xperion

This innovation consortium of partners include educational and research institutions, and also industrial companies with an interest in applications with implemented fuel cell

technology and the features and benefits gained from this, including a competitive edge in the market. Figure 1.1 shows the scope of the *Fuel Cell Shaft Power Pack* project. In fuel cell system applications, the fuel cell system is typically connected to power electronics to condition the voltage and current output of the fuel cell stack before this available power is converted into mechanical torque in an electric machine powering a given application.

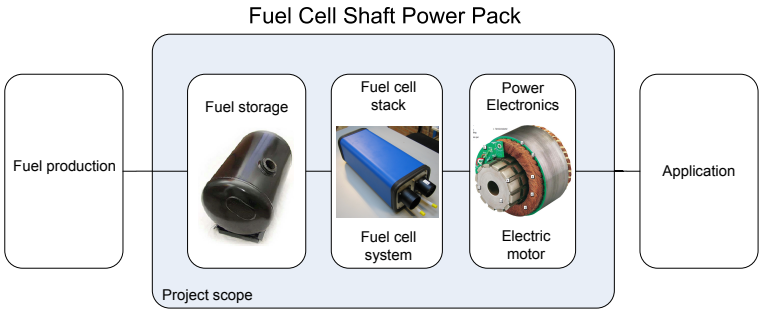

Figure 1.1: Scope of project

The research results described in this work, involves the fuel cell stack and peripherals (balance-of-plant) including the fuel storage system. Moreover different operating and control strategies are examined both experimentally and theoretically. The remaining research regarding the power electronics, electric machines, electrical energy storage control and fuel cell diagnostics, is conducted in separate Ph.D. studies. The final product of the overall study is an implementation and evaluation of HTPEM fuel cell systems in different applications.

1.2 Objectives of this dissertation

The objectives of this dissertation are to give a thorough understanding of the different subjects and methods involved in the design and development of a high temperature polymer electrolyte membrane (HTPEM) fuel cell system. These objectives include identifying the advantages and disadvantages of this type of system when using it as a power supply in an electrical vehicle. Furthermore the operating strategies and control principles for operating such a system reliably are to be analyzed and implemented in working systems to evaluate their performance.

1.3 Methodology

In the design of the above mentioned systems, the following methods are used to support efficient and in-depth engineering of the different system designs.

1.3.1 Steady-state mathematical modelling

Steady-state mathematical modelling is used to determine the general operating conditions of the fuel cell system to determine reasonable stack sizes for the fuel cell system and an expected fuel storage size. This is especially efficient in the initial system design phase, where large parts of the involved applications and system components are unknown. Empirical models based on experimental results can be used in cases where simulation speed is essential, i.e. for example cases where dynamic models are used during system operation.

1.3.2 Transient modelling and simulation

To enable predictions of dynamic behavior during operation of the fuel cell system, dynamic models are developed. These models also support the development of the control system, and ensure safe and reliable operation that does not damage the fuel cells. Full transient system models can often be very extensive, requiring high computational capabilities, and are simplified in order to enable simulations of systems during operation. For use directly in real-time system applications, simplified models using empirically derived expression are preferred for successful implementation of model based controllers that, e.g. replaces sensors or ensure proper redundance in the system.

1.3.3 Experimental test and model verification

To verify model predictions and to simplify and speed up subsystem simulations, experimental analysis are carried out and the developed control strategies are tested. The experimental process plays an important part in fuel cell system design because the fuel cell system is going to be operating in a real application subjected to operating conditions very different from the controlled environment inside a typical laboratory.

The continued development and test of a fuel cell system is an iterative process divided into different phases, initial design and lab system tests, establishing knowledge of advantageous system operating conditions. This phase is followed by implementation

of off-the-shelf industrial components to replace lab equipment resulting in a prototype system which can be subjected to real loading cycles and eventually implemented in a real application, with the development of a proper stand-alone control system. When looking at system dynamics it is important to use similar components as the ones used in the final applications. The final performance of the fuel cell system is evaluated by looking at the total system efficiency and the overall performance of the application.

1.4 Dissertation outline

Chapter 1 presents the overall research project, which this work is a part of. The objectives of the dissertation are outlined, and the primary methodologies used are presented. Finally the papers included in this dissertation are presented.

Chapter 2 provides background information regarding the governing principles of fuel cells, together with a comparative study of different types of available fuel cell technologies. The overview leads to the particular choice of fuel cell technology used in the design of the systems focused on in this work, the HTPEM fuel cell.

Chapter 3 summarizes some of the features of the HTPEM fuel cells and presents the benefits of using fuel cells together with other electrical storage devices, such as batteries or super capacitors.

Chapter 4 presents the concept of compressed hydrogen fueled cathode air cooled HTPEM fuel cell stacks, and shows tests conducted on a 30 cell prototype stack, and a commercial 65 cell stack. The results of these tests include the determination of operating principles during start-up, current load operation, and shut-down.

Chapter 5 focuses on a HTPEM fuel cell system running on steam reformed methanol and the different initial tests of a novel heat exchanger based reformer system, integrated with a 1 kW HTPEM fuel cell stack. The chapter also presents a possible control strategy developed from results on an experimental second generation system.

Chapter 6 shows the development of two different applications where HTPEM fuel cell stacks have been used as power supply, a fuel cell electric vehicle with a 4 kW HTPEM fuel cell on-board traction battery charger, and a utility truck with a battery/fuel cell/super capacitor power system.

Chapter 7 and 8 summarizes this work; concludes on the research and outlines a line of interesting areas for future research.

1.5 List of papers

Papers covering the scope of this doctoral thesis

- **Dynamic Model of the High Temperature PEM Fuel Cell Stack Temperature**
  Søren Juhl Andreasen and Søren Knudsen Kær
  Published in: ASME Journal of Fuel Cell Science and Technology, 2009, Volume 6, Issue 4, p. 041006-(1-8), 12/08/2009.
- **Characterization and Modelling of a High Temperature PEM Fuel Cell Stack using Electrochemical Impedance Spectroscopy**
  Søren Juhl Andreasen, Jesper Lebæk Jespersen, Erik Schaltz and Søren Knudsen Kær
  Published in: Fuel Cells - From Fundamentals to Systems, Wiley-VCH, 2009, Volume 9, Issue 4, p. 463-473, 05/06/2009.
- **Directly Connected Series Coupled HTPEM Fuel Cell Stacks to a Li-ion Battery DC-bus for a Fuel Cell Electrical Vehicle**
  Søren Juhl Andreasen, Leanne Ashworth, Ian Natanael Remón and Søren Knudsen Kær
  Published in: International Journal of Hydrogen Energy, 2008, vol. 33, p. 7137-7145, 1/11/2008.
- **Modelling and Evaluation of Heating Strategies for High Temperature Polymer Electrolyte Membrane Fuel Cell Stacks**
  Søren Juhl Andreasen and Søren Knudsen Kær
  Published in: International Journal of Hydrogen Energy, 2008, vol. 33, p. 4655-4664, 16/08/2008.
- **Experimental Evaluation of a Pt-based Heat Exchanger Methanol Reformer for a HTPEM Fuel Cell Stack** Søren Juhl Andreasen, Søren Knudsen Kær and Mads Pagh Nielsen
  Published in: Electrochemical Society Transactions, 2008, vol. 12, nr. 1, p. 571-578, 01/05/2008.
- **Modeling and Implementation of a 1 kW, Air Cooled HTPEM Fuel Cell in a Hybrid Electrical Vehicle**
  Søren Juhl Andreasen, Leanne Ashworth, Ian Natanael Remón, Peder Lund Rasmussen and Mads Pagh Nielsen
  Published in: Electrochemical Society Transactions, 2008, vol. 12, nr. 1, p. 639-650, 01/05/08.
- **400 W High Temperature PEM Fuel Cell Stack Test**
  Søren Juhl Andreasen and Søren Knudsen Kær
  Published in: Electrochemical Society Transactions, 2006, vol. 5, nr. 1, p. 197-207, 18/06/2007.
- **Design of Propulsion System for a Fuel Cell Vehicle**
  Erik Schaltz, Søren Juhl Andreasen, and Peter Omand Rasmussen
  Published in: Proceedings of the 12th European Conference on Power Electronics and Applications, EPE 2007, 02/09/07.

2

Fuel Cells

2.1 Powering the future

Efficient and new sustainable energy technologies are required to ensure reduced dependence on fossil fuels, stable energy supply and reduction in greenhouse gas emissions. The Intergovernmental Panel on Climate Change (IPCC) report of 2007 has identified the transport sector as one of the large contributors of CO_2 emissions and toxic particles [31]. Transport propulsion systems are primarily combustion engines running on fossil fuels, but the increasing emission restrictions in the automobile industry has led to new car propulsion systems including different types of hybrid power systems combining electric power from batteries with both diesel and gasoline engines in different configurations. These technologies improve the efficiency and driving range of the vehicles, but are still dependent on fossil fuels. Using synthetic diesel or diesel derived from biomass in engines result in a CO_2 neutral fuel economy independent of fossil fuels. Furthermore, the introduction of pure electric cars or fuel cell cars may also reduce the issues of fossil fuel dependence, but often requires a complete rearrangement of the entire energy system. Batteries and fuel cell systems are often considered competing technologies for transport propulsion, but many advantages are gained when combining these technologies in an application. In many applications where batteries are used, long charging time is typically problematic especially if multiple work shifts or long driving ranges are needed. Typically battery packs will need to be switched or additional vehicles are needed. In such situations a quickly re-fuelable fuel cell system would be a better choice. In the case of personal transport, an analysis indicates that over 90% of the

trips made in Denmark are below 127km, as shown in figure 2.1. These typical driving range requirements can be managed with present available battery technologies, but the freedom of operation when using these cars is still limited because of the need for a long term charging period or changing the battery pack.

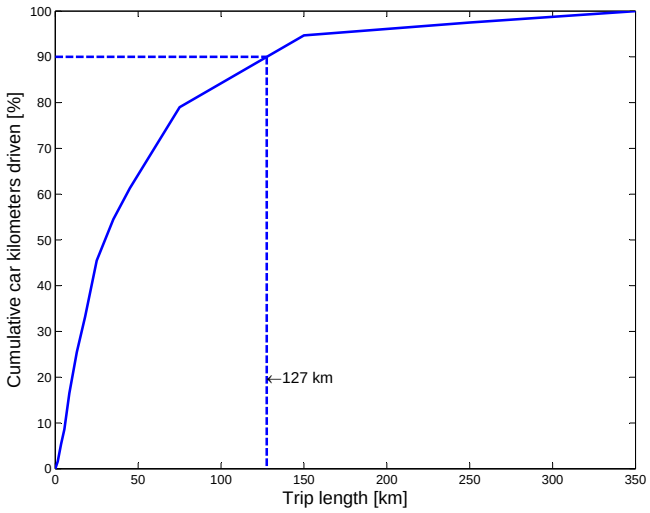

Figure 2.1: Cumulative percent of car kilometers driven as a function of trip length in 2006 in Denmark [53].

In the cases of longer trips, a small fuel cell system could be fitted to a car and run as a range extender for the system providing charging during and after driving, enabling the cars to drive much farther. Finally the combination of fuel cells and batteries and the load sharing between them can in some systems lower the peaks of transients on either of the components and hereby extend their lifetime.

2.2 How a fuel cell works

A fuel cell is an electrochemical device that converts the available energy in a fuel, such as hydrogen, into electricity, heat and water. An example of a fuel cell membrane electrode assembly (MEA) is shown in figure 2.2, and consists of the following components:

- Bipolar plate (BPP)
- Gas diffusion layer (GDL)

- Catalyst layer (CL)
- Polymer membrane

The functions of these different components will be explained in the following.

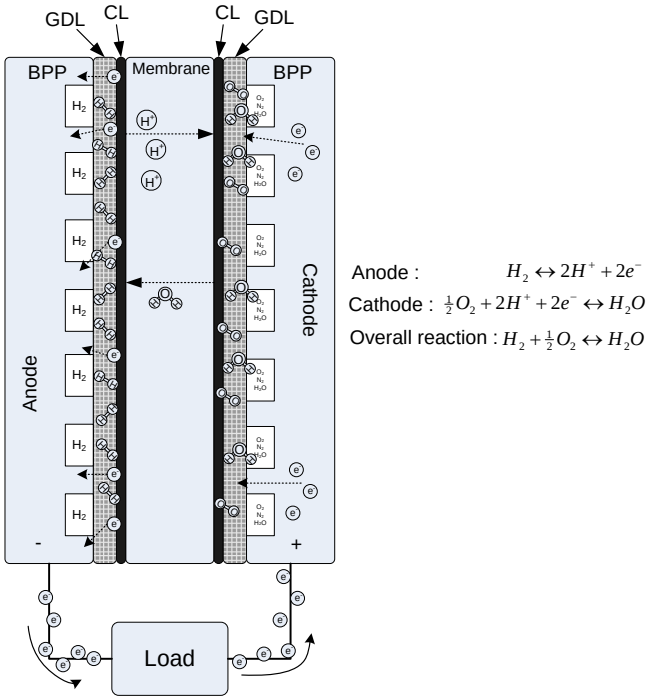

Figure 2.2: The reactions in a hydrogen fuel cell.

The reactions in a fuel cell are divided into an anode reaction and a cathode reaction. The anode reaction includes splitting of the supplied hydrogen on e.g. a platinum catalyst, hereby releasing electrons which are available to do work in an external electric load. The primary task of the catalyst layers on each side of the membrane is to catalyze the desired anode and cathode reactions, and contain many three-phase interfaces, i.e. sites with reactants, catalytic material, and ion conductive abilities. A typical catalyst layer consists of platinum particles deposited on a carbon material, in close contact with the polymer membrane. In hydrogen fuel cells, the free protons migrate through the proton conductive polymer membrane, to the cathode. The membrane should be non-conductive for electrons and have a low proton conduction resistance. The cathode reaction includes a reaction on the catalyst between the protons from the anode side and the oxygen available in the supplied atmospheric air. The resulting product of the

cathode reaction is water which primarily is carried out by the air exiting the fuel cell, but can also diffuse into the membrane. Often water from the cathode side will diffuse through the membrane to the anode side and can cause blocking of catalyst reaction sites and the gas diffusion layer if in liquid form. The functions of the gas diffusion layers are to distribute the incoming reactants over the entire area of the catalyst, and to conduct the electrons released in the anode reaction. Obstruction of catalytic sites can be problematic both on the anode and cathode side and can cause significant performance losses and material damage in the fuel cell. If the supplies of fuel and oxidant, i.e. hydrogen and air is maintained at flows matching the current drawn by the load, the fuel cell will efficiently be generating electric and thermal power.

The different losses and the performance of the fuel cell can be illustrated by looking at a polarization curve, i.e. a plot of the voltage as a function of the current density. These losses are shown in figure 2.3.

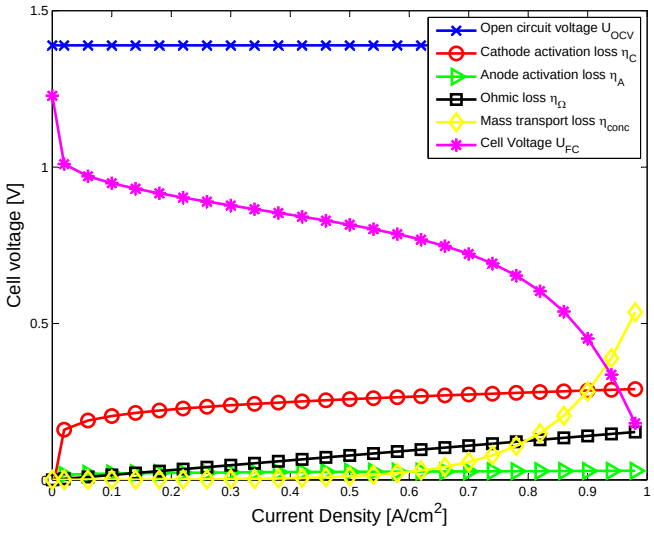

Figure 2.3: Plot of the typical fuel cell losses, for a pure hydrogen fuel cell.

The fuel cell stack voltage U_{FC} consists of a theoretical maximum voltage U_{OCV} and losses connected to the anode η_A and cathode η_C electrochemistry, the ohmic losses in the membrane and electrical connection η_Ω between each of the MEA layers, and finally the losses connected to mass transport of each of the reactants η_{conc}. The fuel cell voltage can generally be calculated as shown in equation 2.1, assuming the

superposition of these losses:

$$U_{FC} = U_{OCV} - \eta_C - \eta_A - \eta_\Omega - \eta_{conc} \tag{2.1}$$

The theoretical open circuit voltage, U_{OCV} can be expressed by the Nernst equation, as:

$$U_{OCV} = U^0 + \frac{RT}{2F} ln \frac{P_{H_2} \cdot P_{O_2}^{\frac{1}{2}}}{P_{H_2O}} \tag{2.2}$$

Where U^0 is the electromotive force (EMF) for the involved reactions at standard pressure and P_{H_2}, P_{O_2} and P_{H_2O} are the partial pressures of the respective reactants and product. R is the gas constant, F is Faraday's constant and T is the temperature. From this equation it is clearly seen that this voltage increases with increased pressurization of the fuel cell. Furthermore U^0 decreases with increasing temperature. Pressurization however often requires additional power consumption by auxiliary components, lowering the overall efficiency [43].

The losses associated with the anode activation are considered negligible when running a fuel cell on pure hydrogen. The electrochemistry involved with the reaction of pure hydrogen on platinum is very fast even at low temperatures. The losses on the cathode are on the contrary normally the largest loss in the fuel cell, and much research is conducted to develop better catalysts and improve this oxidation reaction [8, 40, 41]. It is shown that a large part of the initial drop of the fuel cell voltage at low currents, is due to the contribution of the initial cathode activation. The ohmic losses are, as seen, typically linearly dependent on the current, just as an ohmic resistance, hence the name. They are typically composed by the resistance of the membrane but electrical resistances in the form of contact resistances between the different layers can also be significant. When drawing high currents, there is a need for high flows of hydrogen and oxygen to each side of the fuel cell, hydrogen being a very small molecule has no problems with diffusing through the GDL and reaching catalytic sites. The oxygen which is diluted with nitrogen in atmospheric air can have difficulties reaching the catalytic sites fast enough at very high current loads, so unless very high stoichiometries are applied to the air side at high currents, large losses and possible oxidant starvation can be experienced on the cathode side.

The possible current that can be drawn from the fuel cell is determined by the cell area, but the voltage will remain the same because it is determined by the electrochemical reactions. Thus the power output from a fuel cell can be increased by increasing the active cell area. Normally it is more convenient to increase the power of a fuel cell by stacking the fuel cells, and hereby increasing the fuel cell voltage. A fuel cell stack is the result of a line of series connected fuel cells, resulting in a fuel cell stack voltage increased by the number of fuel cells in the stack. The current drawn from the stack is the same as for a single fuel cell.

With the increase of the power delivered from the fuel cells by stacking them, it is possible to use them in applications replacing other technologies. Often there is a limit as to how large stacks can be made because of the mechanical stability of the stack, in these cases a series of parallel or series connected stacks can be used to further increase the power output of a fuel cell system.

2.3 Fuel cell technologies

Several types of fuel cells exist. To decide which specific types are relevant for the applications considered in this work, an initial delimitation is made by only looking at some of the most advanced technologies. These are the technologies considered to be closest to the market, some of which are already appearing in commercial products. Fuel cells can be divided into different categories relating their properties to the nature of their catalysts, electrolytes, membranes, proton conductive capabilities, fuel type, operating temperatures, etc. The relevant fuel cells described in this work are divided into the following categories:

- Low temperature PEM fuel cells
- Direct methanol fuel cells
- High temperature PEM fuel cells
- Solid oxide fuel cells

2.3.1 Low temperature PEM fuel cells

The category of low temperature PEM (LTPEM) fuel cells include fuel cells using different polymer membrane types, but all have the common operating conditions of needing

liquid water present in the membrane to ensure proper proton conductive capabilities. This criteria includes operation below 100 ^{o}C, if the systems are not pressurized, and utilizes mainly platinum based catalyst. The anode and cathode reactions of a hydrogen fuelled LTPEM fuel cell are shown below in equation 2.3 and 2.4:

$$Anode: \quad H_2 \leftrightarrow 2H^+ + 2e^- \tag{2.3}$$

$$Cathode: \quad \frac{1}{2}O_2 + 2H^+ + 2e^- \leftrightarrow H_2O \tag{2.4}$$

$$Overall: \quad H_2 + \frac{1}{2}O_2 \leftrightarrow H_2O \tag{2.5}$$

The polarization curves of a selection of commercially available fuel cells are shown in figure 2.4, at pressures close to atmospheric. The LTPEM fuel cell voltage is high and the fuel cells are very efficient compared to other fuel cell technologies.

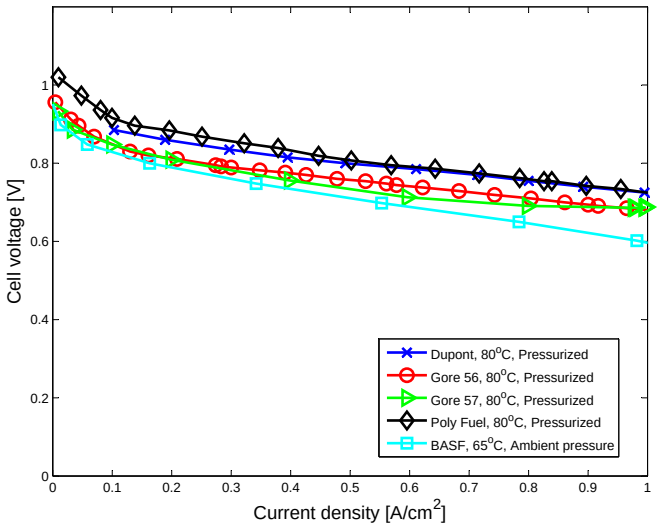

Figure 2.4: Polarization curve of different types of low temperature PEM fuel cells [6, 19, 26, 27, 45].

A widely used membrane polymer is Nafion, which is based on sulphonated polytetrafluoroethylene (PTFE, also know as Teflon). The presence of hydrophilic sulphonic side-chains and hydrophobic areas of the bulk polymer, enables good abilities for proton conduction through the liquid water present in the membrane, and also a good mechanical stability. The membrane humidity is vital to the fuel cell performance. An MEA

with a very high humidity has the risk of flooding, i.e. large water droplets blocking the flow channels and gas diffusion layer disabling the catalytic sites of the cell. A too dry membrane will quickly loose the ability to conduct protons and could lead to failure of an entire stack, because the cells are connected in series. An increased resistance could also form hot spots and increase the cell temperature locally. Although many methods of predicting and diagnosing the flooding or drying of membranes in low temperature PEM fuel cells exist [25, 39, 47, 48], this is still one of the problematic areas of this technology. A list of typical advantages and disadvantages for these fuel cells are summarized below:

Advantages

- High cell voltage and efficiency.
- Well known and established technology.
- Operating temperatures do not require special system components.
- Fast system start-up from low temperatures.

Disadvantages

- Low CO tolerance, and poor dynamic operation with CO.
- Complicated water management.
- External reformer is requires if other fuels are needed.
- Low temperature operation requires large cooling areas.
- Low temperature operation requires expensive catalysts.

2.3.2 Direct methanol fuel cell

The direct methanol fuel cell (DMFC) also uses a polymer membrane, often of the same Nafion based type as the low temperature PEM membranes. A mixture of liquid water and methanol is supplied to the anode side of the membrane, which simplifies the cooling and humidification processes. The cathode reaction is the same as the LTPEM fuel cell, but the anode reaction is different as seen in the following:

$$Anode: \quad CH_3OH + H_2O \leftrightarrow CO_2 + 6H^+ 6e^- \tag{2.6}$$

$$Cathode: \quad (3/2)O_2 + 6H^+ + 6e^- \leftrightarrow 3H_2O \tag{2.7}$$

$$Overall: \quad CH_3OH + (3/2)O_2 \leftrightarrow CO_2 + 2H_2O \tag{2.8}$$

From equation 2.6 it is seen that CO_2 is a product of the anode reaction. This is often associated with difficult stack flow plate design, because gaseous CO_2 bubbles emerge on the anode side and needs to be vented. The anode catalytic loading is often higher than

LTPEM because a mixture of liquid methanol and water is directly supplied. Using methanol and water reduces the fuel storage volume compared to hydrogen because of the much higher volumetric energy density compared to hydrogen as also shown in Paper A.5. The electrochemical anode reactions of the DMFC requires significantly more catalyst than the LTPEM fuel cells. To further improve the reaction kinetics, small amounts of ruthenium is often mixed with the platinum catalyst. Figure 2.5 shows polarization curves for different DMFC manufacturers at atmospheric pressure. The DMFC has a very low fuel cell voltage and is often not used in high power systems because the fuel cell stacks volume is much larger than other fuel cell technologies.

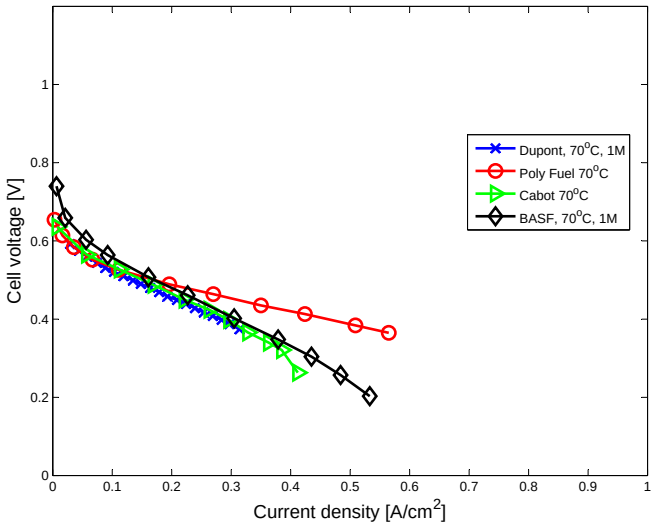

Figure 2.5: Polarization curve of different types of direct methanol fuel cells [7, 12, 18, 46].

DMFC fuel cells are a good choice for small electronics applications using passive diffusion of methanol and air to the anode and cathode respectively. This enables the design of simple system that are completely passively controlled, much like batteries, but refueling is much faster. One of the main problems with DMFC is the crossover of methanol to the cathode side of the fuel cell. Water and methanol molecules are dragged through the membrane via electro-osmosis and are combusted catalytically on the cathode side catalyst lowering the fuel efficiency and the electrochemical potential of the cathode process. The typical advantages and disadvantages of the DMFC are listed in the following.

Advantages

- Efficient fuel storage of methanol and water mixture.
- No external reformer required.
- Inherent anode cooling with fuel/water mixture.
- Anode fuel flow keeps membrane humidified.
- Fast system start-up from low temperatures.

Disadvantages

- Low cell voltage and efficiency.
- High losses increases cooling demands.
- Complicated water recirculation.
- Very high catalyst loading.
- CO_2 bubbles in anode flow.
- Methanol crossover lowers efficiency.

2.3.3 High temperature PEM fuel cells

The previously presented fuel cell types both relied on liquid water as a proton conductor. This can often result in unstable operation and a complicated humidification and water recuperation system. The low temperatures furthermore increase the complexity of the necessary cooling systems, by requiring large heat surfaces. If the temperature is increased to above 100^oC the product water will be steam, but a different membrane and proton conductor is needed at these high temperatures.

An example of a high temperature PEM fuel cell membrane is the phosphoric acid doped polybenzimidazole (PBI) membrane. PBI is a material typically used in the production of heat resistant materials such as fire fighting gear. This polymer is in itself a poor proton conductor, but combined with phosphoric acid, the conductive abilities can be greatly improved. Different methods for adding the phosphoric acid to the polymer exist, and with the phosphoric acid containing the primary conductive abilities of the membrane, it is vital that this acid stays in the membrane. If water droplets condense on the membrane, acid can diffuse to the droplets, and be removed by the gasses exiting the fuel cells. For these reasons, operation with water condensation is fatal to the fuel cell. Figure 2.6 presents polarization curves for HTPEM fuel cells at atmospheric pressures.

Because there is no need for liquid water, there is also no risks of drying out or flooding of the membrane. Therefore there is also the possibility of cooling the stack by supplying large amounts of cathode air and hereby saving the requirement of adding

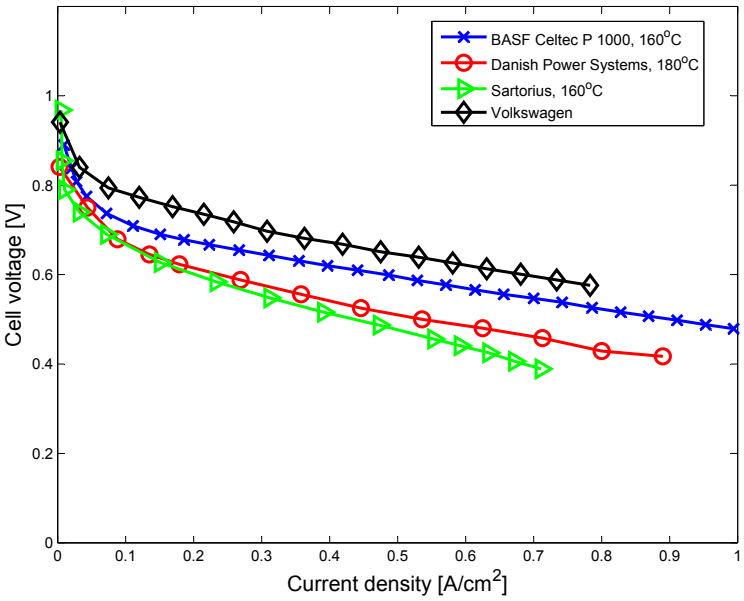

Figure 2.6: Polarization curve of different types of high temperature PEM fuel cells [5, 30, 49, 52].

cooling channels in the fuel cell stack. Because of the high operating temperatures of the HTPEM fuel cell, the anode reactions with CO are much faster, less likely to bond with active sites, and the fuel cell is therefore much more tolerant to this poison. The voltage recovery time is also significantly shorter than LTPEM fuel cells. The advantages and disadvantages of the HTPEM fuel cell are listed below:

Advantages

- No liquid water present increases reliability and simplicity of system.
- Cathode air cooling and dead-end anode operation enables simple system design and low parasitic losses.
- High CO tolerance reduces the complexity of reformer systems.
- No liquid water present.
- High quality waste heat.

Disadvantages

- Lower cell voltage and efficiency.
- High demands for materials and components at high temperatures and in presence of H_2PO_4.
- Slow start-up because of high temperature operation.

2.3.4 Solid oxide fuel cell

All of the previously presented fuel cell technologies rely on proton conduction through a polymer membrane. When reaching the very high temperatures of a solid oxide fuel cell (SOFC), which typically is above 800^{o}C, using polymer based membranes is no longer an option. Instead metal oxides and ceramic materials are used in the MEA. The typical material for the membrane is yttria-stabilized zirconia (YSZ), the cathode can be constructed in YSZ and lanthanum strontium manganese (LSM) and the anode of YSZ and nickel. Because of the very high temperatures, nickel can be used as a catalyst avoiding the expensive precious metal catalysts. Typical polarization curves for SOFC are shown in figure 2.7.

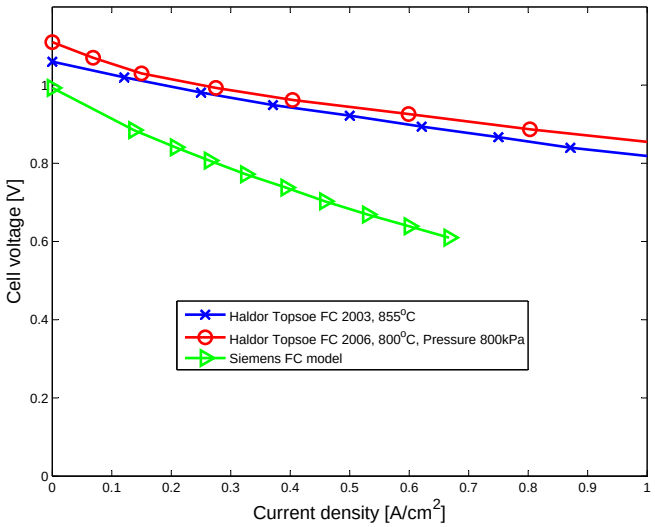

Figure 2.7: Polarization curve of different types of solid oxide fuel cells [15, 33, 42].

The solid oxide fuel cells can be either of planar or tubular shape and they can be stabilized (or supported) on either the cathode side or anode side. Other interesting features are that internal steam reforming is possible [1, 51]. Which both can introduce compact systems running on liquid hydrocarbons, but also potentially simpler systems because the endothermal nature of the steam reforming process acts as an internal cooling of the cells. There are high requirements for the different materials used in the SOFC. Besides the high temperatures, a component such as a bipolar plate exists in an environment with both strong oxidizing and reducing reactions. This requires

special materials and developments are moving towards specially designed steel and nickel alloys, making it easier and cheaper to produce the plates [23, 55].

Advantages

- High cell voltage and efficiency.
- Fuel flexibility.
- Internal reforming possible.
- Can use CO as fuel.
- Cheaper catalysts due to high temperatures.
- High quality waste heat.

Disadvantages

- High demands for materials at high temperatures.
- More volume is needed for insulation.
- Long start-up times due to high operating temperatures.
- Increased issues with thermal stresses.

2.4 Fuel cell technology choice

Comparing the fuel cell technologies and looking at the power range for the applications chosen. The HTPEM fuel cell technology is chosen to supply power for a utility truck (see section 6.2) and a small electric car (see section 6.1). All the presented fuel cell technologies could potentially be used, but the HTPEM fuel cells are chosen because of the stable and reliable operation compared to the LTPEM fuel cells, because of the independence of liquid water. Also the better tolerance to CO compared with LTPEM fuel cells is an advantage of the HTPEM fuel cells which could lead to simpler reforming systems with less CO clean-up stages. The higher temperatures of the HTPEM fuel cells are also close to the possible reforming temperatures of methanol. Using a liquid hydrocarbon could solve the hydrogen storage issues of the two applications, which are both non-stationary applications with high volumetric requirements for fuel storage. The relatively low temperatures compared to SOFC allow the use of more standardized auxiliary components and a smaller amount of insulation. Faster start-up times are also expected due to the lower operating temperatures of the HTPEM. The DMFC technology also fulfills the demands for using a liquid fuel, but the system efficiency is very low, and a DMFC fuel cell system is expected to be much to large, heavy and expensive. Figure 2.8 shows the evolution of the HTPEM fuel cell stacks used during this work.

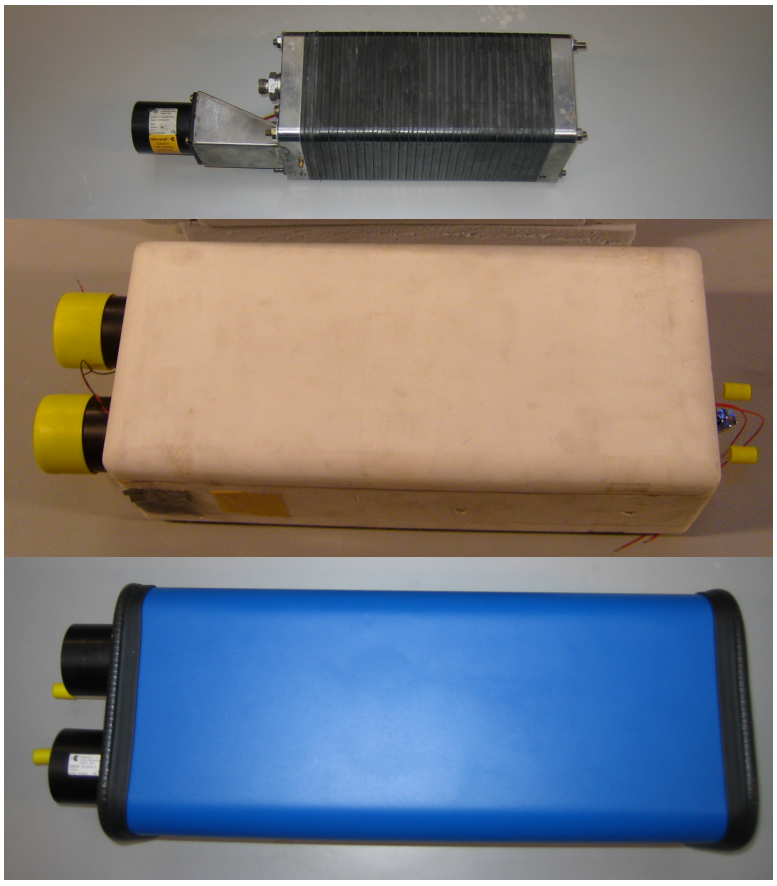

Figure 2.8: Examples of different generations of HTPEM fuel cell stacks.

3

Fuel cell system configuration

Fuel cell systems can be used at electrical power generators in systems where electrical energy is needed. In many cases batteries can be replaced by fuel cells because of smaller weight and volume requirements, and the possibility of continuous operation because recharging is not needed. In some systems the heat generated by the fuel cells can also be used to supply various processes and demands. The choice of using the HTPEM fuel cell technology is associated with various advantages and disadvantages as also explained in section 2.3.3.As later examinations and results also will indicate, the advantages of designing simple systems, the independence of liquid water as a proton conductor, and the good possibilities of using reformed liquid hydrocarbons are some of the strongest advantages of these fuel cells.

3.1 Operating conditions of high temperature PEM fuel cells

The membranes used in this research are primarily BASF Celtec P-1000 and P-2000 PBI-based membranes, with an active area of 45cm^2. The fuel cell performance greatly depends on the purity of the fuel used, and on the temperature. The effects of changing any of these can be seen from the modelled polarization curves of figure 3.1 [34].

Figure 3.1 shows the fuel cell voltage at different currents and CO concentrations as high as 5%. The recommended maximum anode CO concentration operating range is up to 3%, but the degradation rate of the fuel cell is expected to increase during long operation with reformate gas containing larger amounts of CO. The optimal oper-

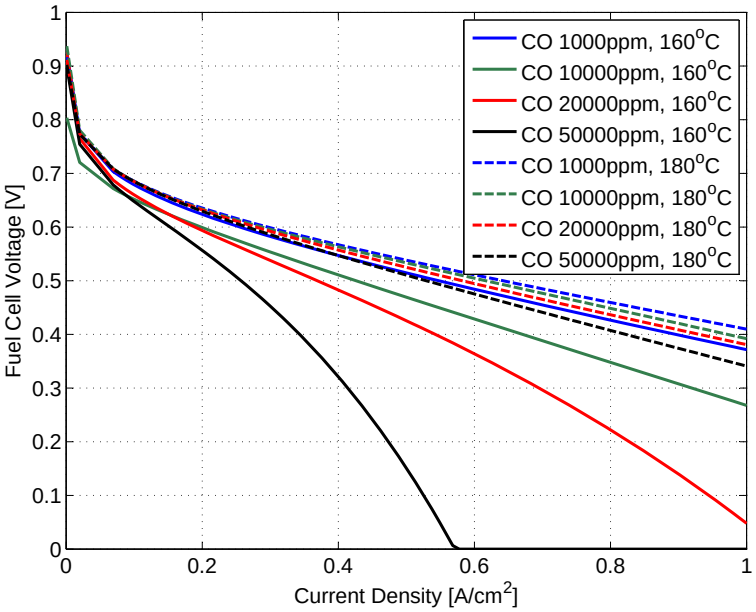

Figure 3.1: HTPEM Fuel cell polarization at different CO concentrations at 160 and 180^{o}C, λ_{Air}=2.5

ating temperature for the fuel cells is 120^{o}C-180^{o}C with the critical upper limit due to increased degradation. The recommended lower boundary of 120^{o}C is to avoid liquid water. At low temperatures, the performance is increasingly poor, whereas high temperature yields more efficient power production. Experiments on single cells have shown at least 6300 hour steady operation in steady state operation at low current density (0.2 A/cm^2), with a registered degradation rate of 5μV/hr [24].

The different failure modes of the fuel cells can be characterized as follows. Anode or cathode carbon corrosion can occur due to e.g. fuel starvation. The catalyst Pt alloy can undergo particle growth, agglomeration or dissolution due to high potentials and acidic environment. Electrolyte removal can occur at very low temperatures. The membrane can be affected by different mechanical stresses during assembly or as a function of temperature, which could result in pinhole formation and degradation.

The use of fuel cells as the only power supply for a given application can, result in very expensive systems considering the novelty of the fuel cell technology and the early stage of the fuel cell market. For this reason, and because other benefits can be gained, the fuel cells can effectively be combined with other electrical energy storages such as batteries and super capacitors. Figure 3.2 shows an example of a simulation

of the power demand for a vehicle undergoing one ECE-15 drive cycle followed by a extra-urban driving cycle (EUDC).

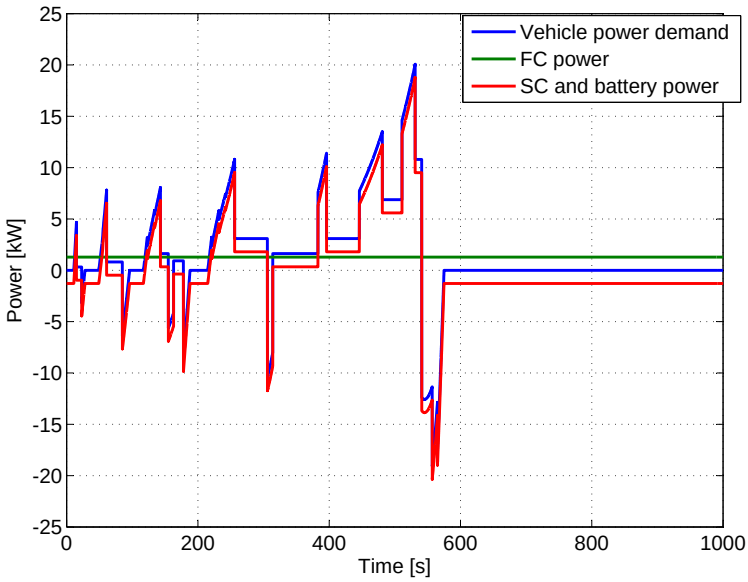

Figure 3.2: Overview of some of the choices made in the design phase of a fuel cell system.

If the vehicle was powered only by fuel cells, the fuel cell system needed to be able to supply the peak power demand of 20 kW. Using a combination of super capacitors, batteries and fuel cells allows the fuel cell system to be significantly smaller, and act as an on-board charger delivering a constant base charge for the battery and fuel cell, operating in it's optimal operating point. Using this strategy, the large power peaks experienced during acceleration is handled by the super capacitors and batteries, and the fuel cells only need to supply the average power over the entire driving cycle. The size of the fuel cell system should be based on the particular drive cycle of the application and depends strongly on the amount of time the vehicle is not using any power. In this period the fuel cell system is able to completely charge the batteries and super capacitors.

3.2 Fuel cell system design and hybrid power system configurations

When designing a fuel cell system for a given application, fuel cell efficiency is of course of importance, but often other practical issues determine the choice of technology and system design. These are issues such as cost, fuel availability, system volume, system load following capability etc. Figure 3.3 shows a typical roadmap of available system choices during a design phase. In this work two types of systems have been designed, one system running on compressed hydrogen and another on reformed methanol.

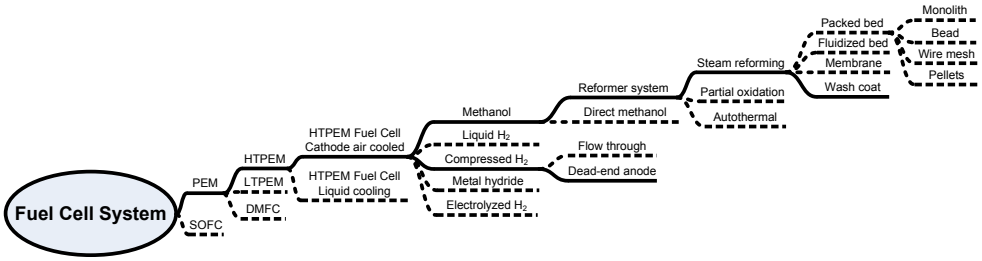

Figure 3.3: Overview of some of the choices made in the design phase of a fuel cell system.

Figure 3.3 shows the choices made and discarded in the design process, starting out with the overall choice of fuel cell technology, which is also described in chapter 2. With the chosen HTPEM fuel cells, using cathode air cooling was explored instead of using a liquid coolant. Typically air cooling will require some large geometries if low pressure losses are needed, but in the case of HTPEM fuel cells the entire fuel cell system is greatly simplified in terms of additional auxiliary components using this strategy. The operation and performance of a HTPEM fuel cell stack using this cooling strategy is analyzed in the following chapters, using compressed hydrogen as fuel. One of the main disadvantages when using hydrogen is the tank volume. Using metal hydrides as H_2 storage only yields a limited weight percent [14] and also involves special refuelling stations. In the case of liquid hydrogen, a cryogenic storage tank is needed, which also greatly complicates a system, and increases the losses. Producing hydrogen onboard the vehicle could be a possible solution to the problem with hydrogen storage. An electrolysis system producing hydrogen from water would require large amounts of electricity which in that case could be more efficiently directly from e.g. batteries. Producing hydrogen from methanol is chosen as a possible fuel for a HTPEM fuel cell

system, utilizing the high CO tolerance of the HTPEM fuel cells. In the design of a methanol reformer a new type of catalytically coated heat exchanger is used in order to benefit from the good heat transfer of such a unit. This reforming system, and some of the measurements and simulations conducted are presented in chapter 5.

Figure 3.3 only shows the overall outline of choices made during the design phase of a fuel cell system. Another aspect to consider when implementing fuel cell systems in electric power systems is how the fuel cell system is to be operated, and how it fits into the electrical system of a given application.

Fuel cell systems deliver electric power at a high efficiency. They are often implemented to replace battery systems, because the long charging time of batteries is inconvenient, and the lifetime in many cases limited. Fuel cells do not need recharging, and will run as long as a sufficient fuel supply is present. Directly replacing batteries with fuel cells is not always possible because the fuel cell voltage is not fixed. Figure 3.4(Top) shows the simplest way of connecting a fuel cell to the motor of a given application. The fuel cell stack is connected directly to the motorcontroller/inverter.

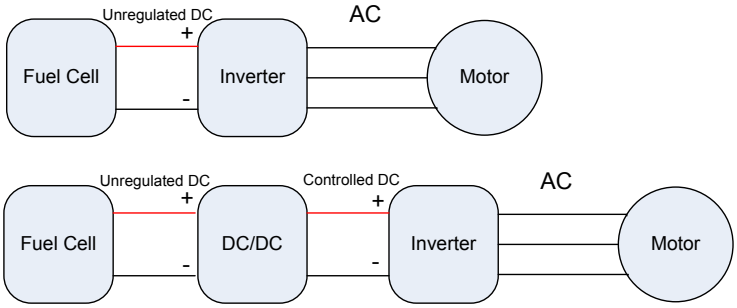

Figure 3.4: Top: Fuel cells directly power the inverter that controls the motor. Bottom: Fuel cell system is connected to the inverter through a DC/DC converter controlling the input voltage and current to the inverter.

Because the fuel cell delivers a DC voltage dependent of the current load which can vary up to 50%, such a system configuration would require an inverter with a wide input voltage range, and a special switching control strategy in order to ensure proper control of the motor. In this case the load from the motor will be determining the operating point of the fuel cell system, and no directly control of the power production is possible. Although no real fuel cell power generation control is possible some systems can benefit from the simplicity of this type of configuration, if the load is well defined

and matches the fuel cell system. An example of such an application is presented in chapter 6.1 and in Paper A.3. If more control of the power generated from the fuel cells is needed, i.e. a fixed input voltage is needed for the inverter, a DC/DC converter is typically used to ensure proper current and voltage control. An example of this is illustrated in figure 3.4(Bottom). As also explained in Paper A.8, combining fuel cells with batteries or other electrical storage units, such as super capacitors, results in more advantageous and cheaper systems. Figure 3.5(Top) shows an electric power system where e.g. batteries are used as the DC link voltage between the fuel cell and inverter. In this configuration, the battery and fuel cell system can share the load required from the motor. The benefit of such a strategy is that the fuel cell system is not required to supply the peak powers during accelerations in e.g. an automotive system, but only the average power requirement, using primarily the battery pack for power, and the fuel cell system as an on-board charger. This enables the system to operate much longer periods without hours of charging that for battery system usually are unfavourable. The price of the entire system could be significantly reduced by dimensioning this hybrid fuel cell/battery system exactly to the load pattern of the given application.

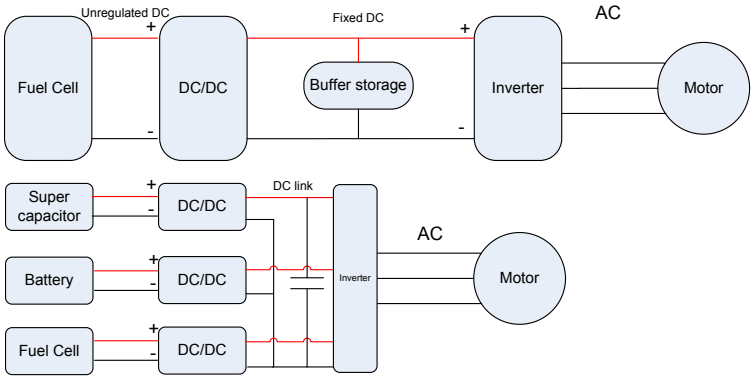

Figure 3.5: Top: Fuel cell system is connected to the inverter through a DC/DC converter and an electrical buffer storage such as a battery or a super capacitor. Bottom: Each electrical power system component is controller by separate power electronic units.

The voltage levels of fuel cells, batteries and super capacitors used in such hybrid systems need to be balanced properly if the benefits from all these components are desired in a given system. This is rarely the case, and can result in very expensive, overdimensioned and bulky systems. It applies for both fuel cells, batteries and super capacitors, that a series connection is needed to raise their voltage. High voltages of

e.g. 400V are usually required in order to reduce wire dimensions and enable the use of standard industrial components. Series connecting capacitors enable them to be connected to higher voltage levels, but also reduces the capacity. Therefore using the strategy proposed in figure 3.5(Bottom), where multiple converters are implemented to boost the voltages of each of the power units reduces the size of the super capacitor pack. In this strategy it is possible to precisely control the charging and discharging of each of the components, but the system complexity is much higher because of the additional power electronic components. And although power electronics are efficient, additional losses are introduced. Choosing the proper configuration strategy depending on the load pattern of the power system, can optimize e.g. cost, performance, operating time or even lifetime.

4

Hydrogen based high temperature PEM fuel cell system

One of the most desirable fuels for PEM fuel cells is hydrogen, because it offers the smallest losses and gives the best performance. There are many different ways of storing hydrogen, as listed below:

- Compressed hydrogen
- Metal hydrides
- Liquid hydrogen
- Reformable fuels

A very straight forward way of storing hydrogen is using cylinders with compressed hydrogen, 250 bar, 700 bar or even 900 bar. The hydrogen is compressed in cylinders but even at high pressures, the density of hydrogen is still very small. High-pressure storage of any gas introduces a safety risk, and the compression often involves a high power consumption affecting the overall efficiency and sustainability [44]. Keeping hydrogen in specially alloyed metal hydrides is another way of storing hydrogen. Metal hydrides exist in both physical form, adsorbing hydrogen in special alloys, or in chemical compounds usable mixed with e.g. water. In physical metal hydrides, the hydrogen is often released by heating the metal hydride and alloys can be designed to match specific temperatures close to ambient. Some of the main problems when using metal hydrides include the storage/release kinetics, i.e. removing the hydrogen at a fast enough rate. When refueling the metal hydride cartridge cooling is needed and much care must be taken, to avoid poisoning the metal hydride. Some metal hydrides can be highly toxic and explosive, and the energy density of the technology is still to be improved for use

in automotive systems [11, 14]. At low temperature (22K) hydrogen condenses into a liquid. This liquefaction ensure storage of hydrogen at lower pressures, with a high energy density. Often large insulated storage containers are needed and ≈30% of the energy content of the stored H_2 is needed to liquefy the H_2 [44]. Issues with hydrogen boil-off also increases the complexity of using this type of storage. The problem of storing hydrogen does not only concern consumption, but also production and distribution. If gaseous and liquid hydrogen are to be utilized for electricity production, large investments must be made in infrastructure. A liquid hydrocarbon based fuel could solve some of these storage and distribution and introduce a lower cost target because of e.g. simpler and more well established infrastructure. Systems using one type of liquid hydrocarbon, i.e. methanol, will be mentioned later (see section 5).

4.1 High temperature PEM fuel cell stacks

At the initiation of this research is was not possible to acquire HTPEM fuel cell stacks, only single cells. Therefore some of the work involved assembling a stack to test the feasibility of using HTPEM fuel cells producing power at a level usable in industrial applications. Figure 4.1 shows two different HTPEM fuel cell stacks. A prototype developed at the Department of Energy Technology at Aalborg University, and a further developed commercial product manufactured by Serenergy A/S.

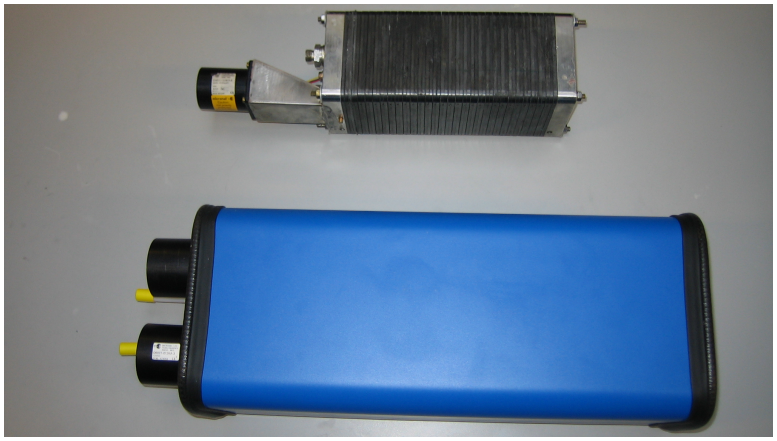

Figure 4.1: Top: 30 cell HTPEM fuel cell stack, initial prototype stack. **Bottom:** 65 cell HTPEM fuel cell stack, commercial stack from Serenergy.

The prototype stack is a 30 cell stack, using PEMEAS (later taken over by BASF) Celtec P1000 MEAs, with an active area of 45 cm^2. A single cell consist of two bipolar plates, teflon gaskets and the MEA. The stack delivers approximately 400W, and is developed to test the performance of stacking HTPEM fuel cells and to test the principle of using high cathode air flows to cool the stack, i.e. not needing an additional cooling circuit in the stack. The prototype stack is shown without the 50mm foam insulation that is applied to avoid insufficient temperatures during operation. The blower shown is a 12V Micronel D483Q which supplies the cathode and cooling air. In the same end of the stack, the hydrogen is also supplied. Both current collectors are led to the same end as the gas connections, to simplify insulation and system integration.

The 65 cell stack produces a nominal power of 1kW and has undergone a product maturation process leading to better stack temperature distribution and flow distribution resulting in an increased performance compared to the 30 cell stack. The membranes used are the same as for the prototype stack, but a new configuration of the bipolar plates has led to the possibility of using only one plate per cell. The cooling principle still utilizes the possibility of using high cathode air flows, which is possible only because the phosphoric acid doped PBI-membrane does not dry out at high air flow as a liquid water based proton conductive membrane would do. In the following examples of two systems using these two stacks will be presented.

4.2 Test of 30 cell prototype fuel cell stack

The purpose of the experiments conducted on the 30 cell prototype stack, are to evaluate the performance of a cathode air cooled HTPEM stack, and to develop control strategies to operate the system efficiently. The initial tests conducted on the 30 cell stack are described in Paper A.7. Figure 4.2 shows a schematic of the setup use for testing the 30 cell stack. The system consists of a the fuel cell stack with mounted thermal sensors, a hydrogen pressure valve and a cathode air blower. For cathode air supply it is also possible to use a Bürkert 8626 mass flow controller (MFC) able to supply up to 1000 L/min of air, for a more well defined air flow. The differential pressure between the air inlet and outlet is measured using an SM5852 differential pressure sensor.

The hydrogen supply for the stack is supplied from a reduced pressure of 8 bar, from pressurized bottled hydrogen. Afterwards it is further reduced by a single stage GO

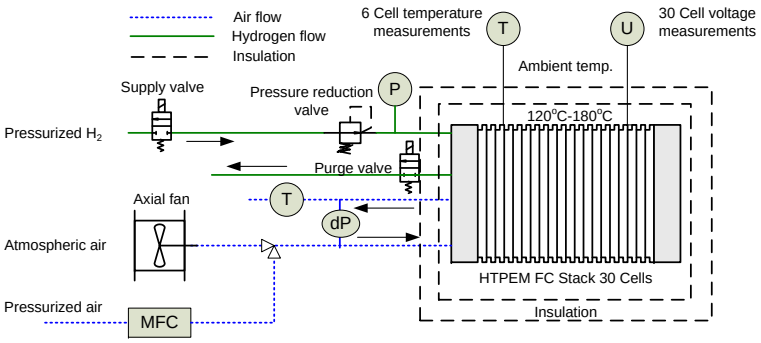

Figure 4.2: System diagram for 30 cell prototype fuel cell stack setup

Regulator LG1 pressure reduction valve to a fixed pressure of ≈0.15 bars in the stack, which is operated at this constant pressure. The hydrogen inlet flow can be restricted by an on/off valve (Bürkert 6011A) and hydrogen purge is possible during operation using the normally closed purge valve. In this type of hydrogen supply, the anode flow is controlled passively by the reduction valve opening to keep a constant pressure when ever hydrogen is removed, i.e. when a current is drawn from the stack. A mass flow controller can also be used, but the introduction of a recirculating system using e.g. an ejector is needed to avoid fuel waste. During long term testing a difference in water production of the membrane was discovered. The constant pressure strategy which has a high pressure on the anode side seems to remove all the water via the cathode exhaust air, whereas a setup using a mass flow controller a significant amount of water can also be condensed from the anode exhaust. This suggests that diffusion of water from the cathode to the anode side of the membrane, which could potentially remove phosphoric acid and increase the degradation of the fuel cells. It also indicates that condensation of water on the anode side is needed if an ejector recirculating circuit is introduced when using a system with a hydrogen MFC.

4.2.1 Pressure and flow characterization

Initial tests made on the 30 cell fuel cell stack includes a pressure and flow characterization to enable the choice of a specific blower for the system. Varying the air mass flow through the stack while recording the differential pressure is conducted, using different air inlet configurations. Measurements showing these experimental results are presented in figure 4.3.

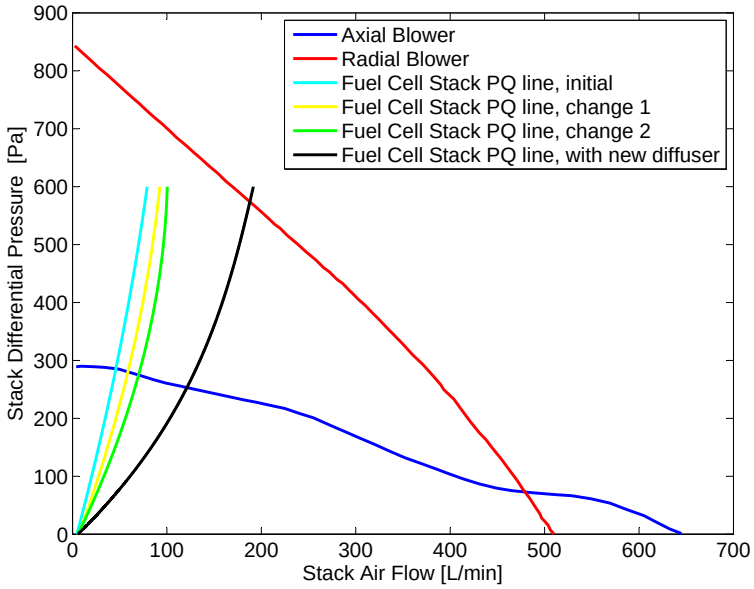

Figure 4.3: Pressure and flow characteristics of two different blowers and 30 cell stack using different air inlet configurations.

Different iterations and improvements were made, increasing pipe diameters, removing 90^o turns and changing manifolds. The characteristics of the axial Micronel D483T blower supplying the cathode and cooling air is seen in the figure. It is in the final system configuration operated at up to 24V, which is twice the rated voltage. During the experiments and many hours of operation at these higher voltages, no signs of failure were detected.

4.2.2 Temperature gradient

During the experiments conducted on the 30 cell prototype stack, one of the disadvantages found was the resulting stack temperature gradient because of the high inlet air flow at a relatively low ambient temperature (22^oC) compared to the high operating temperature (160^oC). Although some heating takes place at the inlet end plate and in the cathode manifold. The inlet part of the fuel cell stack is being cooled significantly as seen in 4.1, which shows the steady-state temperature distribution on the measurements made on the 30 cell stack, in the 6 different points shown in figure 2 in Paper A.1.

It is clear that there is not only a large through-plane temperature gradient from the inlet part of the stack to the end of the stack, but also an in-plane temperature

	Top	Bottom
Inlet stack	142^{o}C	152^{o}C
Middle stack	165^{o}C	172^{o}C
End stack	177^{o}C	177^{o}C

Table 4.1: Temperature measurements during steady-state load of 0.2 A/cm^2.

gradient from the top to the bottom of the stack. The result of this temperature gradient is a lower performance of the fuel cell with the lowest temperature, because the cell performance is strongly dependent on the temperature (see Appendix A.4, A.7 and A.1). This is illustrated by single cell voltage measurements made, which are shown in figure 4.4.

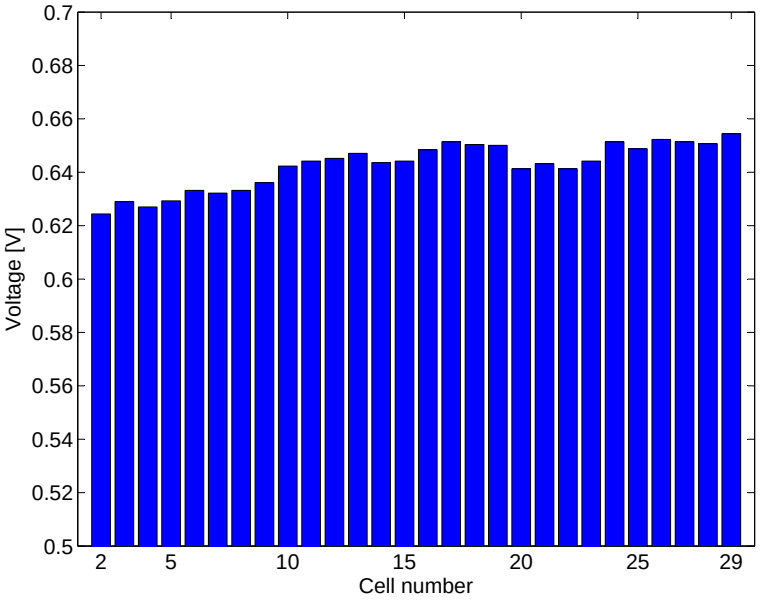

Figure 4.4: Steady-state individual cell voltage measurements at i=0.2A/cm^2

Here it is clear that the temperature has a strong impact on the cell performance, the cells following the temperature gradient with the coldest cell at the inlet have the lowest cell voltage. The losses of the this lower performance can be calculated by looking at the total power loss due to the voltage differences of each cell to the highest cell voltage found at the cell with the highest temperature. These voltage differences sum up to a total power loss at 0.2 A/cm^2 of 9W which corresponds to about 5% of the total

power generated by the stack. The strong temperature dependence is also seen during transient operation, which is shown in figure 4.5, where the temperature distribution is plotted against time, during an experiment where the stack is experiencing a step change in the current, from 0 to 0.2 A/cm^2. Running the stack with a reformate gas with CO, is expected to significantly increase these problems.

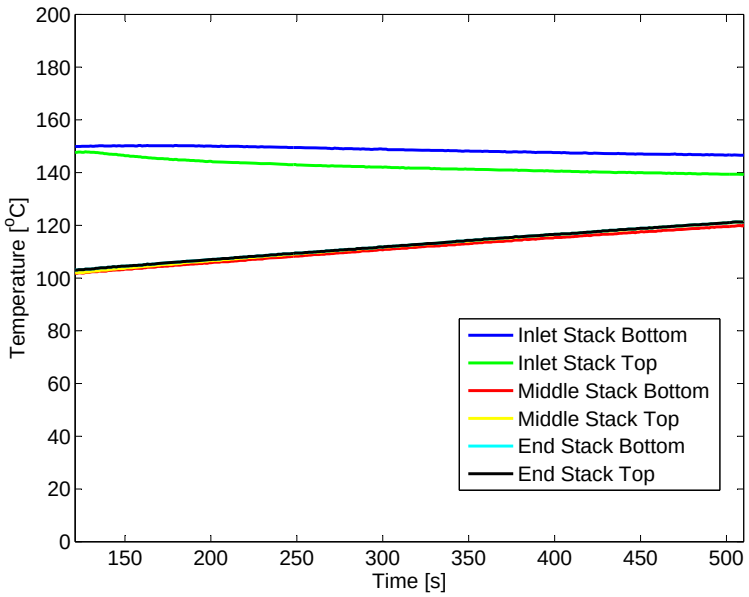

Figure 4.5: Transient stack temperature measurements at i=0.2A/cm^2

The temperatures are increasing due to the heat generated in the fuel cells because of the losses explained in section 2.2. Part of this heat is lost due to convection by the cooling air, conduction through the insulation, but also heating of the fuel cell stack. The resulting cell performance can be seen in figure 4.6, where it is clear that the cell voltages all increase during the shown transient stack temperature, even though the current load is constantly 0.2 A/cm^2.

The temperature of the inlet part of the stack is somewhat constant, slightly decreasing because of the increase in air flow to maintain a constant overall stack temperature. This results in a slightly decreasing cell voltage over time as seen by some of the cells in figure 4.6. If the current is changed very slowly it is possible to produce a polarization curve as shown in figure 4.7.

In the experiment conducted to produce the polarization curve shown, the temperature was controlled manually, and it is because of this, that small voltage changes are

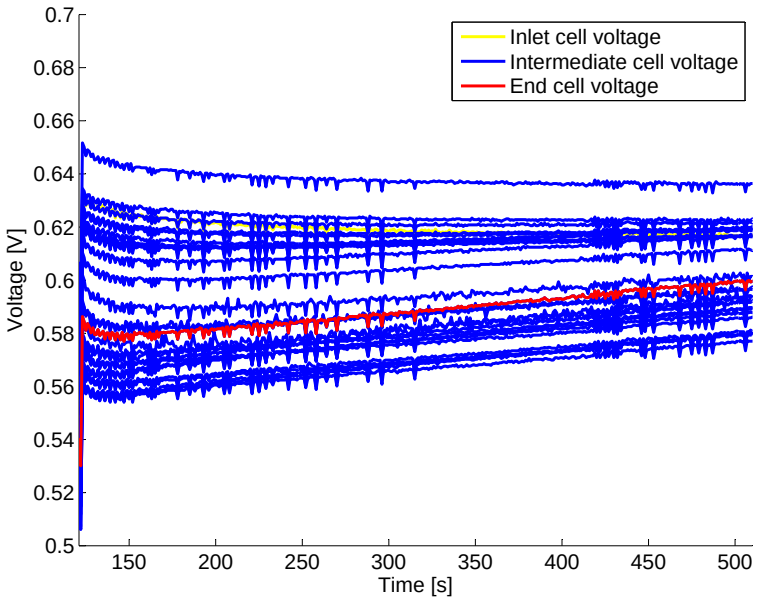

Figure 4.6: Individual cell voltage measurements at i=0.2A/cm^2 during temperature transient.

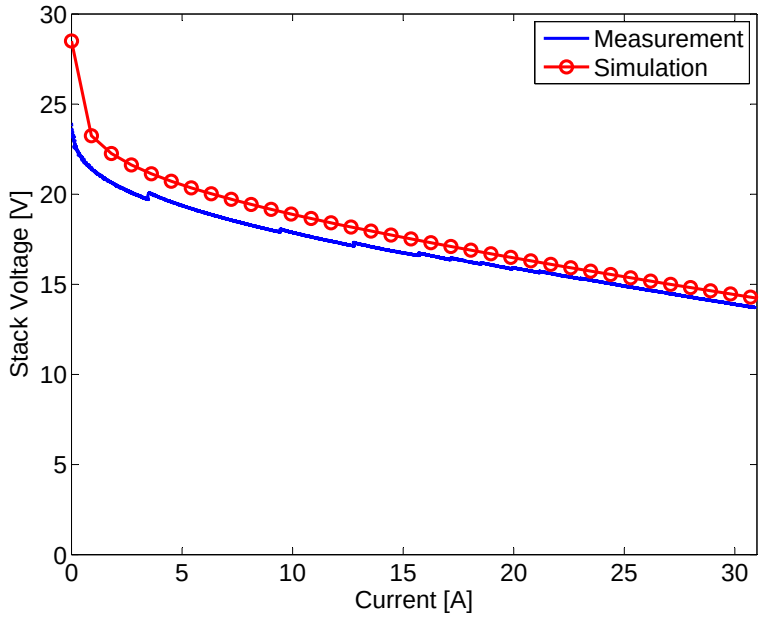

Figure 4.7: Simulated and measured polarization curve of 30 cell fuel cell stack.

present. These changes are where the air flow was increased to maintain a constant stack temperature. In figure 4.7, a simulated polarization curve based on the steady-

state single cell model presented in [34] is also shown, and it is seen that the results are similar even though the simulation is based on a single cell model. The main differences occur in the part of the polarization curve where the current and the air flow is low. These differences could be due to the temperature profile as explained before, and the hydrogen pressure. Problems were identified with the hydrogen pressure, due to the poor turn down ratio of the pressure reduction valve reducing the hydrogen stack pressure from 0.15 bars to 0.05 bars. This effect is seen in figure 4.8, where the hydrogen pressure is seen as a function of time during the creation of the polarization curve.

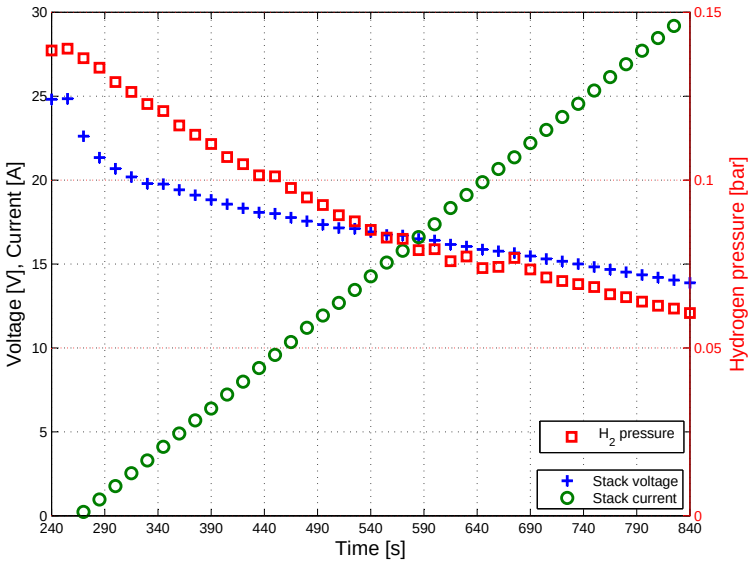

Figure 4.8: Measured fuel cell stack states showing poor pressure reduction valve pressure control.

It is clearly seen that the hydrogen pressure reduction valve is not able to control this low 0.15 bar setpoint pressure, and although there is a constant flow of hydrogen to the fuel cell, the valve is not able to control the pressure in the low pressure region. Another effect which was found relating to the anode pressure, was that at pressures just slightly above 0.2 bars, the cell voltage will drop, contrary to the common fuel cell voltage theory explained in section 2.2, which states that an increase in hydrogen pressure will have a positive impact on fuel cell voltage performance. The drop experienced is concluded to be attributed to increased hydrogen crossover, and the lowered performance involved with this effect.

4.2.3 Stack heating

When drawing a current from a high temperature PEM fuel cell, the stack temperature is required to be at a temperature where no liquid water forms in the cells, in order to avoid the removal of the proton conducting phosphoric acid in the membrane. This requires a pre-heating of the fuel cell stack which can be done using different methods to minimize the heating time. Experiments conducted using the 30 cell stack can be found in Paper A.4. In figure 4.9 an example of pre-heating the 30 cell stack is shown using heating mats placed on the top and bottom of the fuel cell stack.

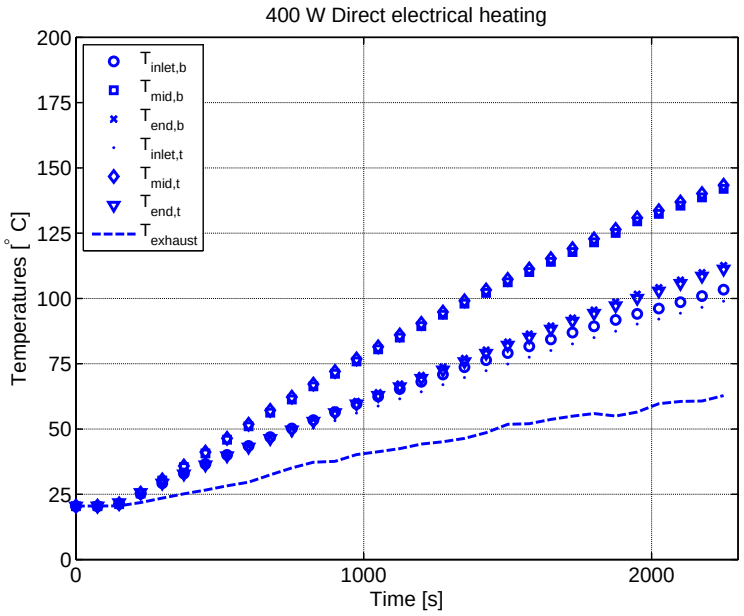

Figure 4.9: Temperature of 400W HTPEM fuel cell stack during heating with 400W surface mounted heating mats.

The electrical input power of the heating pads during this experiment is 400W, and it is seen that the heating time is 2271s . This heating time is defined as the time for the lowest measured temperature to reach 100^{o}C, such that the fuel cell product water will be in vapor phase. If using the fuel cells in an application where system start-up time is critical, another power source needs to be available while the system is heating. Typically a small battery pack could be used to supply the system with power while heating, and the size of this battery pack will depend on the time it needs to be operating, and the power it needs to supply to the heating process itself, if electrical

heating is used. A further elaboration on specific heating strategies for HTPEM fuel cell stacks is presented later in this work.

4.2.4 30 cell stack performance test

One of the great advantages with fuel cells is their ability to be used for dynamically changing loads. Figure 4.10 shows a performance test of the 30 cell fuel cell subjecting it to different load situations. The fuel cell is initially heated, the end of this heating cycle is shown in figure 4.10. The hydrogen is introduced to the stack, resulting in the stack voltage rising, as seen in figure 4.10.

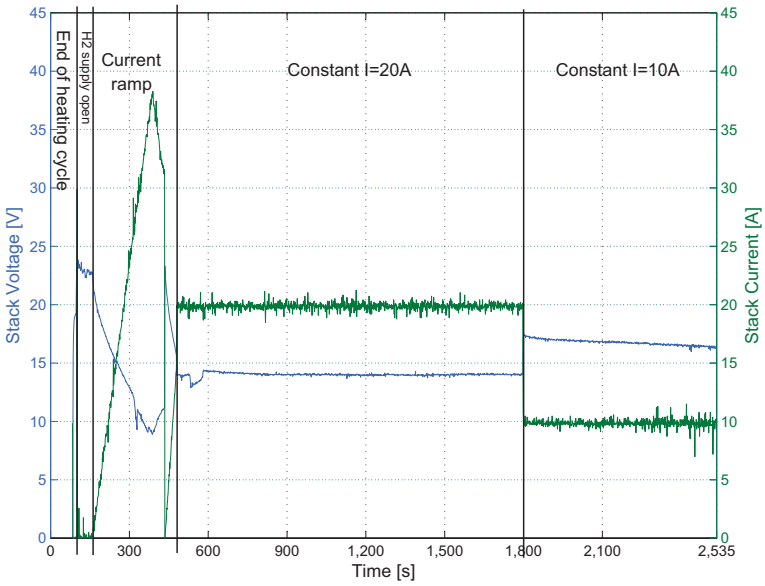

Figure 4.10: Load current and fuel cell stack voltage response in performance test.

For a while during idling, when the hydrogen supply is turned on, the stack voltage drops due to dropping temperatures, because the system heating has been suspended. At around 250s a current ramp is initiated and the voltage drops further. When the current reaches a value where the system is overheating, it is reversed for a short while and then quickly shut off at about 500s. After this, the stack is constantly loaded at 20 A and 10 A. A plot of all the sampled stack voltages and currents for the entire measurement is seen in figure 4.11.

Because of the ramp load, the voltage and current plot has the same shape as a polarization curve, but note that the temperatures during the experiment are changing,

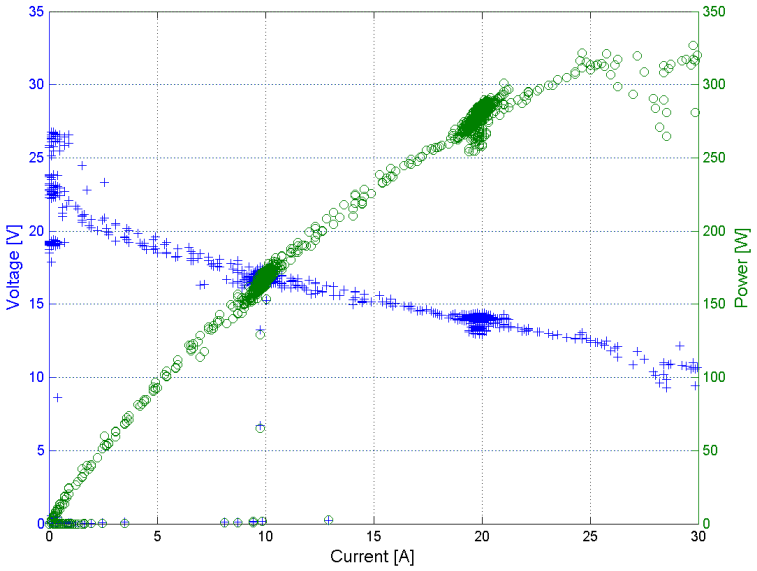

Figure 4.11: Plot of all sampled currents, voltages and corresponding power for the 30 cell stack.

so direct comparison is not possible. Constant load areas can be seen in the power and polarization curve where the measurements are most dense. At the high current loads, the points fluctuate because of the dynamics of the air cooling control.

The fuel cell system efficiency η_{system} of the shown load cycle in figure 4.10 is calculated as in equation 4.1:

$$\eta_{system} = \frac{(U_{FC} \cdot I_{FC}) - P_{Blower}}{\dot{m}_{H_2} \cdot LHV} \tag{4.1}$$

This efficiency is calculated as the ratio between the usable electrical power and the power available in the supplied hydrogen. The usable electrical power is the produced fuel cell electrical power i.e., the multiplication of the stack voltage U_{FC} and the current I_{FC}, and a subtraction of the parasitic losses P_{Blower} from the blower, which changes dependent on the current I_{FC}. The power available in the input hydrogen is calculated by a multiplication of the mass flow of hydrogen $\dot{m}_{H_2}$ and the lower heating values LHV. The efficiency of the performance test shown is seen in figure 4.12.

During the performance test the stack temperature control is active, it will be explained in details later in section 6.2.1. The general performance of the prototype fuel cell stack was satisfactory and showed promising results for the cathode air cooling

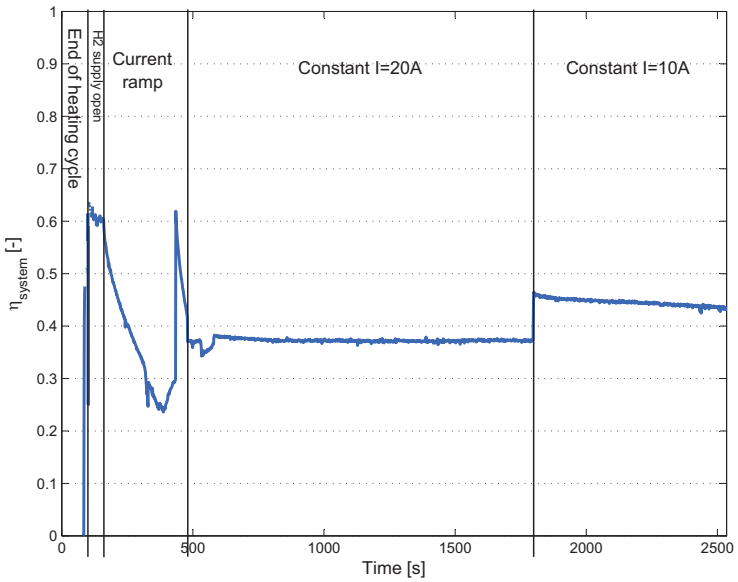

Figure 4.12: Fuel cell system efficiency during load cycle.

strategy. The primary problems with the stack developed was the temperature gradient both through each of the cells in the stack, but also from top to bottom, i.e. in the plane of each single cell. The system required to run such a system efficiently from pure hydrogen is remarkably simple.

4.3 Test of 65 cell fuel cell stack

The Serenergy Serene 1002 and 1003 are 65 cell, 1 kW HTPEM fuel cell stacks. It is, as the 30 cell prototype stack, based on the principle of using excess amounts of cathode air to cool the stack. The Serene stacks have many improved features compared to the 30 cell prototype, including only one bipolar plate per cell, where the prototype stack used two plates per cell. These changes have resulted in a smaller and lighter system, with improved thermal characteristics and a reduced temperature gradient, which improves the performance of the system. The improved temperature behaviour of the fuel cell due to the lower mass gives advantages both during stack heating and operation.

4.3.1 Fuel cell stack heating

The tests with the 30 cell prototype stack show a very slow heating of the system with electrical heating mats, and the same is the case for the 65 cell stack, which has a start-up time of 3423s using 400W on a top mounted 230VAC heating foil. Increasing the electrical input power did not improve the heating time significantly for the 30 cell stack, but changing the heating strategy to convective heating, results in a larger reduction of the heating time. Paper A.4 also examines different heating conditions for the 1kW HTPEM fuel cell stack. Figure 4.13 presents results of stack heating using preheated air at different air flows.

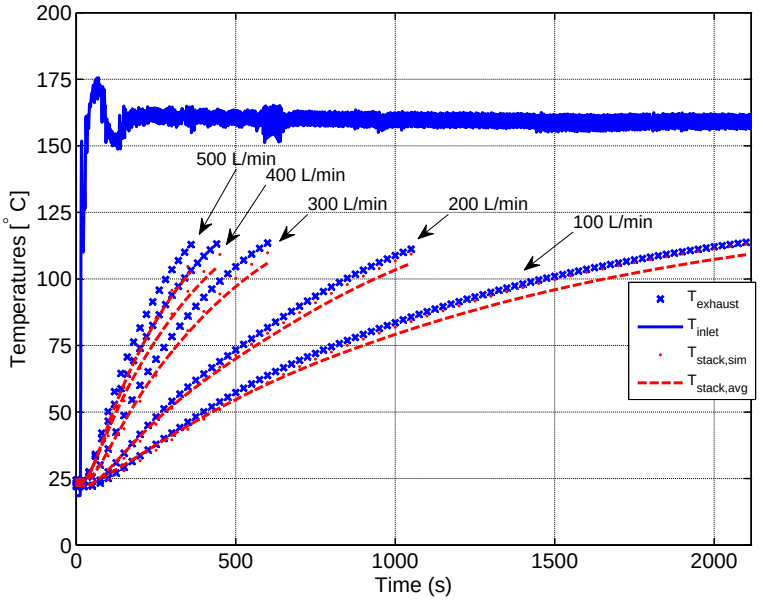

Figure 4.13: Temperature as a function of time at different air flows during heating of a 1kW HTPEM fuel cell stack.

It is clearly seen that the improvement in heating time using air is significant, needing only 359s for the lowest temperature in the stack to reach 100^{o}C at 500 L/min, which is well within the operating conditions of the blower. Because of the long start-up period different strategies should be considered for different applications. If requirements for quick start-up exist, a good choice is strategies where the system is kept at a standby temperature, such that it is ready for operation at any given time. If the user pattern is more unpredictable a long start-up time where power is supplied from batteries during

start-up could be feasible.

4.3.2 65 cell stack performance test

As described earlier, the stack needs preheating before a current load can be applied to the fuel cells. The following experiments show a series performance data of the 65 cell HTPEM stack. Initially the fuel cell stack is heated to a temperature of 100^{o}C. Figure 4.14 shows four temperature measurements made during operation of the stack. The temperature probes are mounted on the top surface of the stack in the front, middle and end part of the stack, and an additional sensor is mounted in the exhaust cathode gas.

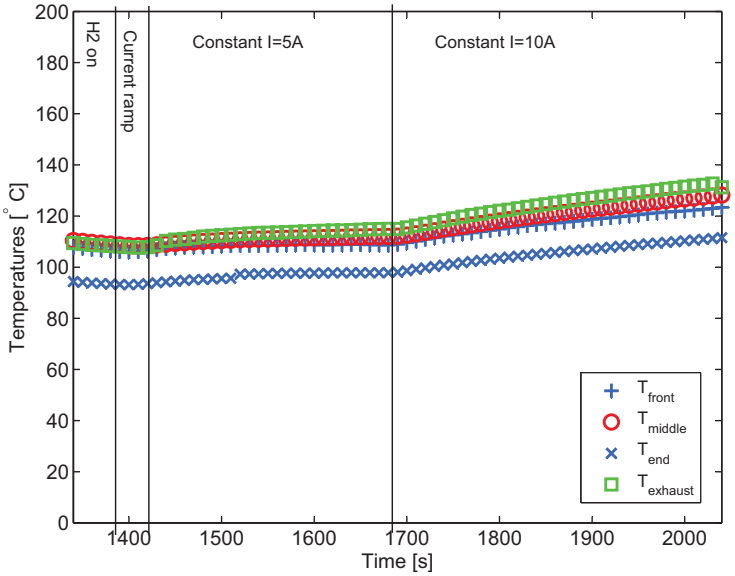

Figure 4.14: 1 kW HTPEM fuel cell stack temperatures during steady-state loads.

Figure 4.14 shows the stack temperatures immediately after heating. It is seen that the temperatures slowly start rising, more rapidly just before 1700s. The lowest stack temperature is T_{end}, which is the temperature, measured at the end away from the cathode air inlet and outlet. In this end, the temperature rise during heating is at it's slowest, also described in A.4. The reason for the temperature gradient change at around 1700s, is that the fuel cell current load is changed. The current and voltage of the fuel cell stack can be seen in figure 4.15. In the beginning of the experiment shown, hydrogen and a cathode air flow is introduced to the stack, resulting in the voltage

build-up seen at 1350s. Following the rise of the fuel cell stack voltage is a slow current ramp to 5A, which is held for ≈300s. The constant load causes a very small overall temperature rise of the fuel cell stack.

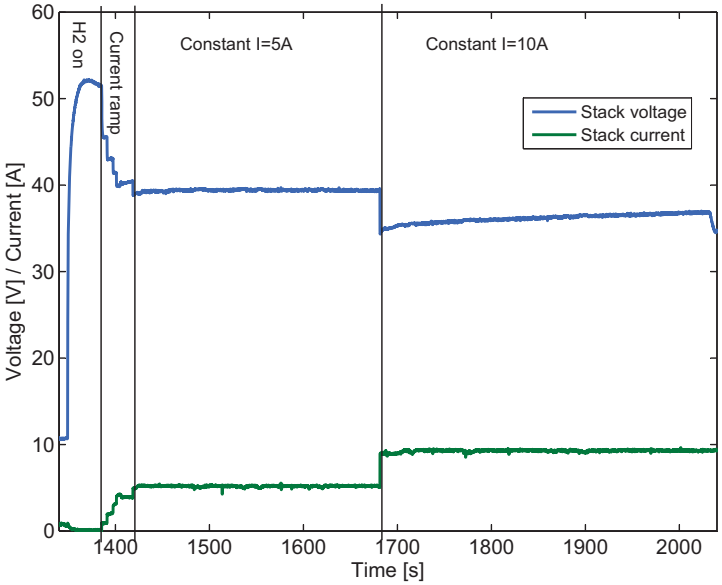

Figure 4.15: 1 kW HTPEM fuel cell stack voltage and current.

As explained before, at ≈1700s, the load is changed to 10A (0.2A/cm^2), which can be seen as an increase in the temperature gradient. Also because the air flow is changed simultaneously, the exhaust temperature starts separating from the other temperature measurements. The fuel cell system efficiency (LHV) during this load pattern can be seen in figure 4.16, and is around 40%. In the 5A part of the load, the efficiency is constant, and there is a small step down at the load change, due to the increased current drawn by the cathode blower. During the 10A load it is seen that the efficiency rises resulting from the increased performance due to the increasing temperatures, i.e. the current load is the same, but the fuel cell stack voltage increases because of the higher temperatures.

Fuel cells are often not only subjected to stable current loads, as shown in figure 4.15, but more dynamic loads. An example of a more dynamic load pattern is shown in figure 4.17. In this example the fuel cell stack has been operated for a long time and reached the desired operating temperature. The cathode air supply is being controlled by a current feedforward control, and a stack temperature feedback. Because of the low

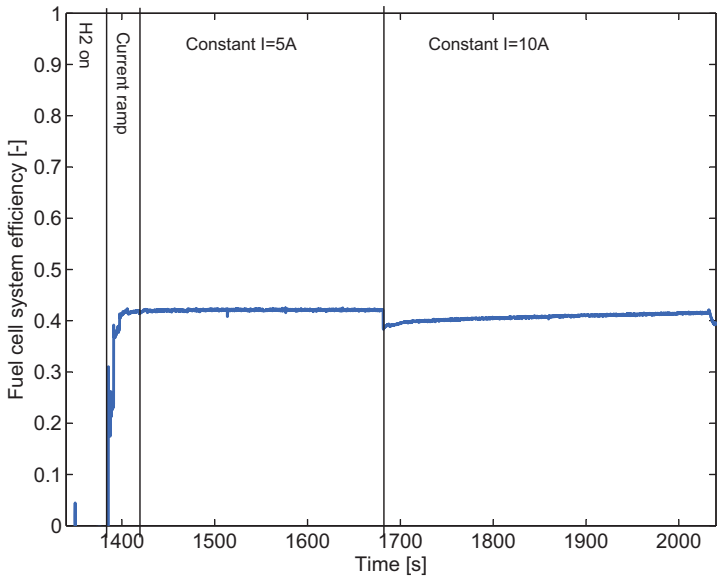

Figure 4.16: Fuel cell efficiency during experiment, also accounting for parasitic losses.

average load in the case shown, the control signal dominating cathode air supply is the feedforward.

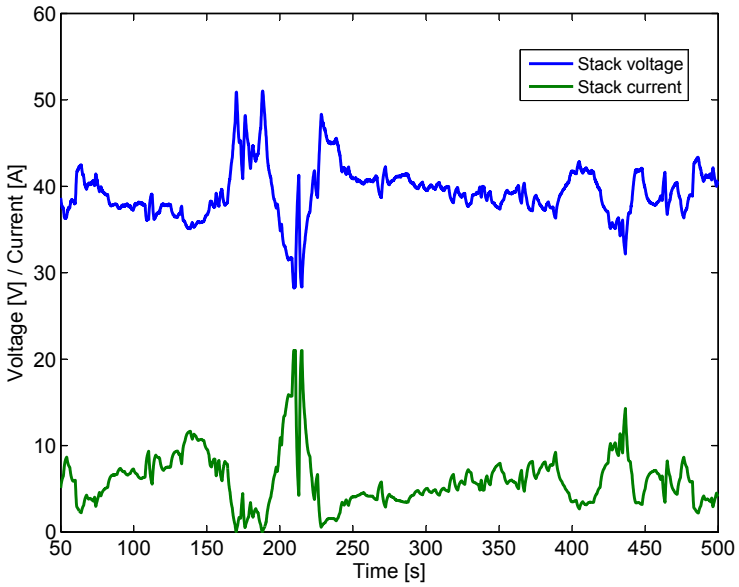

Figure 4.17: Fuel cell stack voltage and current during dynamic load situation.

The typical voltage behaviour of the fuel cell stack is clearly seen during this situa-

tion, when the current increases, a drop in the fuel cell voltage is experienced. The fuel cell stack is easily following all the ripples seen in the dynamic load pattern. The stack temperature behaviour can be seen in figure 4.18, and because of the thermal mass present in the fuel cell stack, the temperature changes are heavily filtered compared to the current although the increased losses at higher currents are directly related to the current. At around 200s, where the largest current change is experienced, some small temperature gradients are experienced.

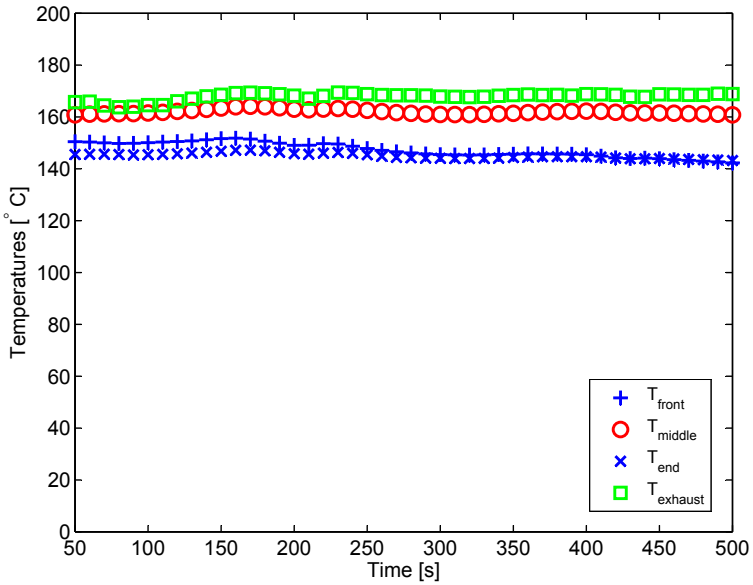

Figure 4.18: Measured fuel cell stack temperatures during dynamic load.

Compared to the temperature at the steady load in figure 4.14, the stack has been running for a longer time, and the temperature distribution is more uniform. The typical steady-state temperature profile shows the exhaust and middle stack temperatures as the highest, and the front and end temperatures as the lowest because of the increased conductive losses in these parts. The fuel cell system efficiency is shown in figure 4.19 and is also around 40% throughout the experiment, also showing some of the dynamic behaviour seen in the current and voltage.

At the points where the current reaches 0, equation 4.1 does not apply, and yields false results. This is seen in the areas around 200s where a current of 0A is experienced multiple times.

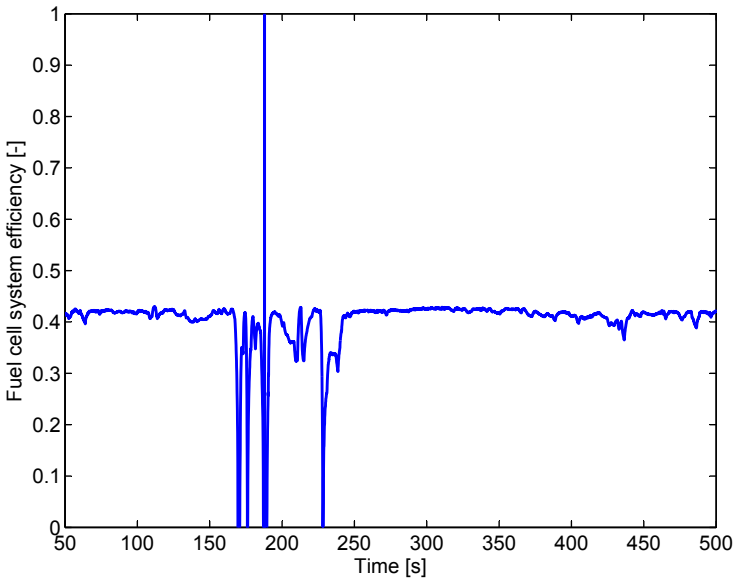

Figure 4.19: Fuel cell system efficiency during dynamic load.

The 65 cell HTPEM fuel cell stack shows a stable and predictable performance during both steady-state and dynamical operation. Many improvements have been made between the 30 cell stack and the 65 cell stack, but primarily the through plane temperature distribution has been made more uniform increasing the efficiency of the system.

4.4 Discussion

The work presented here regarding analysis of cathode air cooled HTPEM fuel cell stacks running with pure compressed hydrogen shows the advantages and disadvantages of this technology. The main advantages being the very simple system design and reliable system operation. This is primarily possible because of the low pressure drop through the stack, and the possibility of using large stoichiometric cathode air flows, without the risk of significantly lowering protonic conductivity of the membranes. Furthermore these fuel cell stacks have higher tolerances regarding the purity of the hydrogen used, enabling them to use reformed fuels efficiently. The disadvantages of these fuel cell stacks relate to the high operating temperatures, and the extended start-up time due to this. The presented work shows a method to minimize this start-up time, by using new

heating methods, but also the presence of small batteries in e.g. hybrid systems, could solve these issue for systems with quick start-up requirements. Using pure hydrogen as a fuel is in many cases not recommendable due to the very low volumetric energy density, but also due to the lack of infrastructure and the costs involved in such an investment. Therefore other fuels can be preferable and show promising results integrated with HTPEM fuel cells, as the next chapter will present.

5

Methanol reformer based high temperature PEM fuel cell system

One of the most ideal fuels for fuel cells is hydrogen, but it is not a naturally occurring resource, so it has to be produced from other sources. Many ways of producing hydrogen are available such as reforming methane or other hydrocarbons, water electrolysis and other chemical methods. Production from renewable energy sources such as using wind turbines, wave energy, or photo voltaic panels would ensure the reduction of CO_2 emissions, but often depends on different random weather phenomena. When using hydrogen as an energy carrier in the transport sector problems arise because of the low density of hydrogen even at high pressures. Not only the on-board fuel storage in a vehicle, but also the distribution of the fuel [11, 28, 37]. In many cases a liquid based fuel would be preferable because already established supply systems used for fossil fuels can be used. Storing hydrogen as a liquid involves very low temperatures, and complex storage systems. An alternative way of storing hydrogen is by using a hydrocarbon based fuel such as e.g. methanol, which can be produced by methanol synthesis, from biomass or potentially by solid oxide electrolysis using water and CO_2 [29, 32]. The use of on-board reformers using such liquid hydrocarbons require very pure reformate hydrogen when using LTPEM fuel cells, with CO concentrations of only 10-100ppm [2, 10, 16]. With HTPEM fuel cells being more tolerant to CO, on-board reformer systems could be made less complicated with smaller fuel purification components.

The use of a heat exchanger methanol reformer has been analyzed in this work. In the following, the initial tests with the reformer system will be presented, and fur-

thermore the system has been integrated with a 1 kW HTPEM fuel cell stack, and the possible operating strategies of this system are analyzed.

5.1 Initial methanol reformer system design

The concept of using a catalyst coated heat exchanger is to utilize the thermal advantages of the heat exchanger, which include optimized heat transfer, compact design and low thermal mass for fast temperature dynamics. Furthermore the plate heat exchanger is a well known and reliable product which easily can be scaled to larger sizes. The heat exchanger reformer is coated with at platinum based reforming catalyst and a burner catalyst by Catator AB. The initial test setup for the system can be seen in figure 5.1.

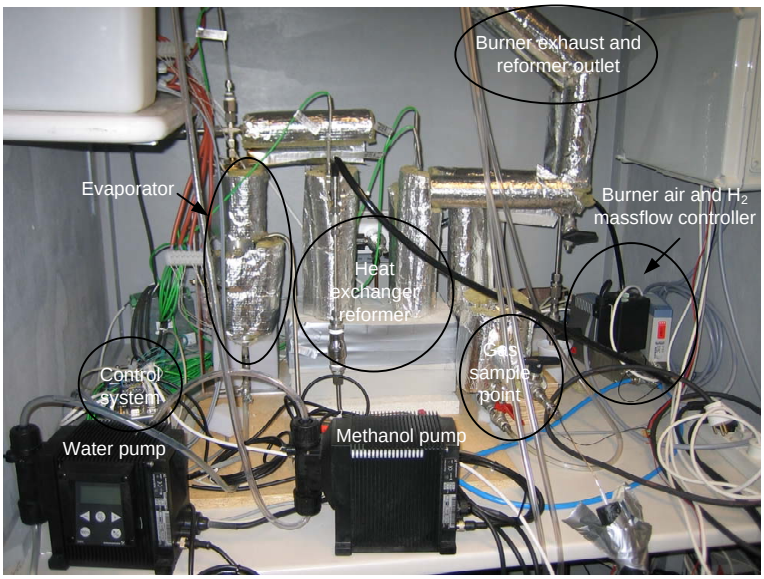

Figure 5.1: Picture of the initial system setup

In figure 5.1 the reformer is visible in the center of the setup, insulated with 5cm Microtherm insulation to reduce heat losses to the surroundings for a more uniform reformer temperature. Six type K thermocouples have been mounted on the top and bottom surfaces of the heat exchanger to analyze the temperature development of the bulk reformer. The reformer catalyst is Pt-based due to the higher robustness than e.g. a Cu-based catalyst [54], the disadvantage being an increased operating temperature.

Reforming of methanol can be done in different ways, and equation 5.1, 5.2 and 5.3, shows three typical ways of reforming methanol:

$$SR: \quad CH_3OH + H_2O \leftrightarrow 3H_2 + CO2(49.5kJ/mol) \tag{5.1}$$
$$POX: \quad CH_3OH + (1/2)O_2 \leftrightarrow 2H_2 + CO2(-192.3kJ/mol) \tag{5.2}$$
$$ATR: \quad 4CH_3OH + (1/2)O_2 + 3H_2O \leftrightarrow 4CO_2 + 11H_2(0kJ/mol) \tag{5.3}$$

The first reaction is the steam reforming (SR) reaction, where water and methanol reacts to form hydrogen and carbondioxide. Steam reforming is the most common method for reforming methanol, and many systems using this type of reformer have been made [20, 21]. The reaction is endothermic and therefore requires a heat input. The reaction shown in equation 5.2 is the POX reaction, where a source of oxygen is used together with the methanol to form hydrogen and carbondioxide. The partial oxidation (POX) reaction, although it has a lower hydrogen yield than SR, often uses less catalyst because of higher reaction rates, in the production of hydrogen and can result in very compact reformers [3, 13, 22]. Because parts of the fuel flow in the POX reaction is oxidized, the reaction is exothermic. The autothermal (ATR) reaction is a combination of the two prior reaction, i.e. both water and oxygen is used, to combine the advantages of the SR and POX in a reaction that balances the heating requirement, such that no external heating is required [17, 35]. The heat exchanger reformer presented in this work is also capable of autothermal reforming, but only pure steam reforming will be shown in the following. The overall steam reforming reaction presented in equation 5.1, including in this reaction are also the two following chemical reactions:

$$MD: \quad CH_3OH \rightleftarrows 2H_2 + CO(90.7kJ/mol) \tag{5.4}$$
$$WGS: \quad CO + H_2O \rightleftarrows H_2 + CO_2(-41kJ/mol) \tag{5.5}$$

The methanol decomposition (MD) is the direct conversion of methanol to hydrogen and carbonmonoxide. Carbonmonoxide is in PEM fuel cells viewed as a poison, while for SOFC it can be used as a fuel. With water available in the reaction the water-gas-shift (WGS) reaction can convert the carbonmonoxide into hydrogen. The balance of the water and methanol fuel flow is referred to as the steam-to-carbon (SC) ratio:

$$SC = \frac{\dot{n}_{H_2O}}{\dot{n}_{CH_3OH}} \tag{5.6}$$

This ratio is defined as the ratio between the molar flow of water $\dot{n}_{H_2O}$ and methanol $\dot{n}_{CH_3OH}$.

5.1.1 System setup

In the initial system setup it is possible, by a separate water and methanol pump, to change the steam-to-carbon ratio, during operation of the system. The pumps used are Grundfos DME 12 dosing pumps able to deliver 12 L/hr water and 2.5 L/hr methanol. The pumps deliver a pulsating flow, but the size of the liquid bulk volume entering the evaporator and the expansion during evaporation, ensures a stable gas flow in and out of the reformer side. The methanol and water mixture is pumped into an electrically heated evaporator, and is evaporated and superheated before it enters the reformer. This is mainly to avoid using part of the HEX to evaporate and superheat the methanol and water mixture. The evaporator is a cylindrical aluminium block with four 400W heating cartridges at the top and in the bottom of the block. A sketch and picture of the plate heat exchanger reformer is seen in figure 5.2, where it is seen that one side of the heat exchanger acts as the steam reformer which is an endothermic process requiring heat, and the other side acts as a burner supplying this process heat.

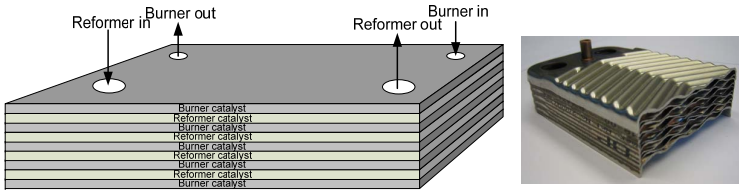

Figure 5.2: Picture and sketch of the reformer principle.

The fuel for the burner is in these initial tests, a supply of pure hydrogen mixed with air, via two mass flow controllers a Bürkert 8626 MFC 200 L/min for air supply and a Bürkert 8712 MFC 30 L/min for supplying hydrogen. The catalytic combustion is easily started from room temperature, but a too high hydrogen concentration can results in flashback, which results in critical temperatures, that could sinter the catalyst. A sketch of the initial system and the measurement points, are shown in figure 5.3.

In the final system the stack will be running at an overstoichiometric anode flow because of the different dilutants in the reformer outlet gas. The excess hydrogen exiting

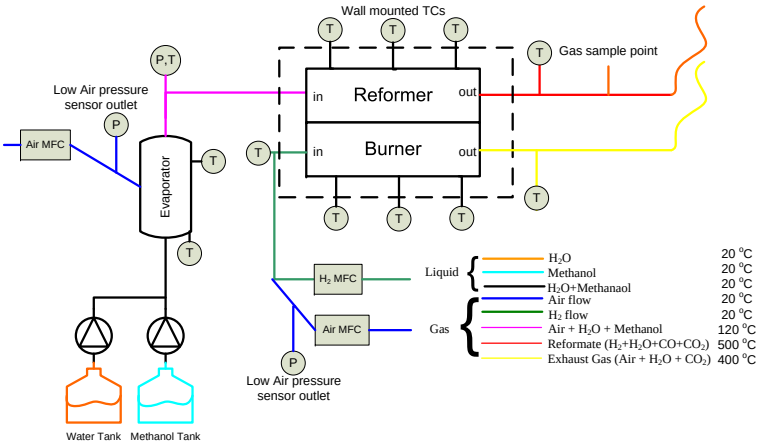

Figure 5.3: Diagram of the initial system setup

the fuel cell stack will finally be catalytically combusted in the burner, supplying the heat needed. In the initial system, the temperature of the evaporator is measured in the lower part of the bulk aluminium as close to the liquid as possible, and also in the vapor exiting the evaporator. The temperatures of the different gas flows in and out of the reformer and burner are measured, and air pressures can also be measured at the sites where air is supplied. Notice that it is possible to add air in the evaporator for autothermal operation. To evaluate the performance of the heat exchanger reformer, the gas can be sampled when exiting the reformer, and is measured by a Pfeiffer Omnistar mass spectrometer.

5.1.2 Gas composition

The expected gas composition of the exiting reformate gas can be estimated by calculating the chemical equilibrium of the steam reforming reactions. The measured gas composition can be somewhat different depending on the catalyst, space velocity, local reformer temperatures, and pressures throughout the reformer. As presented in Paper A.5, the Gibbs free energy G has a minimum at chemical equilibrium at a given pressure p and temperature T, expressed by:

$$G = \sum_{i=1}^{N} n_i \left[G_{mi}^{0}(T) + RT \left(ln\left(\frac{p}{p^0}\right) + ln(X_i) \right) \right] \tag{5.7}$$

Where i is the i'th specie. The gas composition will be at equilibrium with respect to the molar balance of the A'th atom, expressed by:

$$\hat{A}_j = \sum_{i=1}^{N} b_{ji} n_i - a_j = 0; j = 1...A \tag{5.8}$$

Using Lagrange multipliers λ, the following two equations can be solved to yield the molar fractions X of the chemical equilibrium.

$$\frac{\partial L}{\partial n_i} = G_{mi}(T) + RT\left(ln\left(\frac{p}{p^0}\right) + ln(X_i)\right) + \sum_{j=1}^{A} \lambda_j b_{ji} \tag{5.9}$$

$$\frac{\partial L}{\partial \lambda_i} = \hat{A}_j \tag{5.10}$$

The derived steady-state model, can be used to predict the output of the reformer under conditions of varying temperatures and SC. Figure 5.4(Left) and 5.4(Right), show the gas composition as a function of temperature at two different SC.

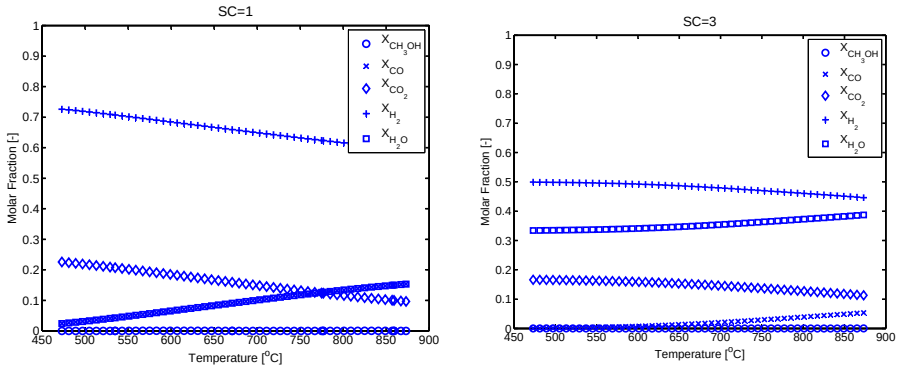

Figure 5.4: Left: Gas composition as a function of temperature at SC=1. Right: Gas composition as a function of temperature at SC=3.

To obtain the best conditions for fuel cell stack performance and lifetime, the CO content of the reformer outlet gas is required to be as low as possible. It is seen that from a theoretical point-of-view, using chemical equilibrium, increasing the temperature will increase the CO concentration, and lower the hydrogen concentration. Adding more water, i.e. increasing the SC will decrease the CO concentration at higher temperatures due to a more active water-gas-shift, this will in turn decrease the efficiency of the system because more power is needed to evaporate the additional water. In general operation

at low temperatures give the lowest CO concentrations. The reforming catalyst used in the reformer is typically used at 350-400^{o}C for optimal hydrogen production, and the water-gas-shift reaction is only significantly active at temperatures above 350^{o}C. The impact of adding CO to the anode hydrogen gas is illustrated by the single cell polarization curves shown in Figure 5.5.

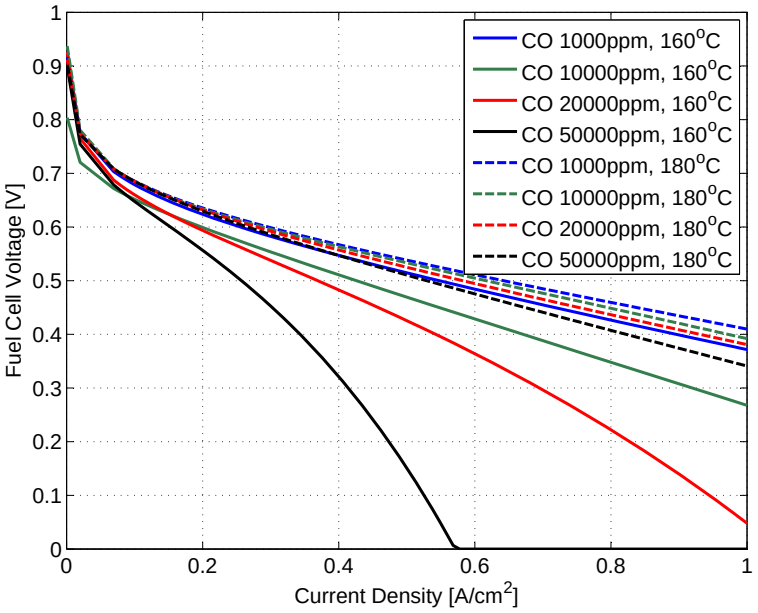

Figure 5.5: HTPEM Fuel Cell Polarization at different CO concentrations at 160 and 180^{o}C, λ_{Air}=2.5

The simulations in Figure 5.5 are based on an empirical model [34], and clearly show the impact on the fuel cell voltage, when increasing the CO content of the anode hydrogen gas. The reason for the CO lowering the performance of the fuel cell stack is the adsorption of CO on the platinum catalyst sites on the fuel cell anode catalyst layer, leaving fewer active sites for hydrogen to react. Furthermore the CO adsorption is slower than hydrogen adsorption. Some performance increase of the fuel cell can be gained by increasing the temperature, as seen on figure 5.5, but increased temperatures can also accelerate fuel cell degradation.

5.1.3 Initial methanol heat exchanger reformer performance test

The initial experiments performed on the heat exchanger methanol reformer are described in Paper A.5. Measurements conducted in some of the typical operating regimes are presented in the following. During system start-up using this initial system setup, a mixture of pure hydrogen mixed with air is supplied to the burner side of the heat exchanger reformer, supplying the heat needed for the steam reforming process. If the air to fuel ratio is too small, and the burner inlet temperature reaches high temperatures, hydrogen flash backs occur, which should be avoided due to very high temperatures. Figure 5.6 shows temperatures measured on the heat exchanger reformer during system operation. Three points on the top and bottom one, in each end of the reformer, and one in the middle of the reformer are measured. These temperatures are measured at the reformer surface on the inside of the insulation.

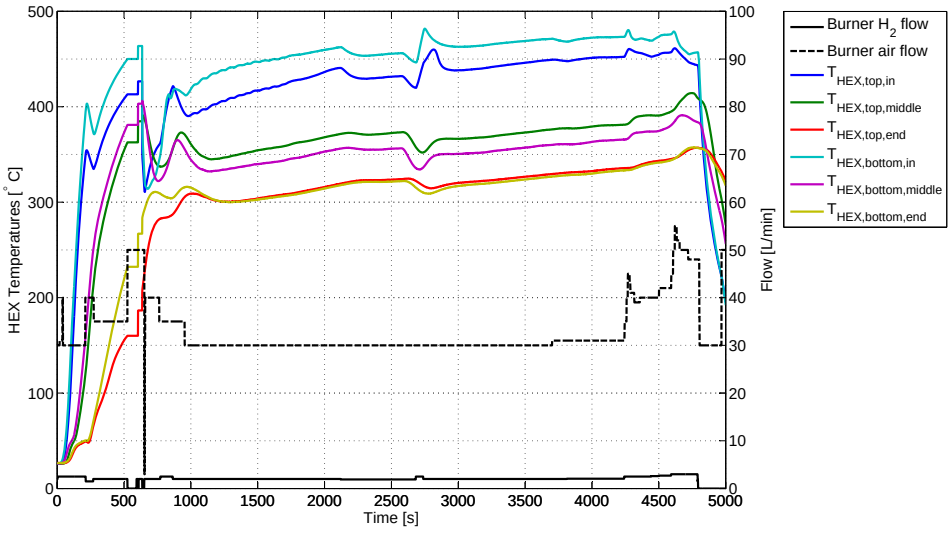

Figure 5.6: Reformer surface temperatures during steam reforming heated using pure hydrogen.

During the initial heating of the system (up to around 800s) the temperature starts rising soon after the introduction of hydrogen to the burner. The reformer temperature is controlled manually, with an introduction of a hydrogen fuel flow of 3-4 L/min using an increase in air flow to control the temperature, and avoid too high temperatures. As soon as average temperatures above 350 ^{o}C are reached, the methanol and water pumps

are started. The fuel flow introduced by these two pumps is shown in figure 5.7. The initial high water flow is needed to empty air out of the water fuel pipe in the system.

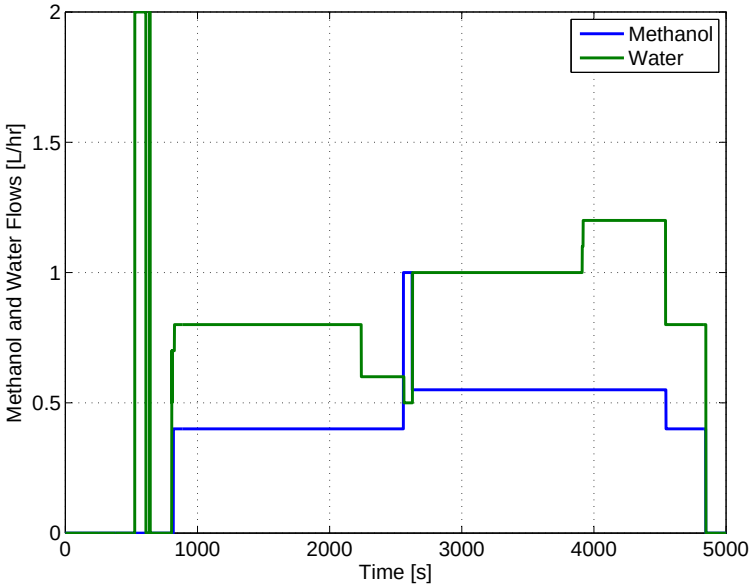

Figure 5.7: Methanol and water flows during system experiment.

At around 800s a constant water flow of 0.8 L/hr and a methanol flow of 0.4 L/hr is started. This corresponds to a steam-to-carbon ratio of 4.5, and introduces a hot steam gas into the reformer by heating in the evaporator. After this constant fuel flow, a step change in the water flow is made, reducing it to 0.6 L/hr (S/C 3.4), and afterwards the sizes of the water and methanol flows are switched for a short while, i.e. the methanol flow is 1 L/hr and the water flow is 0.5 L/hr. This change is made in order to see a short dramatic change in the gas composition response, which is much dependent of steam-to-carbon ratio. A large increase in methanol flow and simultaneous decrease in water flow is expected to decrease the water-gas-shift activity and hereby increase the amount of CO in the reformate gas. The gas composition is measured using a mass spectrometer, and clearly states this change in fuel and water flow which can be seen in figure 5.8, where the CO shortly increases and the CO_2 decreases.

The time axis in the gas composition measurement shown in figure 5.8 is a bit different due to the difference in start time of the datalogging started on the mass spectrometer, and the other reformer states. While using the mass spectrometer, different calibration procedures were conducted in order to measure the content of different

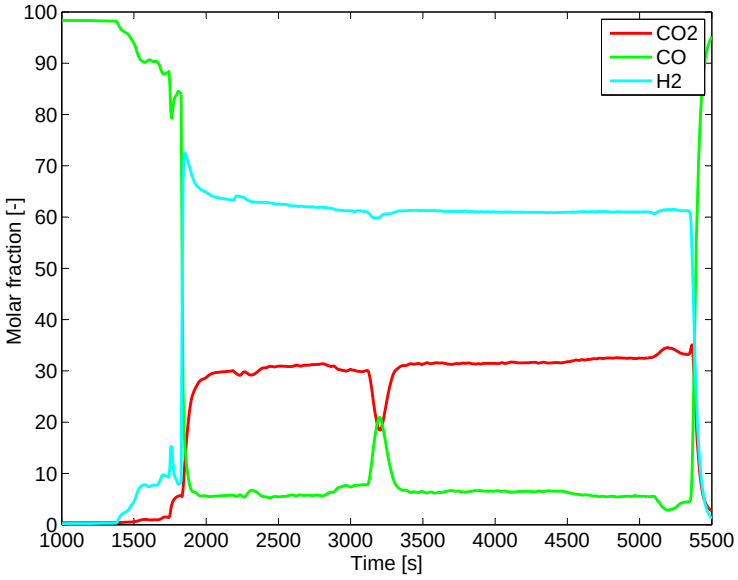

Figure 5.8: Dry volumetric gas composition during reformer operation.

species in the reformate gas. Particularly with measurement focusing on CO in hydrogen, it was found that the ion current calibrations were somewhat nonlinear, i.e. calibrations using many different CO concentration gasses were needed in order to yield the correct gas concentrations. Due to this, an uncertainty in the CO measurement shown in figure 5.8 is expected in the concentration more than a few percent away from the 5% calibration gas used in the calculation of the volumetric fractions. After the rapid switch in flows, a steady steam-to-carbon ratio of ≈ 4 is kept for 1300s, also yielding a steady reformer output concentration of 65% H_2 30% CO_2 and 5% CO.

The evaporator itself initially heats the liquid fuel mixture to the boiling point, and afterwards superheats it before it enters the reformer. The temperatures in and out of the reformer during the test is presented in figure 5.9.

The burner input temperature $T_{Burner,in}$, is constantly at ambient temperature, and the output burner temperature $T_{Burner,out}$ follows the behaviour of the surface mounted temperature measurements, initially rising during heating, to around 300 ^{o}C during start-up and afterwards slowly rising throughout the experiment. The reformer input temperature is controlled in the evaporator, which is the reason for the step changes seen in the measurements. This is due to changes in the evaporator temperature set point, to examine the response of the implemented controller. Oscillations are encountered in the

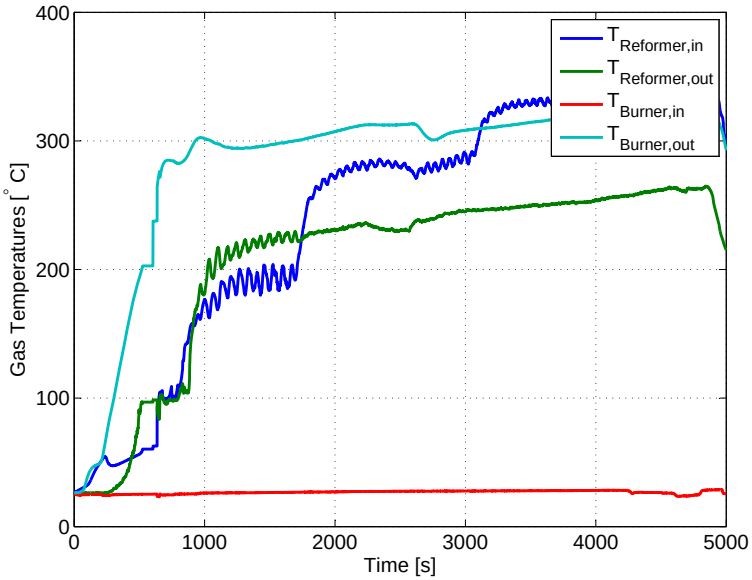

Figure 5.9: Temperatures if the gasses entering and exiting the heat exchanger reformer during operation.

evaporator exit temperature, and they seem to be decreasing in amplitude at increasing set point values. This behaviour could indicate stability problems with the implemented controller, but in the experiments conducted the PI controller parameters could not be found to stabilize this behaviour. During close examination of the step response of the evaporator temperature a few seconds of dead time were found, i.e. a time delay exists from when the evaporator electrical power is turned on until the evaporator temperature start rising. In order to compensate for this dead time a Smith-predictor is implemented, using a derived model of the system and the time delay. The principle of this predictor is shown in figure 5.10.

The principle of the Smith-predictor shown in figure 5.10 is to use a linear model of the evaporator, in this case a first order system as shown in the figure. The used PI controller output is fed into the evaporator model and the model output is used as a negative feedback which is subtracted from the difference between the reference temperature and an outer feedback signal. This outer feedback signal is the model response of the PI controller output including the estimated system dead time subtracted from a measurement of the controlled state. The difference is used as a negative feedback together with the temperature setpoint, and creates part of the error signal for the PI

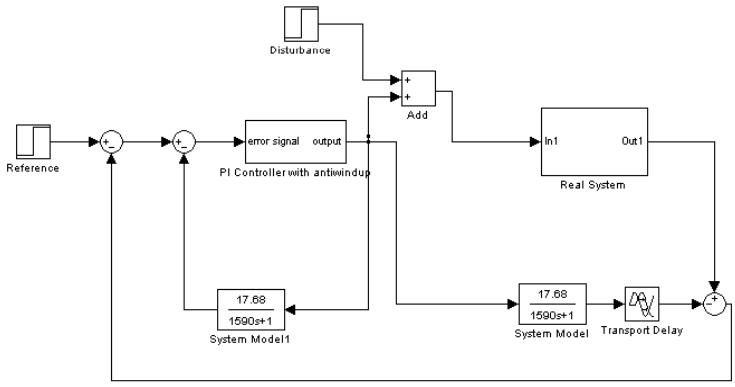

Figure 5.10: Smith-predictor used as dead time compensator.

controller. In this way, if the system model is correct, a dynamic compensation for the dead time will be made. This strategy works, and avoids the oscillations shown in figure 5.9, but a precise linear system model, and dead time estimation is needed. The means, that some areas of operation could exist, where the system shows more nonlinear behaviour, than the linear model predicts. Figure 5.11 shows the top gas temperature and bottom solid temperature of the evaporator using the Smith predictor, during a constant feed flow and using and different temperature set points.

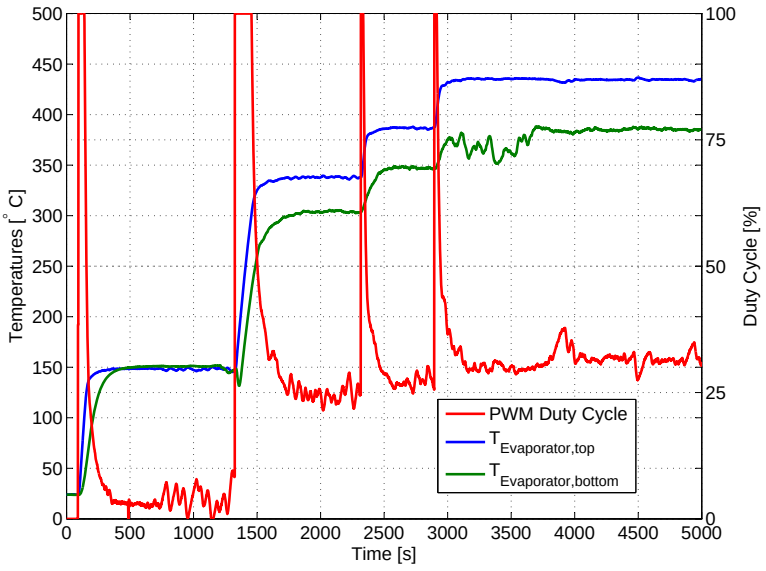

Figure 5.11: Evaporator temperature as a function of time using a PI controlled Smith-predictor to compensate for system dead time.

The dead time compensation seems to work, but a more thorough system analysis might show that the region of controller parameters that offer non oscillating operation exists, but simply is very narrow, but still possible to control the system acceptably.

The concept of using a catalytically coated heat exchanger to steam reform methanol was successfully demonstrated, utilizing good heat transfer and low thermal mass, showing promising results for use together with a HTPEM fuel cell stack. The main disadvantage being the high CO content in the anode gas due to the use of platinum based catalyst.

5.2 Integration of heat exchanger methanol reformer system with fuel cell stack

The initial results of the heat exchanger reformer presents a system with an acceptable performance and a proof of concept for the catalytically coated heat exchanger as a reliable strategy for steam reforming of methanol. The efficiency of the system could be further analyzed and improved by integrating the reformer with the stack, utilizing some of the available waste heat from the fuel cell stack to run the evaporation of the methanol and water mixture flow.

A typical air flow through the stack is approximately 350 L/min at the nominal power, where the electrical efficiency running on pure hydrogen is typically 40-45%. When introducing CO to the inlet anode gas, which is typically the case when reforming methanol, the electrical efficiency will be lower depending on the CO concentration; which in turn increases the cooling demand and the heat removal from the fuel cell stack. Using the heat available in the exhaust cathode cooling air to evaporate the methanol water mixture will increase the overall system efficiency and remove the dependence of using the electrical power generated from the fuel cell to supply the supportive system, as when e.g. using electrical heaters during operation. The exhaust from the burner also contains a lot of heat, which could support the evaporation process.

Figure 5.12 shows the system operation during normal operation, where the system is running in standard fuel cell power production mode at a varying or fixed current load.

A small KNF FMM20 membrane pump able to deliver up to 30 ml/min, pumping a mixture of water and methanol into the evaporator which is heated by the fuel cell

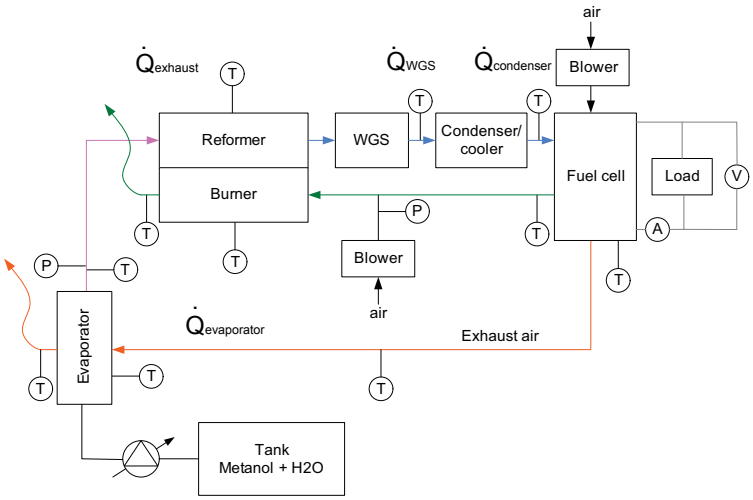

Figure 5.12: System diagram where the flow path is visible during operation of the fuel cell system.

stack cathode exhaust air exiting at 160-180°C in normal operation. The evaporated fuel enters the reformer where it is converted to H_2, CO, CO_2 and H_2O. The exiting reformate gas enters a water gas shift catalyst to lower the CO content, and is afterwards cooled to stack temperature, where condensed water is removed before the fuel flow enters the stack at anode stoichiometry of ≈1.2. The residual combustibles, i.e. H_2 and CO is afterwards mixed with air and catalytically combusted in the burner side of the heat exchanger where it transfers heat to the reforming process.

A picture of the system is shown in figure 5.13, where the main system components are outlined.

The methanol/water pump is seen in the bottom of the picture, pumping the feed flow into the evaporator, where heat is added by using two electrical heaters, and by a preheated air flow, that acts as a fuel cell stack emulator. After the evaporator, the steam based methanol and water enters the reformer, which is heated by a supply of hydrogen from the shown mass flow controller, mixed with an air flow. The reformate gas enters a water-gas-shift and is afterwards cooled to a temperature that matches the fuel cell stack temperature. The reformate gas is sampled in a mass spectrometer, and an additional condenser is placed in the gas sample flow, to ensure that no liquid water is present in the mass spectrometer used to measure the system gas composition. A close-up of the uninsulated system is seen in figure 5.14, where the reformer connections

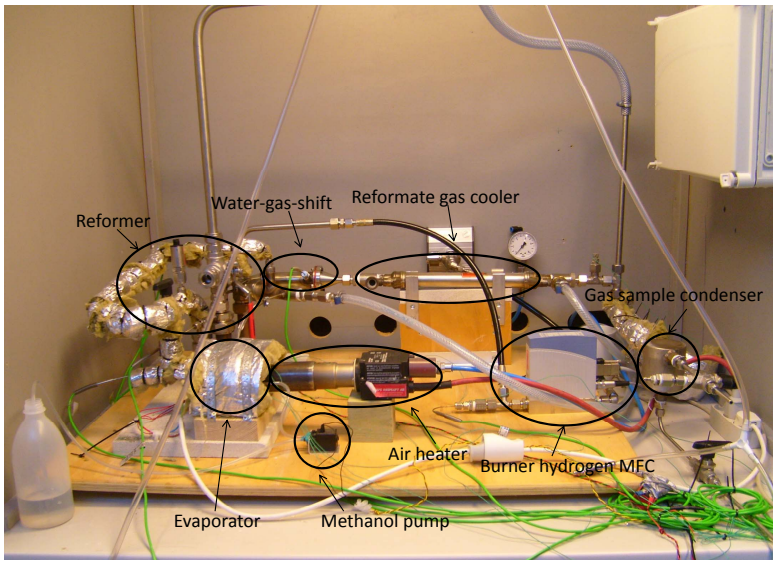

Figure 5.13: Picture of the system setup using hot air for methanol evaporation.

are visible in the bottom left part of the picture.

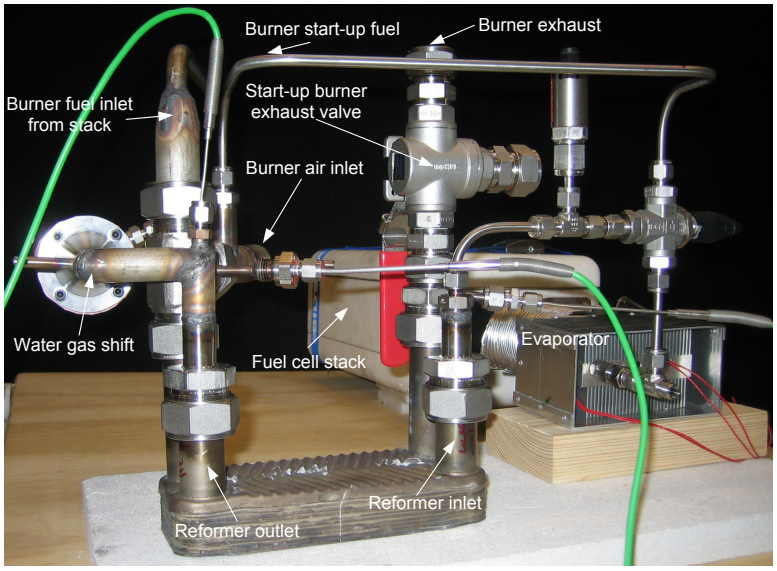

Figure 5.14: Picture of the integrated system setup

During the start-up of the system, different strategies can be used, initially using electrical heaters, but preferably combustion of available fuel which is more efficient, and does not depend on an additional electrical source i.e. a battery. The system has two three way valves which redirect some of the gas streams during the start-up of the

system. The initial evaporation of the methanol and water mixture is done electrically and the evaporated fuel is directed directly to the burner side of the reformer where it is mixed with the burner air flow. The configuration of the system during start-up, is shown in figure 5.15.

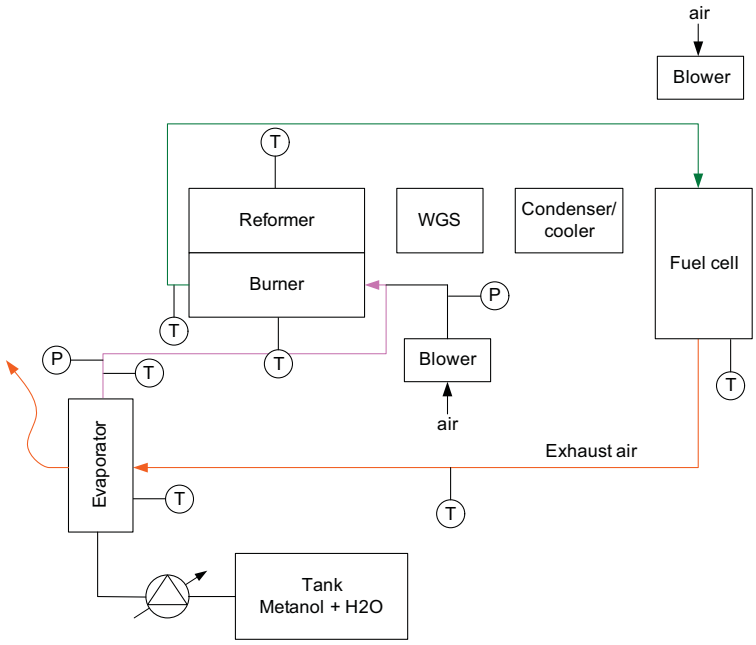

Figure 5.15: System diagram where the flow path is visible during start-up of the fuel cell system.

Once the combustion process is running, the burner exhaust is redirected to enter just after the stack cathode blower, where it can be mixed, and the inlet temperature controlled. The gas flow heating the stack will gradually decrease the need for electrical power used for the evaporation process, and after a while both the reformer and fuel cell stack will be at operating temperatures and ready to deliver electrical power and switch back to operating mode.

5.2.1 Control of integrated system

To test different control strategies for running the system, estimate efficiencies and derived controller parameters, a simple simulation model has been derived using Simulink. The model generally uses the method of modelling each of the components in the system

as a lumped thermal mass, as in Paper A.4. This method together with an equilibrium model of the steam reforming reactions described in Paper A.5 yields the model of which an overview is shown in figure 5.16.

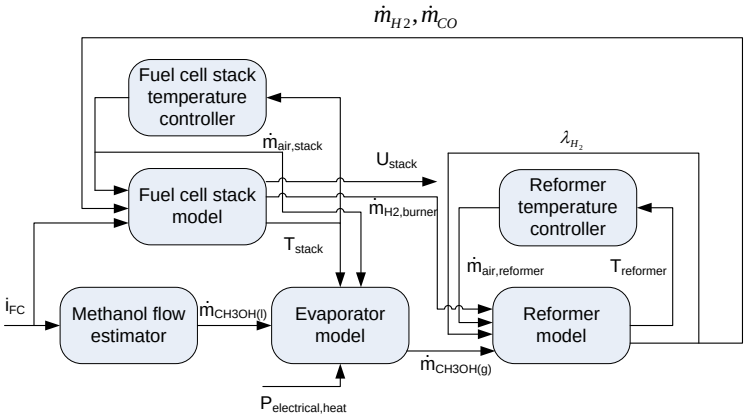

Figure 5.16: Overview of the dynamic simulation model

This model predicts the different dynamic states of the fuel cell stack and methanol reformer system. The primary assumptions are that the gas composition can be looked at as chemical equilibrium at a temperature a bit lower than the actual reformer temperature. The temperatures of the system have been determined using a lumped approach and are expected have significantly larger time constants compared to fuel cell stack voltage dynamics and reformer chemical reaction rates, such that these can be neglected. The different controllers acting in the system are listed below :

- Fuel cell stack temperature control
- Reformer temperature control
- Fuel feed flow control

The fuel cell stack temperature control is carried out by using PI controlled cathode air cooling of the stack, which is elaborated in section 6.2.3. The fuel cell feed flow is based on an estimated hydrogen conversion ratio at the desired stack hydrogen flow and a λ_{H_2} ensuring proper excess hydrogen for the heat supply to the burner. The function of the stack temperature control is explained in detail in Paper A.1 . The reformer temperature is controlled as follows. The hydrogen exiting the fuel cell stack is mixed

with air and catalytically burned to supply heat for the reforming process. To ensure proper temperature control, the burner air flow is increased when the temperature rises above a specified set point, increasing the convective losses, hereby cooling the system and lowering the combustion temperature. The fuel feed flow is estimated by the expression in equation 5.11:

$$\dot{q}_{CH_3OH} = K_{estimator} \cdot \frac{n_{cells} \cdot A_{MEA} \cdot i \cdot \lambda_{H_2}}{2 \cdot F \cdot \rho_{CH_3OH} \cdot x_{H_2}} \tag{5.11}$$

Using a constant value of the gain $K_{estimator}$ is usable, but as it relates to the ratio between the molar gas flow into and out of the steam reformer, it is strongly dependent on both the temperature and steam-to-carbon ratio. The number of cells in the stack are noted by n_{cells}, A_{MEA} is the active MEA area, i is the current density, and x_{H_2} is the molar fraction of hydrogen. The importance of choosing the correct value for $K_{estimator}$ is vital for efficient operation of the system due to the direct impact on system efficiency.

A dynamic system simulation using the determined system controllers using a dynamic current load pattern has been carried out. The particular load profile, and resulting fuel cell stack voltage curve is shown in figure 5.17.

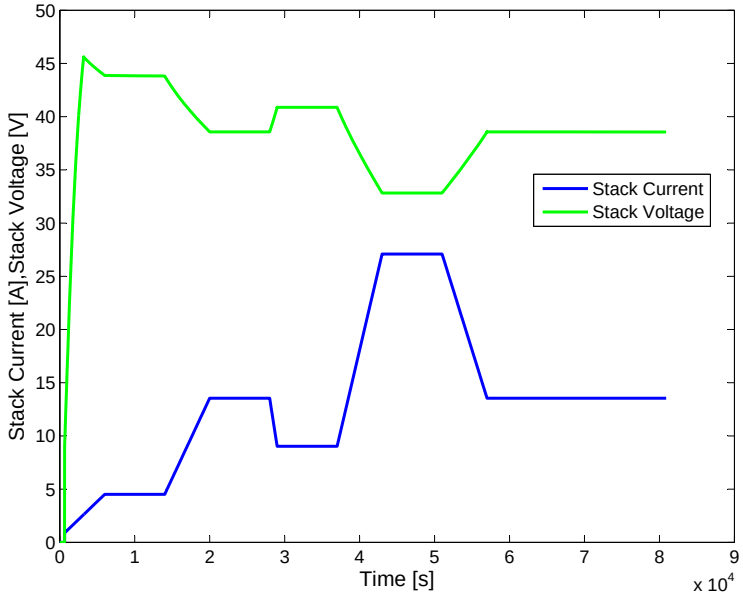

Figure 5.17: Simulated fuel cell stack current and voltage of reformer system.

During the shown loading simulation, the system is allowed to switch between different operating modes in order to avoid singularities in the system equations. These two modes are operating mode and start-up mode. Because a current is not to be drawn until the stack temperature is within reasonable temperature ranges. Figure 5.17 also shows that the step changes made in the current is limited to change load states in at maximum of 500 seconds. The dynamics of the temperatures in parts of the system during operation is shown in figure 5.18.

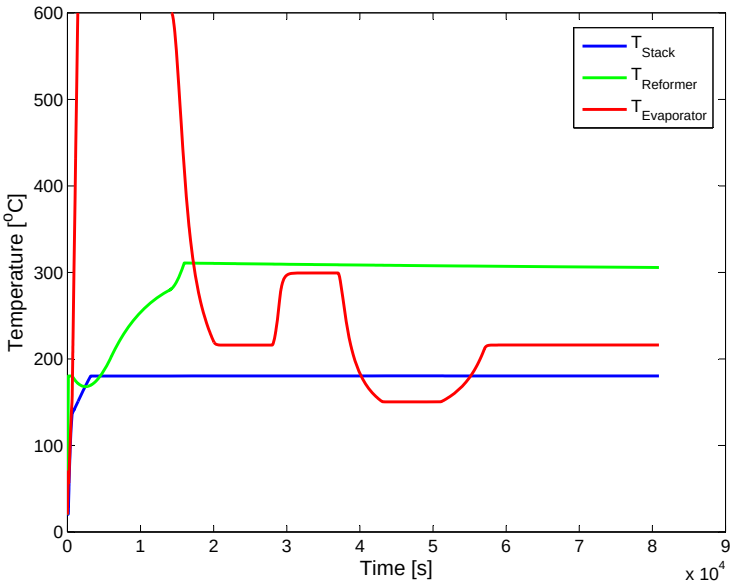

Figure 5.18: System temperatures during simulation using constant 300 W electrical power input to evaporator.

It is seen that the fuel cell stack and reformer temperatures are properly controlled, but that the reformer, only slowly reaches the set point temperature of 320^{o}C. The fuel cell stack reaches the set point temperature of 180^{o}C much fast due to the lower temperatures. The high temperatures of the stack is in this case chosen because the system is running on gas with a CO content. The evaporator temperature is initially very high, because 300W of constant electric power is input to the system from the starting point to ensure constant evaporation of the fuel. Very large temperature gradients are seen in the initial time steps due to the low thermal mass of the evaporator and the surplus of heat input. Figure 5.19 shows the different power levels present in the system in the duration of the simulation. During the initial part of the load pattern,

the current is low, and the fuel cell efficiency is high, which decreases the losses, and hereby the heat removed in the fuel cell stack. Because this heat is used to evaporate the methanol and water mixture, and the temperatures in this case are below the evaporator temperature, convective cooling is actually occurring at the evaporator. A rising evaporator temperature is only possible due to a constant 300W electrical power input. Only at higher current loads will the evaporator be heated by the stack cathode exhaust air.

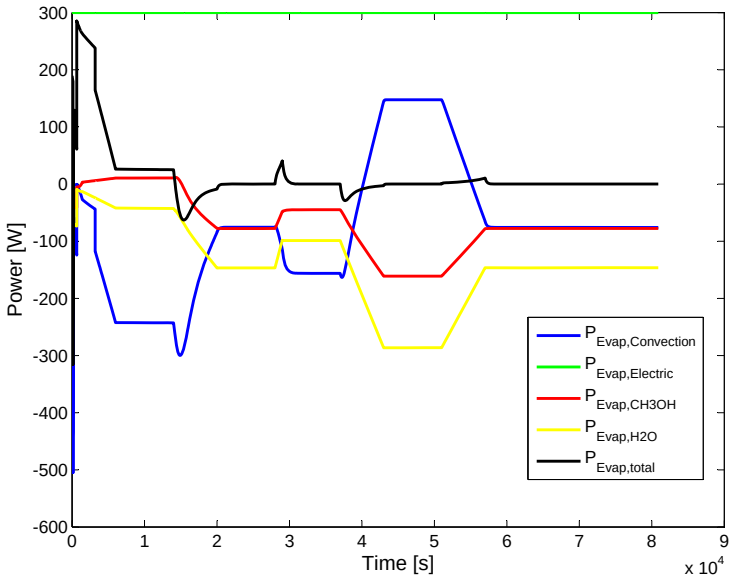

Figure 5.19: General power levels in the evaporator using 300 W electrical power input.

The critically high temperatures of the evaporator during the initial phases of the system simulation of the load pattern, are not acceptable. Furthermore all use of electrical power will give additional parasitic losses which will lower the system efficiency significantly. Implementing a controlled electrical power source to the evaporator can improve this strategy of operation, and avoid high temperatures as shown in figure 5.20.

Figure 5.20 shows that the 300 W initial heating is only needed initially to evaporate the methanol used in the heating process. After this heating, the system will gradually start to generate hydrogen, which can be used in the fuel cell and add heat by convection instead. Here the electrical heating power can be turned down, and the system is supplied primarily by the heat losses from the fuel cell. It is also seen that the evaporator generally needs more power than can be input from the convective heat

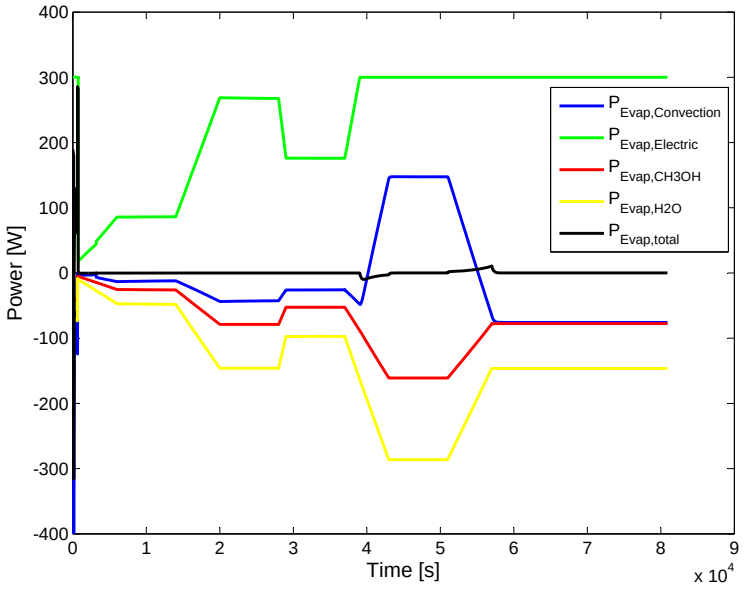

Figure 5.20: General power levels in the evaporator using a controlled 300W power source.

added. Additional heat for the evaporation must be supplied other than the heat available from the fuel cell stack. The resulting system temperatures from this controlled electrical heating strategy are shown in figure 5.21.

During the operating conditions using the controlled electrical evaporator strategy, the gas composition of the reformate before the water-gas-shift is shown in figure 5.22. It is seen that the gas composition is kept quite constant after the initial reformer warm up procedure with approximately 64% H_2, 19% CO_2 14% H_2 and 5%CO. From 0 to 18000s it is seen that the gas composition indeed is quite dependent on the reformer temperature.

The water-gas-shift is in this simulation simplified to assume a conversion of 80% of the molar flow of CO to hydrogen. This yields an expected CO concentration of around 0.8 % into the fuel cell stack.

The efficiency of the different operating procedures described are presented in figure 5.23. The fuel cell efficiency η_{FC}, is the ratio between the fuel cell stack electrical output power and the input power available as heating value of methanol (based on the HHV of methanol). The efficiency is varying at the highest value of 44 % at ≈0.04 A/cm^2, to 32 % at 0.6 A/cm^2.

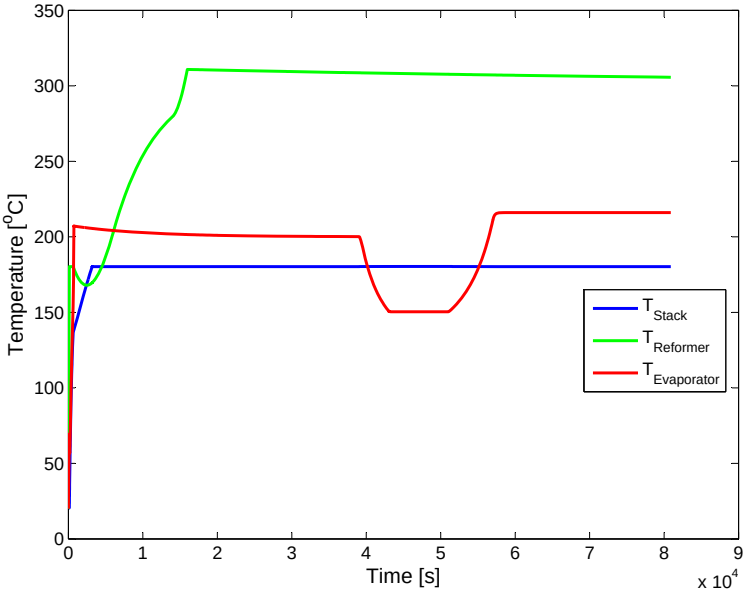

Figure 5.21: System temperatures during simulation using controlled electrical power input to evaporator.

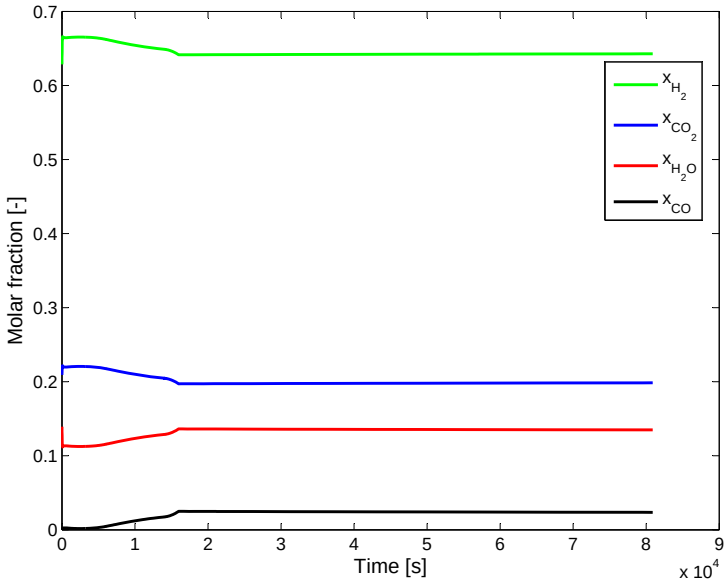

Figure 5.22: Gas composition of reformate during simulation before water-gas-shift.

Because of the extra heat needed to evaporate the methanol and water mixture, and other parasitic losses, will lower the system efficiency further. $\eta_{System,300Wevap.heat}$ is

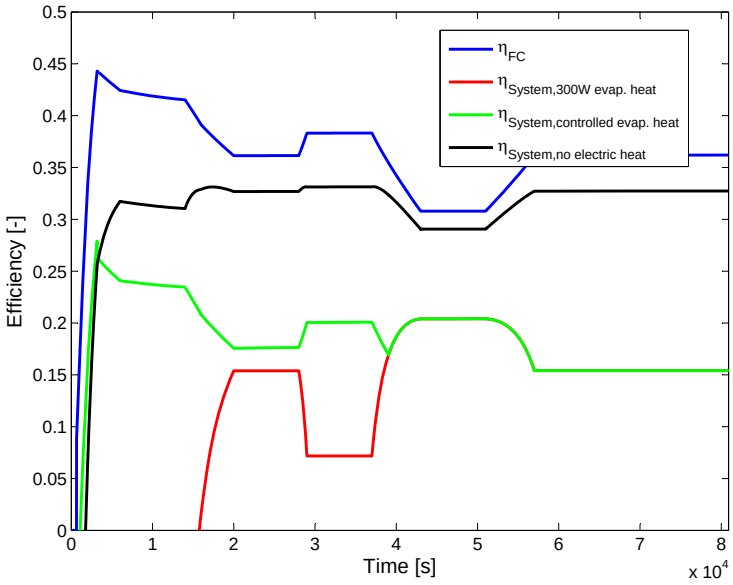

Figure 5.23: Efficiency of different presented operating strategies.

the system efficiency using ratio between the electrical fuel cell output and the methanol power input, subtracting an the additional 300W heat for evaporation from the generated fuel cell power. This strategy renders the system with a significantly poorer efficiency, even with operating points during the load pattern, where the system uses more power than it produces. Using a controlled electrical power input as explained earlier increases the efficiency significantly in some areas, but still only reaches about 15% during the final current load of 0.3 A/cm^2. The effect of controlling this supplemental evaporation power is seen for $\eta_{System,controlledevap.heat}$. Maximizing the efficiency could be done by using some of the many mentioned hot sources in the system, this is shown as $\eta_{System,noelectricalheat}$, where the system is assumed self sufficient in evaporation heat, and with parasitic losses of 50W.

5.3 Theoretical maximum efficiency

In order to compare the methanol reformer based fuel cell system with a system running on pure hydrogen, and to evaluate the possibilities of better heat integration of the hot and cold gas streams, an analysis is conducted using an energy balance of the system, and a pinch analysis is performed to ensure that the second law of thermodynamics is not

violated [36]. The energy balance is used to find the minimum hydrogen stoichiometry λ_{H_2}, that is required to support the reforming process and the pinch analysis is used to evaluate the temperature levels and energy available in the different gas streams. Moreover the possibilities of implementing heat exchangers to utilize unused energy in the system can be evaluated. The system efficiency is calculated at ideal reforming conditions, with the following assumptions:

- Steam-to-carbon ratio of 1.
- Full conversion of CO, witch yields a reformate gas composition of 75% H_2 and 25% CO_2.
- Stack performance is not influenced by λ_{H_2}.
- If the reformer temperature is higher than the stack temperature, additional superheating is done by increasing λ_{H_2}.

If assuming a reformer temperature of $T_{reformer} = 250^oC$, a stack temperature of $T_{FC} = 160^oC$, and an ambient temperature of $T_{amb} = 20^oC$, the primary flows to and from the different system components are shown in figure 5.24.

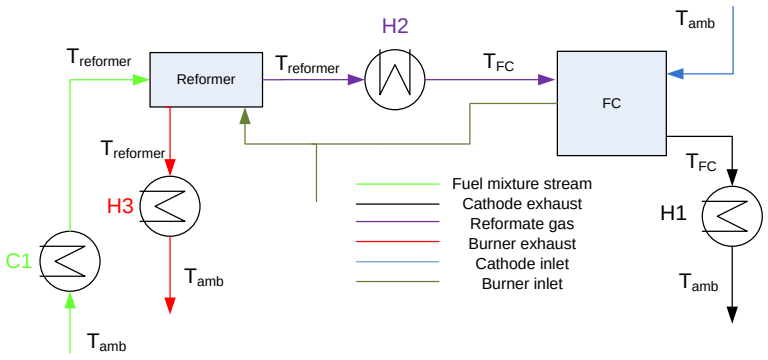

Figure 5.24: Overview of hot and cold gas flows in the methanol reformer system.

In figure 5.24 the only cold gas stream present, i.e. the only gas stream that needs heating, is the methanol/water mixture. This stream is labeled C1, and is to be heated from ambient temperature to reformer temperature. The three hot gas streams are noted as H1, H2 and H3 in figure 5.24. H1 is the primary heat source available, the hot cathode exhaust air. H2 is the heat available in the reformate gas stream if the reformer

temperature is higher than the fuel cell stack temperature. H3 is the gas stream exiting the burner assumed to be at the reformer temperature. All gas streams are assumed to be adjusted to the temperature of the component they are entering or exiting.

The anode stoichiometry λ_{H_2} plays an important part in the efficiency of the system, and in the ideal case described here, it is a constant value independent of fuel cell stack current density. This is shown in equation 5.12, calculating the anode stoichiometry by using the required hydrogen flow for the fuel cell $\dot{n}_{FC,H_2}$ and the required hydrogen flow exiting the fuel cell stack to the burner $\dot{n}_{Burner,H_2}$.

$$\lambda_{H_2} = \frac{\dot{n}_{FC,H_2} + \dot{n}_{Burner,H_2}}{\dot{n}_{FC,H_2}} \tag{5.12}$$

Inserting the equivalent molar flow of methanol required to sustain the reforming process yields the following expression for the stoichiometry of the anode gas:

$$\lambda_{H_2} = \frac{\frac{In}{2F} + \frac{49.5[kJ/mol]}{LHV_{H_2}}\dot{n}_{CH_3OH}}{\frac{In}{2F}} \tag{5.13}$$

$$\begin{aligned}
\lambda_{H_2} &= \frac{\frac{In}{2F} + \frac{49.5[kJ/mol]}{LHV_{H_2}}\dot{n}_{CH_3OH}}{\frac{In}{2F}} \\
&= \frac{\frac{In}{2F} + \frac{49.5[kJ/mol]}{LHV_{H_2}}\frac{In}{6F}}{\frac{In}{2F}} \\
&= \frac{\frac{In}{2F} + \frac{49.5[kJ/mol]}{LHV_{H_2}}\frac{In}{6F}}{\frac{In}{2F}} \\
&= \frac{3 \cdot LHV_{H_2} + 49.5[kJ/mol]}{3 \cdot LHV_{H_2}} = \frac{3 \cdot 242[kJ/mol] + 49.5[kJ/mol]}{3 \cdot 242[kJ/mol]} \\
&= 1.068
\end{aligned} \tag{5.14}$$

In the situation where $T_{reformer}$ is larger than T_{FC}, the cathode air will not be able to super heat the fuel and water mixture to reformer temperatures. In that case, heat exchanging with the reformate gas might be feasible. In the case where $T_{reformer}$ is equal to T_{FC}, it is also possible to supply the reformer heat from the cathode air removing the need for burning hydrogen. A Sankey diagram of the system running at a current density of 0.6 A/cm^2 where the reformer temperature is 250^{o}C and the fuel cell stack temperature is 160^{o}C is shown in figure 5.25.

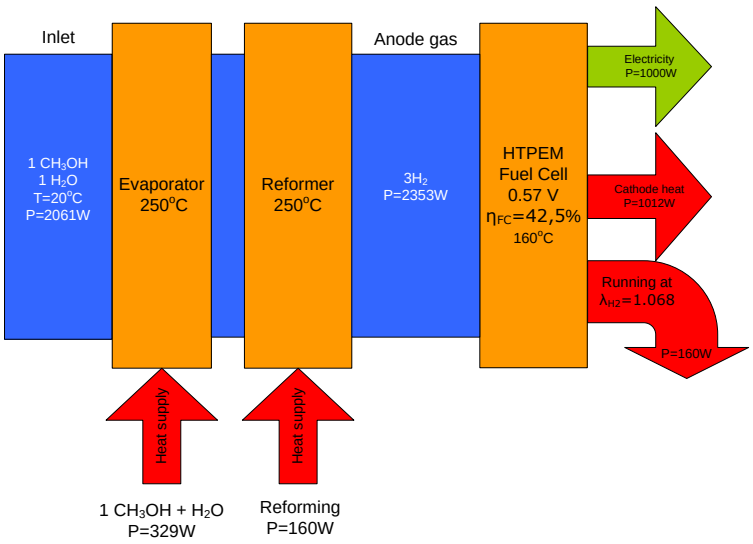

Figure 5.25: Sankey diagram with an overview of power and efficiency available in fuel cell methanol reformer system. LHV is used in calculations.

In the Sankey diagram, the power distribution is seen throughout the system, at a constant current production of ≈0.6 A/cm^2. It is seen that the energy demand for the system is for preheating, evaporation and superheating of the fuel flow. At this particular current density, the available power in the cathode exhaust air is more than enough to support the heating and evaporation process. The Sankey diagram only shows the available energy for one operating point. As stated earlier, varying the current density, reformer temperature and fuel cell temperature changes the power available and needed in the different gas streams. Using the energy balance, a minimum fuel cell stack current density can be found, i.e. the point where the heat produced by the cathode exhaust air is the same as the heat needed to heat and evaporate the fuel mixture. The system will not be able to run at current densities below this value without increasing λ_{H_2}, because the heat generated in the fuel cell is not able to heat the incoming fuel flow. Figure 5.26 shows the powers available in the system as a function of current density, and at different reformer and fuel cell temperatures.

Two cases are chosen, one case where $T_{reformer} = 250^oC$ and $T_{FC} = 160^oC$ and then another where $T_{reformer} = 200^oC$ and $T_{FC} = 180^oC$, to analyze the impact of changing the temperatures. When changing the reformer temperature, changes are also experienced in power requirement for the superheating of the fuel/water mixture. The

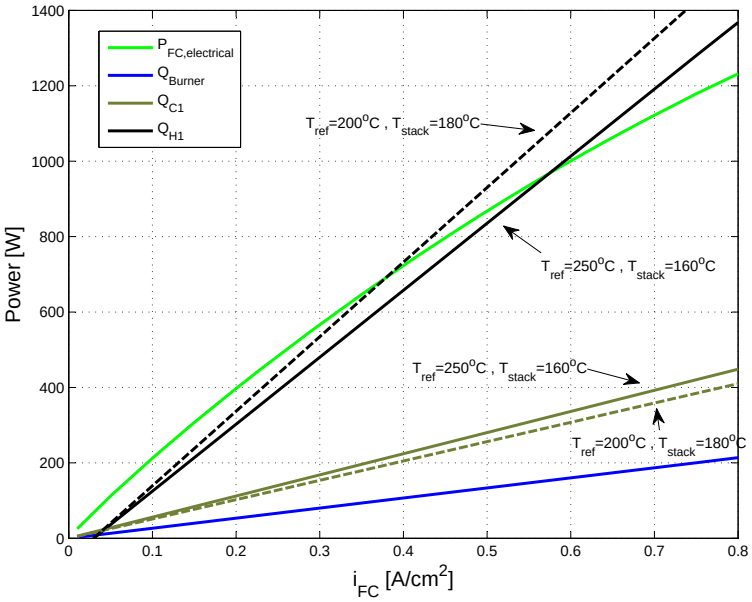

Figure 5.26: Power available and required in the system as a function of current density. (-) are lines at $T_{reformer} = 250^o$C and $T_{FC} = 160^o$C and (- -) are lines at $T_{reformer} = 200^o$C and $T_{FC} = 180^o$C.

largest difference between the two cases exist in the power required to superheat the fuel/water mixture, it is slightly increased in the first case. In the first case, the output cathode air temperature is lower and therefore the minimum current density will be smaller than the other case where more power is available for heating and evaporation. The changes experienced in the burner exhaust stream (H3) and the reformate gas stream (H2) are negligible compared to the other gas streams. The hydrogen fuel cell anode stoichiometry λ_{H_2} also includes a calculation of the additional superheating of the fuel flow mixture, in the situations where the fuel cell temperature, and hereby the cathode air exhaust is lower than the reformer temperature. Figure 5.27 visualizes the minimum fuel cell stack current density $i_{FC,min}$, i.e. the current density at which the system is self sufficient as a function of T_{FC} at different reformer temperatures.

From the figure it is clear that the self sufficient point of operation decreases with increasing temperatures of the reformer and decreasing fuel cell stack temperature. Super heating the fuel and water mixture from stack temperature to reformer temperature at i_{min} without using burning excess hydrogen, i.e. running the fuel cell at λ_{H_2}, would require using a heat exchanger either at H_2 or H_3. From an energy balance point of

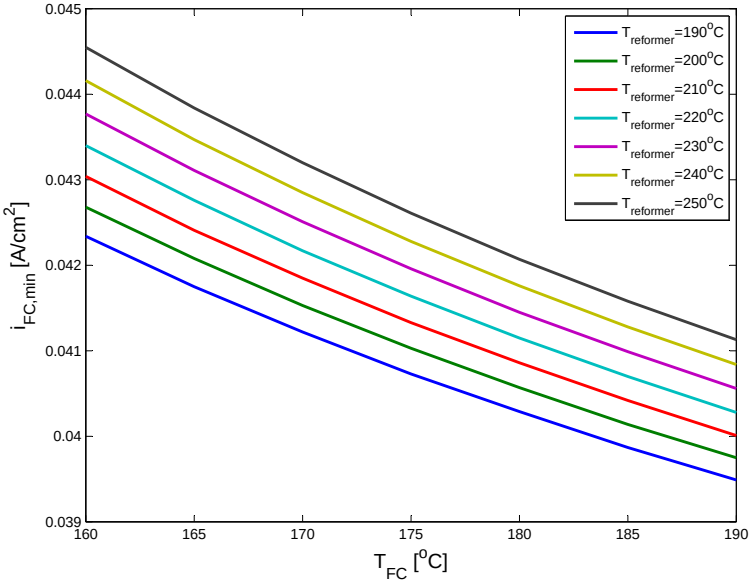

Figure 5.27: Self sufficient current density as a function of temperature, with constant T_{FC}.

view, although it may require an unrealistically large heat transfer surface area, this is possible, and illustrated by figure 5.28.

$Q_{Superheat,C1,FC->reformer}$ is the power required to heat the input methanol and water mixture from T_{FC} to $T_{reformer}$, $Q_{H_3,ref->FC}$ is the power in the exhaust burner gas when cooling it from $T_{reformer}$ to T_{FC}, $Q_{H_2,ref->FC}$ is the power in the reformate gas when cooling it from $T_{reformer}$ to T_{FC} and $Q_{H_2+H_3}$ is the sum of $Q_{H_2,ref->FC}$ and $Q_{H_3,ref->FC}$. The figure reveals that it is possible to run the system at λ_{H_2}=1, by using the heat available in e.g. the cooling of the reformate gas to stack temperature to superheat the methanol and water mixture from stack temperature to reformer temperature. In a practical system it is not feasible to run a fuel cell stack at λ_{H_2}=1, in addition the required heat exchanger could be problematic because of the requirement of very large heat surfaces. From a thermodynamic point of view the heat is available in the system to run at λ_{H_2}.

5.3.1 Pinch analysis

In many cases thermal systems can have potentially large energy content in e.g. a hot gas stream, like the cathode air exhaust. However, it must also be ensured that a

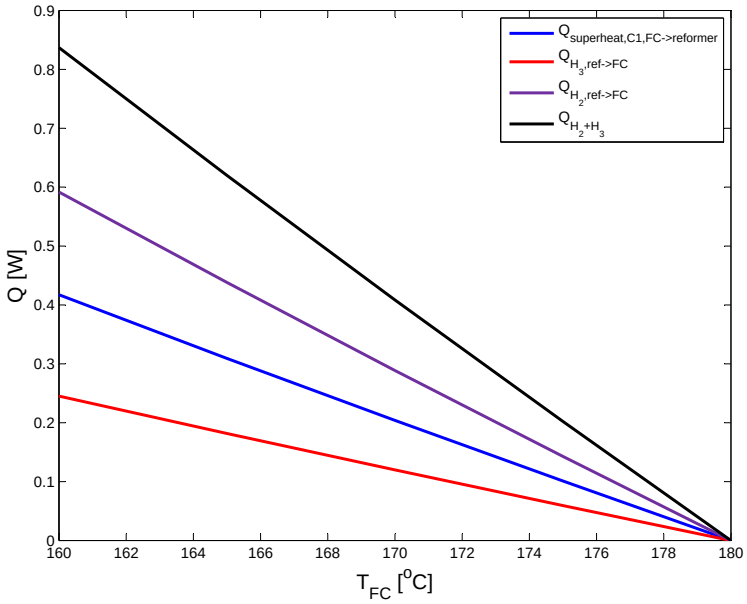

Figure 5.28: Available power and power demand in gas streams at i =0.6 A/cm^2 as a function of T_{FC} at $T_{reformer} = 180$.

sufficient ΔT is available in the heat exchangers to transfer heat from the hot stream to the cold. In order to ensure this, a pinch analysis is carried out and the resulting composite curve is shown in figure 5.29 for the gas streams shown in figure 5.24.

As long as the composite curves for the hot and cold streams do not cross, the second law of thermodynamics is not violated. A minimum temperature difference ΔT_{min} between heat exchanged streams of 30 degrees is assumed realistic in the implemented heat exchangers. The distance between the starting points of the hot and cold composite curves is the required cooling power,usually supplied by a utility. This large cooling amount is only required if the cathode air is desired to have a temperature of T_{amb}, when exiting the system. The cathode exhaust air has in this analysis only been used to support the preheating, evaporation and superheating of the methanol and water mixture. Additional available energy available in the cathode air is assumed not to be used elsewhere because of the lowered temperatures after exiting the evaporator. The only place in the system where cooling is necessary is the cooling of the reformate gas to fuel cell stack temperature. The top horizontal distance between the two composite curves shows the heating requirement in the system by an external source. This is the

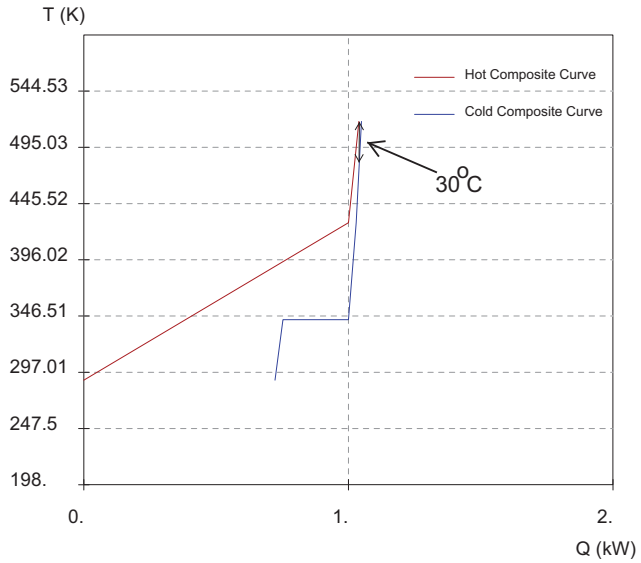

Figure 5.29: Composite curve for ideal methanol reformer fuel cell system using ΔT_{min} of 30^{o}C, at a fuel cell stack power production of $P_{FC,electrical}$=1000W.

heat required for raising temperatures above the fuel cell stack temperature, i.e. the superheating of the fuel stream once evaporated. From a practical point of view the best way to supply this heat could be by burning additional hydrogen by increasing λ_{H_2}. In figure 5.28 it is shown that implementing heat exchanges in e.g. the anode gas stream could be used for superheating, but depending on ΔT_{min} it is unlikely that it will be an practical solution. In systems where the temperature difference between stack and the reformer is larger, implementing heat exchangers in the anode or burner exhaust may be a feasible. ΔT_{min} will directly affect the value of i_{min} and thereby the turn-down ratio of the system.

5.3.2 Reformer system efficiency

The efficiency for the ideal system running on methanol, i.e. the ratio between the electricity produced and the lower heating value of the input methanol can be seen in figure 5.30. The figure also shows the efficiency of a similar pure hydrogen fed system.

The figure shows that the methanol reformer system and the pure hydrogen fed system have comparable efficiencies. In the idealized case shown, the methanol reformer system has a higher efficiency. This is primarily due to the fact that in the pure hydrogen

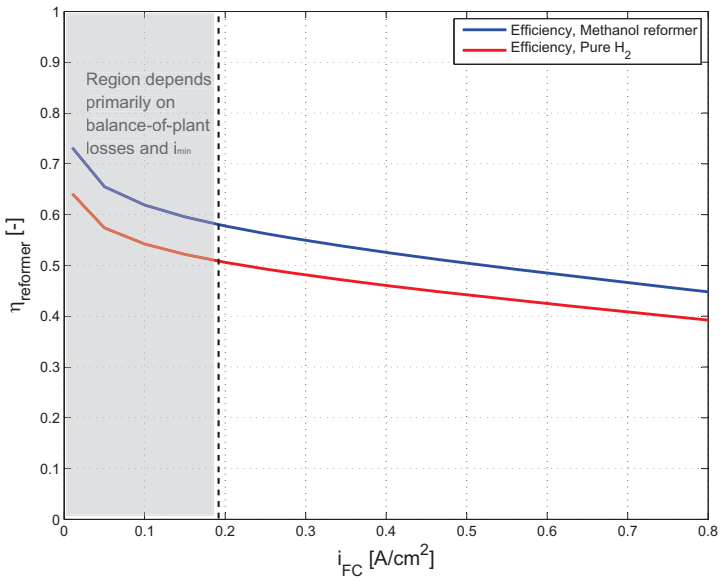

Figure 5.30: Electrical fuel cell system efficiency of methanol reformer system, and hydrogen fuelled system as a function of current density using LHV in both cases.

fed system, the energy available as heat in the exhaust cathode air remains unused, while in the methanol reformer system, some of the heat output assist the reforming process and evaporation of the fuel/water mixture. The efficiencies do not take into consideration the losses related to the system balance-of-plant, such as blowers, pumps etc. These losses are assumed to be larger for the methanol reformer system, and will (also for the hydrogen system) especially affect the efficiency at low current densities (see Paper A.3, Fig. 7 for example). The efficiency of the methanol reformer system will also for a practical system drop further because of higher CO content in the anode gas, but for practical systems the efficiencies of the two types of systems are considered comparable.

Using a methanol reformer system complicates the fuel cell system by adding a chemical reactor and the controls for this additional component, but the great advantage is that a liquid, non-exotic fuel can be used, which solves many practical issues both relating to fuel storage and distribution. Further studies however, are required to integrate the heat exchangers that are needed for a real system to operate.

5.4 Discussion

Although many assumptions exist in order to simplify the system enough for fast simulation time and controller development, the different time constants in the system are visible and show that the discussed control strategy for the system is a feasible, and effective means of operating the system. The primary drawbacks of this strategy is that a good reformer temperature control can be achieved even if too much fuel is burned, by controlling the reformer temperature by adding more air to the process and hereby remove heat convectively. This is an undesirable situation because the hydrogen flow exiting the fuel cell stack is too large, and the system efficiency will be significantly decreased.

The gain $K_{estimator}$ is in the shown simulations chosen as a constant value, but in order to make the system more robust to temperature changes, it could be implemented as a function of reformer temperature and steam-to-carbon ratio. A model based approach could also add the benefit of predicting the reformer output gas composition and give a more precise prediction of the needed methanol input flow to the system.

Heating of the reformer could be improved by adding air to the reforming process initially and hereby running the reformer autothermally. The smaller requirement for process heat will result in a faster reformer start-up. The start-up procedure of the system needs further testing to verify the possibility of using the evaporated methanol and water mixture directly in the burner. Alternatives are using a separate pure methanol supply if available or pressurized gaseous buffer storage captured during operation. Separating the water and methanol could also yield new methods of optimizing the efficiency online, by controlling the steam-to-carbon ratio.

Knowing the time constants in the system is important in order to dimension proper control parameters if long life time of both the fuel cell and reformer is desired. Proper control of the system during load changes and transients is also important to benefit from the advantageous part load abilities of the fuel cells. Using the current load pattern in figure 5.17 with step load changes and a slow reformer temperature control shows the importance of knowing these time constants. A new simulation of the temperatures of the system with this new load pattern is shown in figure 5.31.

Figure 5.31 shows that the slow dynamic abilities of the reformer temperature controller makes it overshoot at one of the initial load steps. Because of the methanol

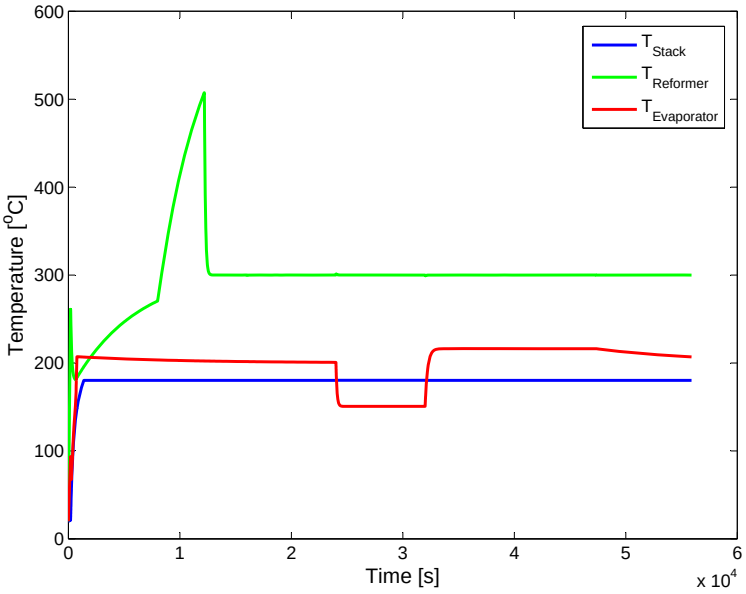

Figure 5.31: Reformer system temperature simulation using non-ramp limited step loads and poor reformer temperature control.

conversion temperature dependence, the gas composition is also affected by this overshoot, which is visible in figure 5.32.

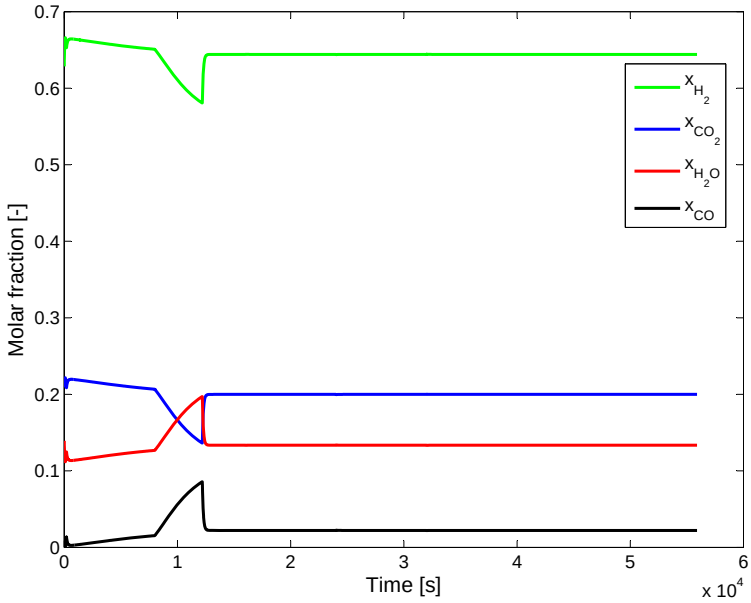

Figure 5.32: Gas composition before water-gas-shift during poor temperature control.

The CO concentration in the gas composition before the water-gas-shift makes a small step from about 1% to 8%. Because of the importance of the CO concentration it is important knowing the dynamics of the system and designing proper controllers to avoid such problems. Analysis of a reformer system using a different type of catalyst has also shown similar problems in simulations during load changes [4]. Figure 5.33 shows the CO dynamics during a load step down in the methanol and water mixture.

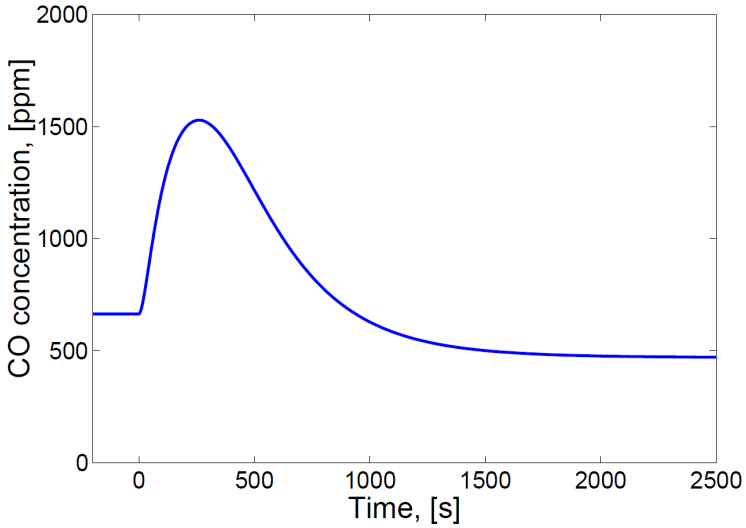

Figure 5.33: Simulation of CO concentration of methanol reformer during feed flow rate step change to a lower value[4].

The spike in the CO is around three time larger than the steady-state values, which could prove problematic in situations and systems with higher CO output concentrations and a fuel cell stack operating in a start-up situation, where some fuel cells may have low temperatures.

The CO concentration of the fuel entering the stack is one of the most important states in a reformer system, and measuring it on-line in real systems is too expensive and therefore it is important to be able to predict it in other ways. A promising tool for analyzing fuel cell behaviour both for single cells, and stacks is electrochemical impedance spectroscopy (EIS). The use of EIS as explained in Paper A.2 could prove important to diagnose fuel cell stack behaviour during operation with reformate gas. The stack impedance behaves differently when operating with CO in the anode gas and EIS might be a useful tool for predicting e.g. CO concentrations.

The system steam-to-carbon ratio of the experimental system is around 1 to 5 in the shown simulations. But further system optimization could be carried out to improve this value. The optimal steam-to-carbon ratio for the system has not been found, and this particular parameter is important for the system efficiency, because the evaporator uses much more power when increasing amounts of water are in the fuel flow mixture. By integrating more of the hot flow streams with the evaporator, such as cooler air flow, water-gas-shift cooling and burner exhaust, the power delivered by the electrical heating in the evaporator can be minimized. Using the system in applications able to utilize some of the excess heat would also improve the overall efficiency.

The use of the equilibrium model to calculate the gas composition does not give the full picture of the exact behaviour of the reformer, because the water-gas-shift happening on the catalyst activates properly at quite high temperatures, and will not increase with the temperature, as the equilibrium model predicts. Instead the CO content will actually decrease with increasing temperature for a period, as illustrated in figure 5.34.

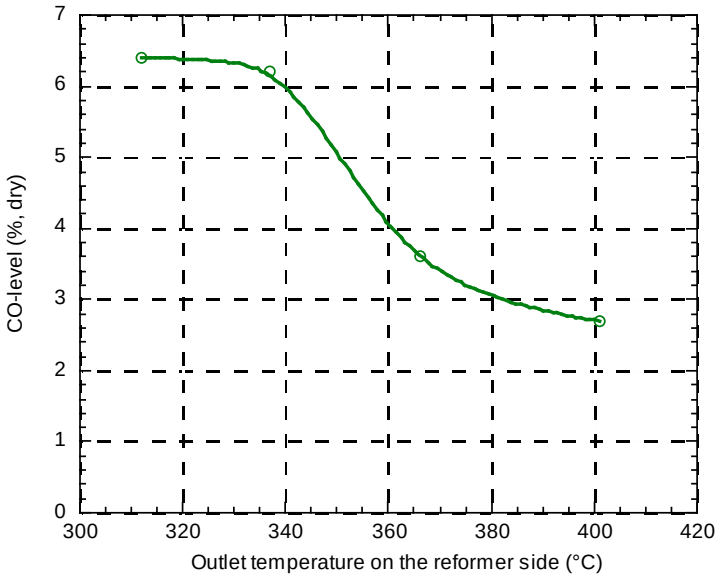

Figure 5.34: Water-gas-shift activity activates at temperature above 350°C, decreasing the CO content of the reformate gas.

An overall lowering of the reformer temperature could improve the efficiency and make a better temperature match between the reformer and fuel cell stack; it would also

possibly simplify the system, not needing cooling of the anode gas before entering the fuel cell stack. Future work will explore the use of reforming catalysts that are active at lower temperatures and steam-to-carbon ratios and the heat integration of the system.

6

Fuel cell system implementation

The transport sector has been identified as a large contributor to particle emissions, CO_2 and other green house gas emissions [31]. Using battery electric vehicle (BEV) or fuel cell electric vehicles (FCEV) can potentially reduce the dependence on fossil fuels, and can be an integrated part of renewable energy systems. Combining the two vehicle types into a fuel cell hybrid electrical vehicle (FCHEV) is often interesting in order to minimize some of the disadvantages of using a purely battery powered system, where the vehicle driving range often is limited. Fuel cell systems have been implemented in the following two electrical vehicle applications, where their performance has been tested:

- Hywet electrical H_2 car
- GMR utility truck

The Hywet is a small hydrogen powered electrical car produced in Norway (originally named the Kewet or Buddy). This car is an urban transport vehicle and carries up to 3 people and has a maximum speed of 80 km/hr. Another line of vehicles where electricity generation using fuel cells can be beneficial, are utility trucks. The company GMR Maskiner A/S produces such trucks which are used in many different places, in gardening associations or different industrial facilities as a means of transportation of tools, personnel and different payloads up to 1000 kg. Each of the fuel cell systems implemented in these two applications will be presented in the following together with a test of their performance.

6.1 Series connection of HTPEM stacks for a fuel cell electric hybrid vehicle

The Hywet was developed to test the performance of a series connection of the before mentioned 1kW HTPEM fuel cell stacks, and also to test the direct connection of such a configuration of fuel cell stacks to a Li-ion battery pack. The Hywet is shown in figure 6.1, and is an example of a small FCHEV.

Figure 6.1: Picture of the Hywet

The original Norwegian electric car, the El-jet Buddy, was initially powered by a 72V lead acid battery bus consisting of 2x6 series connected 12V 182Ah batteries. The batteries power a 13kW separately excited DC motor through a Curtis 1244 DC motor controller. A new 13kWh Li-ion battery pack and 4kW fuel cell system has been introduced to evaluate the performance of this new hybrid system, also described in Paper A.3.

As also explained in section 6.2, there are many ways of configuring a hybrid electrical system for a mobile unit. The system implemented in the Hywet shows one of the simplest ways of connecting a hybrid battery/fuel cell system, i.e. a direct connection

using no power electronics. The main disadvantages of using such a solution is that the current drawn from the fuel cell is determined by the battery pack impedance, and cannot be limited to a specific operating point of the fuel cell stacks. Figure 6.2 shows the principle of the direct connection of the fuel cell stacks onto the battery pack.

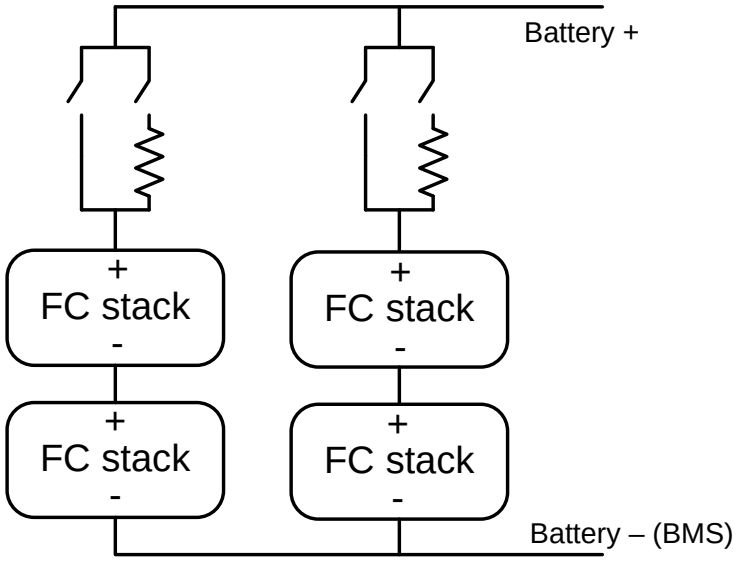

Figure 6.2: Fuel cell stack and battery connection principle.

The stacks are arranged such that two branches of series connected stacks connected directly to the battery pack through a series of relays. To avoid large current peaks, in the case of a battery pack with a very low state-of-charge, the fuel cell stack connection is initially made through a power resistor which limits the current in order to protect the fuel cell stack. After current stabilization, the resistors are bypassed, and the stacks are directly connected to the batteries. During operation, the state-of-charge of the batteries determines the voltage of the fuel cell stacks and hereby the charging current. This way of operating the system efficiently, is only possible because the battery and fuel cell stack voltages are very similar. The fuel cell system is in this case operated with pure compressed hydrogen stored in two bottles in the rear end of the car. The disadvantages of using hydrogen, as also seen in figure 6.3, is that large storage volumes are required.

With two 20L bottles of 250 bar, the energy available in the hydrogen is approximately 27kWh. This is enough energy to fully charge the battery pack about one time

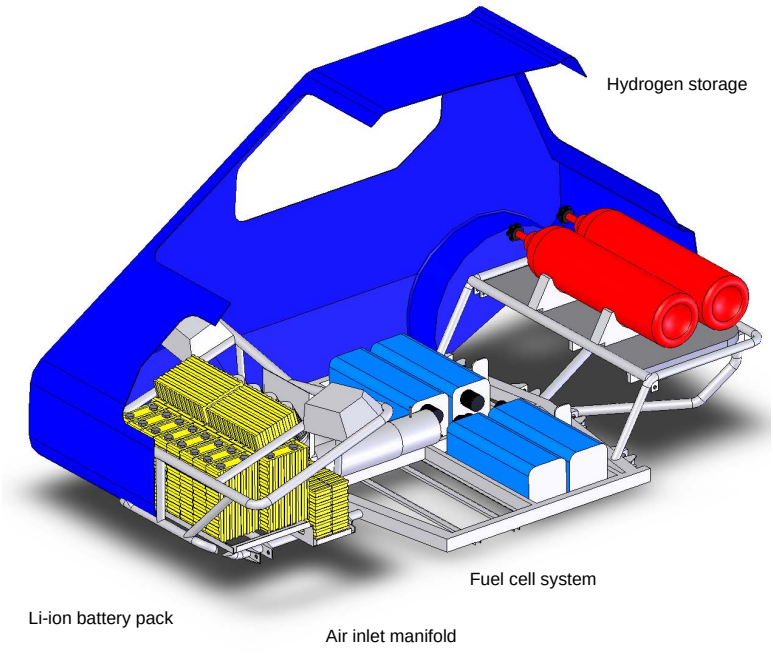

Figure 6.3: 3D image of Hywet where primary system components are visible

using the fuel cells. For general use in automotive vehicles a liquid fuel is preferred in order to increase the volumetric density of the energy stored and to use the existing fuel distribution system.

6.1.1 Hywet system operation

As also stated in A.3, and chapter 4 one of the disadvantages of using high temperature fuel cell systems is that some applications require fast start-up times, and it can take a while to reach the required operating temperatures. When using a car, the driver needs to be able to drive immediately when turning the key. Because of this, the battery pack needs to supply the traction power while the fuel cell system is heating. The balance between the size of the battery pack and the fuel cell system needs to match the general way that the car is used. Generally a cars spends a lot of time parked, which could be utilized e.g. for charging using an external electric source, or an on-board fuel cell system. Another way of ensuring that the fuel cell system is always ready to generate power is to keep it hot. With properly insulated fuel cells, this might prove more energy efficient than repeated heating and cooling in periods where the car is used frequently.

Figure 6.4 shows a graph of the fuel cell stack temperature during the cool down phase of a stack, from around 120^{o}C.

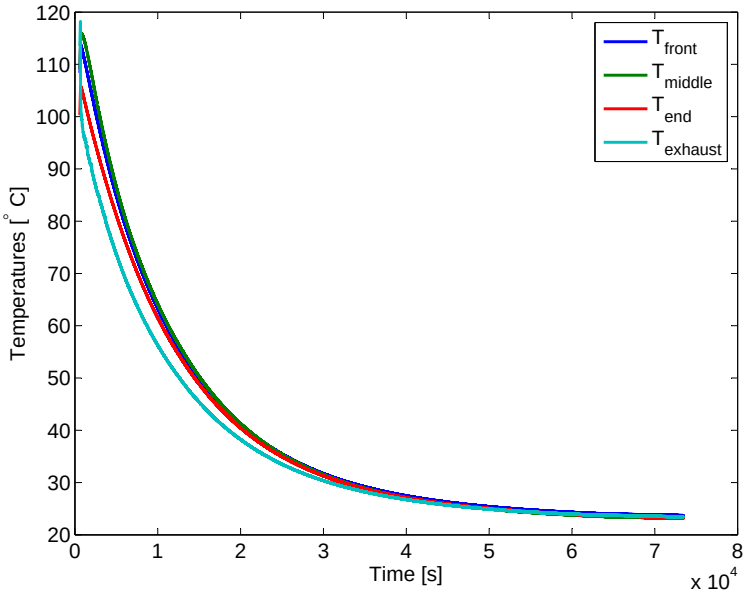

Figure 6.4: Stack temperatures as a function of time when passively cooling.

The temperature falls below 50^{o}C after 15000s, which is around 4 hours. After 15 hours, the stack has reached ambient temperature. As mentioned before, determining the right heating strategy for heating such a stack, is one of the key factors when using fuel cells operating at high temperatures. Keeping the stack at hot standby could be a solution for some systems, while others should include start-up and shutdown sequences.

6.1.2 System performance

The Hywet fuel cell system operation can be divided into two categories, stationary and dynamic charging. These different modes of operation are explained in Paper A.3, and an example of stationary charging is shown in figure 6.5, where the battery pack voltage is seen together with the stack current and voltages of one branch of the system.

In the figure, the fuel cell stacks have just ended their heating procedure, and at 400s, hydrogen and air is introduced to the stacks, and they are connected directly to the battery bus. The initial small drop in battery voltage is due to the battery pack supplying part of the power required for some of the balance-of-plant of the fuel cell system. Following the connection of the two series connected fuel cell stacks, the fuel

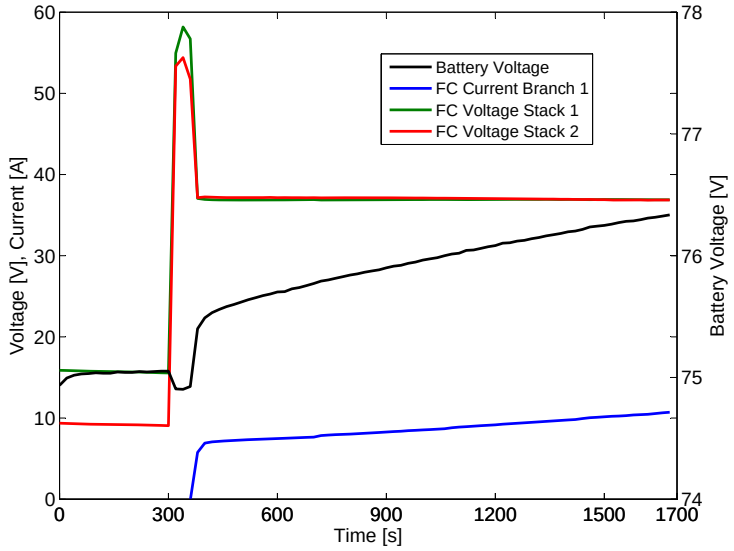

Figure 6.5: Fuel cell and battery system performance during stationary charging.

cell stack current jumps to about 7A, and the battery voltage starts climbing as the batteries are charged. The reason for the constant climb in fuel cell current is primarily due to changes in the fuel cell temperatures, which are presented in figure 6.6.

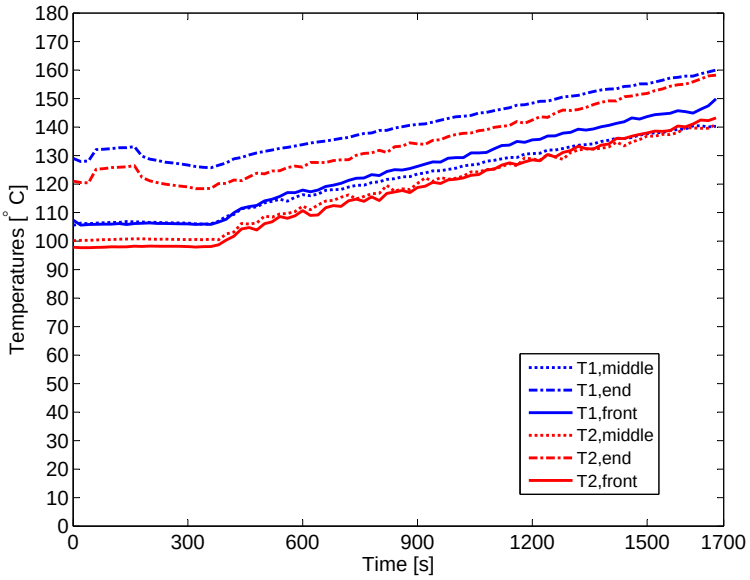

Figure 6.6: Temperatures of the fuel cell stacks in branch 1 during stationary charging.

The temperatures of the fuel cell stacks start at an average temperature of around

110^{o}C and start climbing as soon as the fuel cell starts charging the battery pack. With the fuel cell stack voltage fixed at the battery voltage, the higher temperatures will increase the performance of the fuel cells, and enable them to produce more current at the same voltage. The primary advantages of the Hywet fuel cell system are the very simple connection of the fuel cell system and the battery pack, a longer runtime of the car, and solving the problem of using a long time for recharging. The system operation is not limited to stationary charging, but also hybrid operation, where the fuel cell supply part of the power for acceleration during driving. The disadvantages include not having power electronics to control the operating point of the fuel cells. Fixing the fuel cell stacks at the battery voltage does not allow charging at high power if needed, which means, that the voltages of the battery pack and fuel cell stacks must match according to the desired charging current.

6.2 GMR utility truck fuel cell system

In the GMR truck, a new electrical power traction system has been developed, and a 1 kW HTPEM fuel cell system has been implemented to deliver electric power to the vehicle power system. Figure 6.7 shows the small utility vehicle and the different main parts of the power system.

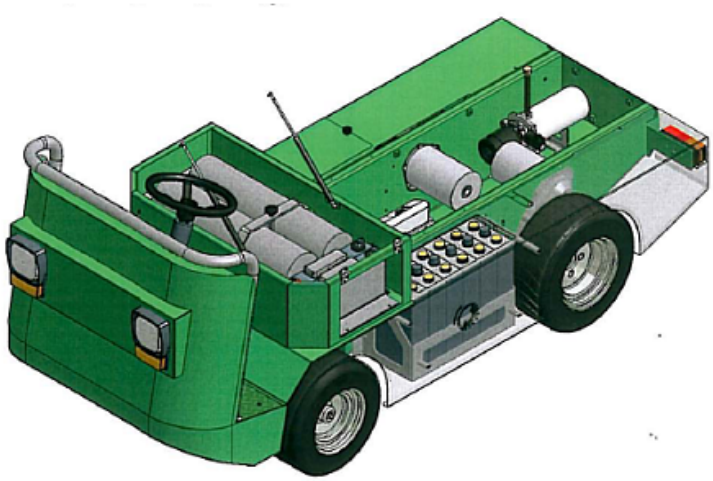

Figure 6.7: Stama utility truck from GMR Maskiner A/S

The original power supply consists of six 6V 185Ah tubular flooded lead acid batteries, series connected to at 36V DC battery pack of 180kg. A Curtis 1244 motor con-

troller controls the two separately excited 2 kW DC machines, with the field windings connected in series and the rotor windings in parallel. The new power system consists of a 1 kW HTPEM fuel cell stack, an Exide Sonnenschein A512/40A, 48V, 40Ah sealed lead acid battery pack, and four 500F Maxwell BMOD Energy super capacitors. The traction power of the vehicle is delivered by two 3 kW permanent magnet synchronous motors (PMSM), attached to each of the rear wheels. The conversion of the DC current to 3 phased AC power is conducted by two Semikron SKAI 6001MD10-1450L inverters. An overview of the implemented system is shown in figure 6.8, where the placement of the individual components is shown.

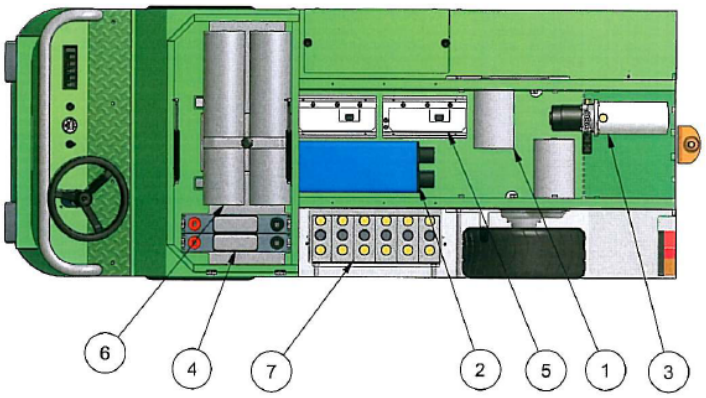

Figure 6.8: Stama utility truck from GMR Maskiner A/S.1:PMSM, 2:FC Stack, 3:Hydraulic pump, 4:Super capacitors, 5:Inverter, 6:Hydrogen tanks, 7:Battery pack

The fuel cell system is fuelled by two 5L bottles of compressed hydrogen at 200 bars situated below the driver seat. Different configurations of the fuel cell/battery/super capacitor power system have been analyzed in Appendix A.8, and the initial electrical configuration is as shown on figure 6.9. The main DC bus is the 48V battery pack, on which the super capacitor bank is connected in parallel, all though this limits the capacity, no additional power conversion is required and the system is quite capable of supplying high power acceleration bursts without overloading the batteries.

With the possibility of experiencing continuous powers of 3kW per motor, and even higher peak powers, the fuel cell stack is not able to supply the full system power. An analysis of the typical load pattern for such a truck has been carried out and is outlined in A.8, where many idling periods are present. The 1 kW fuel cell stack functions in

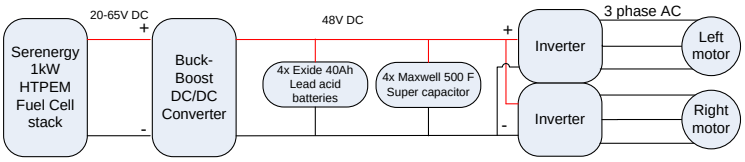

Figure 6.9: The power system configuration for the utility truck

this type of operation mainly as an on board battery charger, or range extender also capable of supplying electrical power during transients.

6.2.1 Final system operating strategy

The knowledge gathered in testing the two different fuel cell stacks presented in 4, is used to specify a system state diagram, visualizing the different operating states of the system, the control strategy. This state diagram is shown in figure 6.10

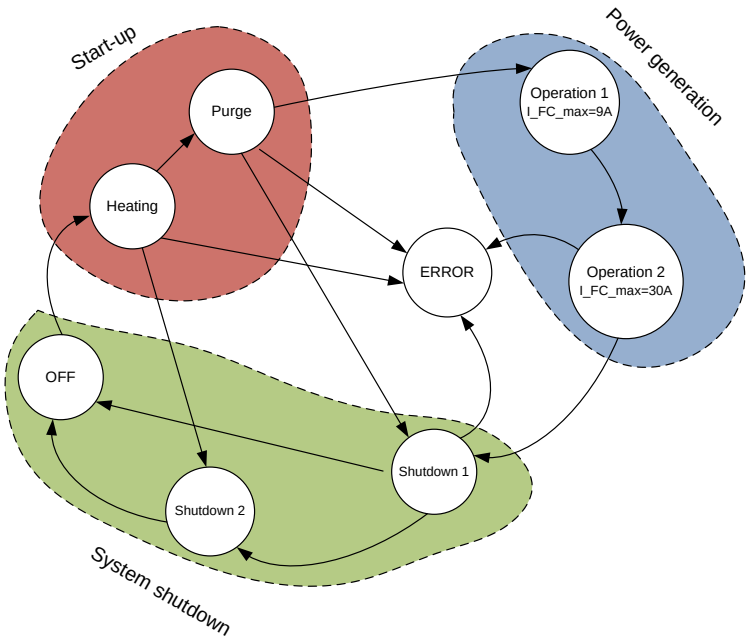

Figure 6.10: State diagram for 1kW HTPEM fuel cell system running on pure hydrogen

The system operating strategy is divided into 4 main areas of operation:

- Fuel cell system heating

- Fuel cell system power generations
- Fuel cell system shut-down
- Error state

The operating strategy of each of these states will be explained in the following, and have been tested on a stack similar to the one implemented in the truck itself.

6.2.2 Fuel cell system heating state

The system heating state includes the initial system heating from ambient temperature to minimum operating temperature of 100^{o}C. When the key in the truck is turned, the truck will drive on power from the batteries, while the fuel cell system initiates a heating sequence. The heating state includes the following operations, when a start signal is given, the system initiates heating if the hydrogen pressure is above a certain threshold value, in order to avoid start-up of a system with no more fuel. An air pre-heater is used to heat the inlet air to an average temperature of 120^{o}C at a blower voltage of 22V. The temperature development is seen in figure 6.11, together with a picture of the heater which, as it is shown, is mounted in front of the blower.

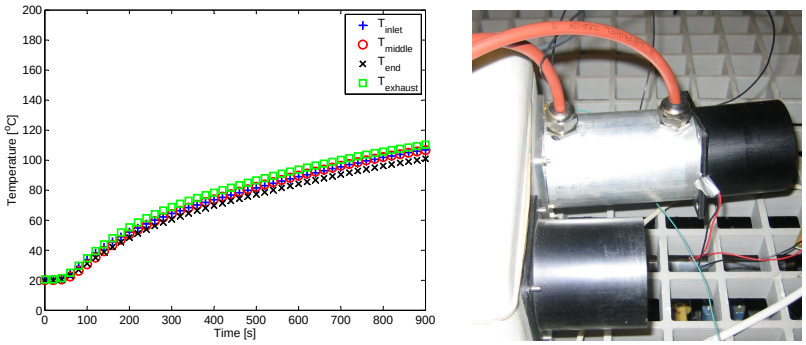

Figure 6.11: Left: Temperature development during heating with 48V DC 1kW air heater. Right: Developed stack DC heater, matching the 48V battery bus voltage..

The heater is designed using a series and parallel connection of resistive heating wires to a total resistance of 2.5 Ω. During heating, this resistance is connected directly to the 48V DC bus voltage and delivers 1kW of heating power. The heating time for the case shown, i.e. the time for all temperatures to reach a temperature above 100^{o}C

is about 800s. This yields a requirement for energy input of 0.2kWh. In the time during heating, the truck should be able to run solely on battery and super capacity power. Following the heating process, the heating element is shut off, the blower is still running, and the hydrogen inlet valve i opened followed by a 2 second hydrogen purge, to introduce hydrogen in the stack. With both air and hydrogen present, the stack voltage will rise to the open circuit voltage and the system will enter the system operation state.

6.2.3 Fuel cell system operating state

At low temperatures only small current loads can be accepted, but even loads as low as 0.1 A/cm^2 will heat the system to temperatures above 100^{o}C. When reaching 140^{o}C, the nominal current load of 0.67 A/cm^2 is allowed. The nominal current load is often application specific depending on operating conditions and expected end-of-life voltage. If no current is drawn from the stack, the temperature will start dropping, and the heating element will need to be turned on because even the small standby air flow is cooling the stack. The stack temperature is controlled during operation using the strategy illustrated in figure 6.12, where a combined current feedforward and PI-controller is used.

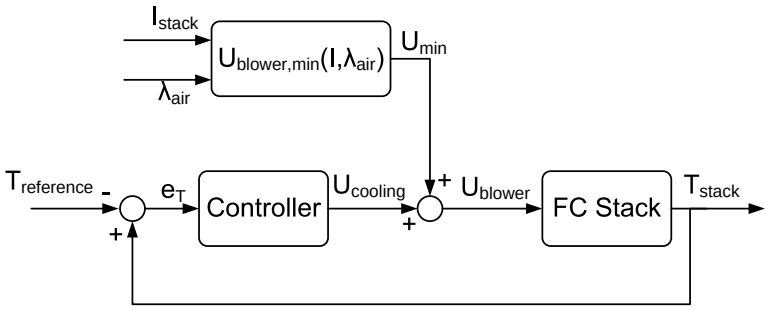

Figure 6.12: Stack temperature control strategy for HTPEM fuel cell stack during general operation of the system.

The feedforward control ensure that a minimum airflow is flowing through the stack depending on a stack current measurement, and at a specified air stoichiometry. At current loads where the temperature starts to rise above a specified reference stack temperature, a feedback control ensures a constant stack temperature. The temperature gradient of the fuel cell stack affects the choice of feedback temperature. As soon as

a current is drawn from the fuel cell stack, the temperatures will start rising, and due to the manifold heating and differences in cooling throughout the stack, different parts of the stack will behave differently as also shown in Paper A.1. Figure 6.13 shows a simulation using the 30 cell stack, where it has been initially heated and is experiencing a current load step.

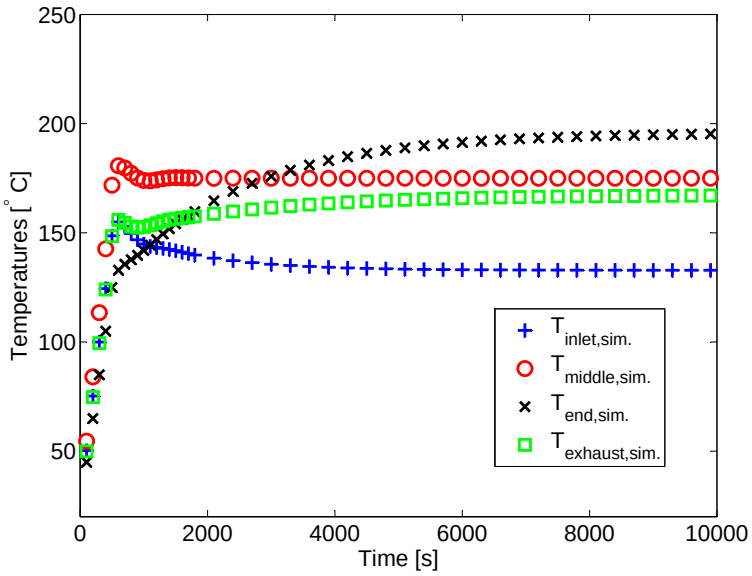

Figure 6.13: Simulation of stack temperature control during fuel cell system start-up and steady current load using middle stack surface temperature as control feedback.

In figure 6.13 the middle cell temperature is used as the feedback temperature. But it is seen that the end stack temperature increases to temperatures above the middle stack temperature. It is found that at higher reference temperatures, the end temperature can reach critically high temperatures. Concluding that the end temperature is the highest temperature, controlling this temperature would avoid the critically high temperatures if the cooling capacity of the blower is sufficient. Figure 6.14 shows a simulation using the end temperature as feedback temperature.

The problem of controlling the steady-state temperature is overcome by choosing the end temperature, but different controller parameters are needed during heating as shown. Because of the slower thermal dynamics of the stack end temperatures, the transient period of the stack temperature is much longer, leading to some situations with poor performance. Similar tendencies are found in the 65 cell stack, but because of the

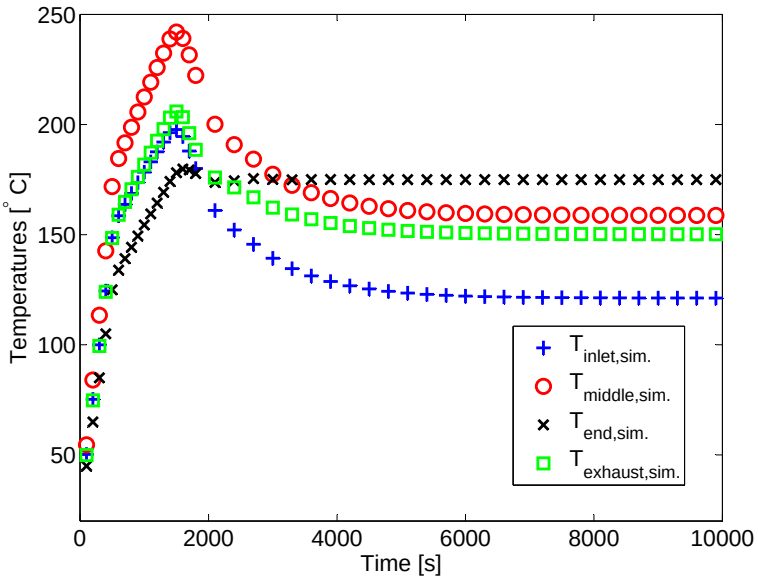

Figure 6.14: Simulation of stack temperature control during fuel cell system start-up and steady current load using end stack surface temperature as control feedback.

lower thermal mass, temperature response to load changes are much quicker than for the prototype stack. Also the improvements in the stack temperature distribution lowers the significance of these problems. Various tests of different choices of temperature feedback points, using sensors mounted in different places on the stack surface and in the manifolds have led to the use of the middle stack temperature as feedback temperature for the controller. An example of the temperature control strategy applied, is shown for the load situation in figure 6.15.

In this example the current load is changing between 9A and 15A. During this load pattern, the stack temperature set point is initially 160^{o}C, but at 8700s it is changed to 180^{o}C, and then to 140^{o}C at 10400s. The temperature response and control signal to the blower is shown in figure 6.16.

When the first change from 9A to 15A is seen, there is an immediate change in the blower voltage because of the feedforward of the current. Afterwards a steady-state control voltage for the blower is found, in order to keep the constant middle stack temperature of 160^{o}C. At 8650s, the current is reduced to 9A and the temperature set point is changed to 180^{o}C after this. This results in a rapid drop in the blower voltage, and the hereby reduced cooling of the stack, giving a temperature rise. The temperature

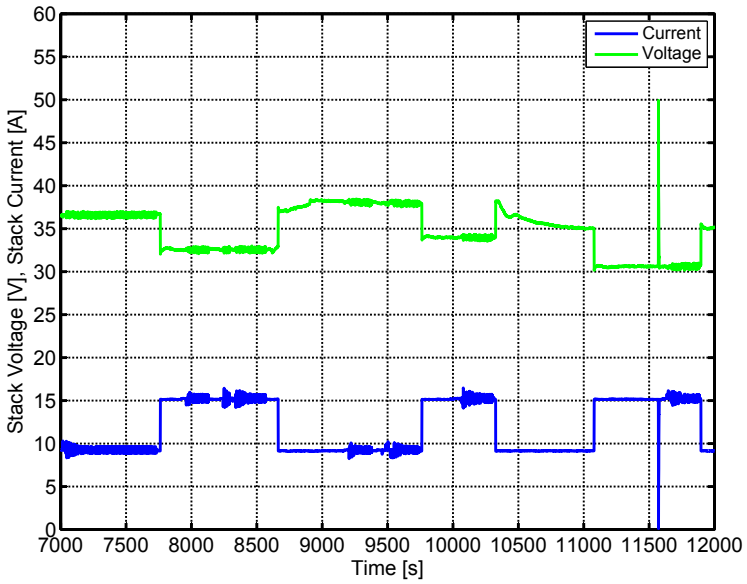

Figure 6.15: Fuel cell stack current load pattern and voltage response.

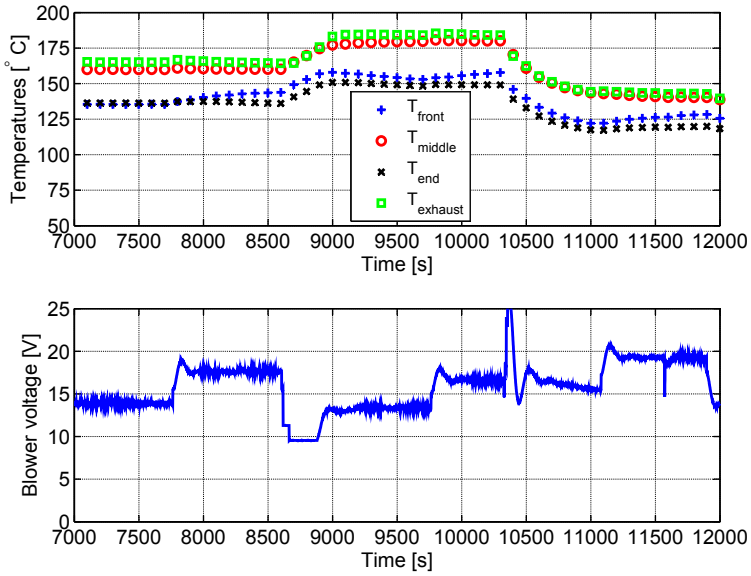

Figure 6.16: Top: 65 cell HTPEM fuel cell stack temperature development during experiment. Bottom: Blower voltage control signal during load pattern.

rises linearly from 160^{o}C to 180^{o}C in around 4 minutes. Similar changes in the current and temperature set points are carried out through the rest of the presented experiment to test the control strategy.

6.2.4 Fuel cell system shut-down state

Different shut-down strategies are relevant when planning proper shut-down of a HT-PEM fuel cell system. The shut-down produce depends on the power cycle and use of the particular application. For example if the standby power consumption for the system, to keep a constant standby temperature, is very small, cooling of the system to ambient temperature might not be required. The shut-down procedure of a HTPEM fuel cell system includes a complete stop of hydrogen fuel flow and reduction of the fuel cell stack voltage to a level that minimizes the degradation involved with high cell voltages [9, 38, 50]. There are different ways of lowering the stack voltage to a level that is not significantly degrading for the fuel cells. One way is presented in figure 6.17, where the voltage and current is shown during an experiment with shut down procedures.

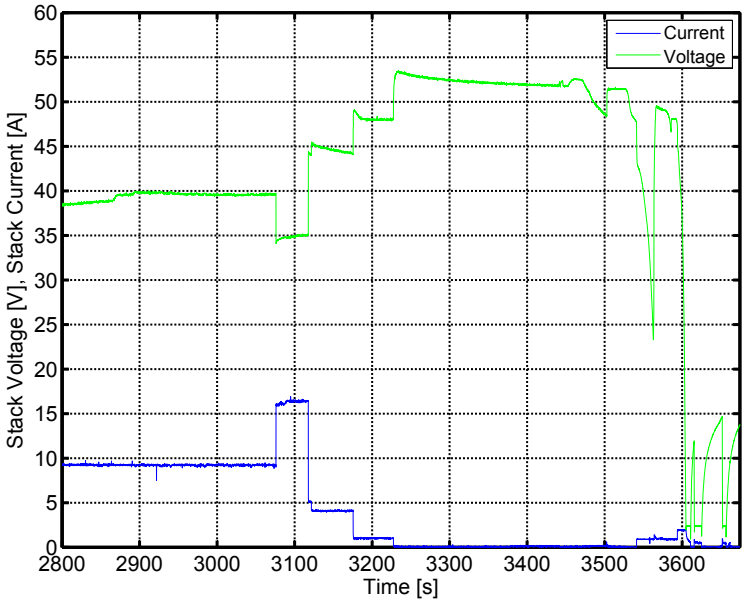

Figure 6.17: Fuel cell stack voltage and current during shut-down procedure.

In the shown example an initial constant current of 0.2 A/cm^2 is drawn from the stack and this current load is changed in steps, to a final complete disconnection of the fuel cell. It is seen that the final stack voltage is about 54V, where, in this case, the average stack temperature is around 130^{o}C. The stack voltage is dropping due to the decreasing temperatures. A voltage of 54V gives an average fuel cell voltage of 0.83V in a 65 cell stack, which is critically high and introduces increased degradation of the

fuel cells. The initial lowering of the fuel cell stack voltage at 3500s is due to a test of reducing the blower voltage. At 3530s the hydrogen supply is shut off, the stack is purged, and a small bleeding current is drawn from the fuel cell stack which results in a fast drop in stack voltage. The rise in voltage is due to an increase in the blower voltage, matching the small current load of 0.01 A/cm^2. The principle of this procedure is to remove the hydrogen left in the system which in the end will lower the fuel cell stack voltage. For a short while at 3600s, a test is made with an increased current of 0.05 A/cm^2. The result is seen to clearly lower the fuel cell voltage, which is now at a level where, when the load is removed, where no significant degradation will occur.

Another example of a shut down procedure is shown in figure 6.18, where the stack voltage is seen in a situation were it is not loaded. At 3175s the blower is shut off, and the following drops in fuel cell stack voltage is due to the lack of air supply to the cathode.

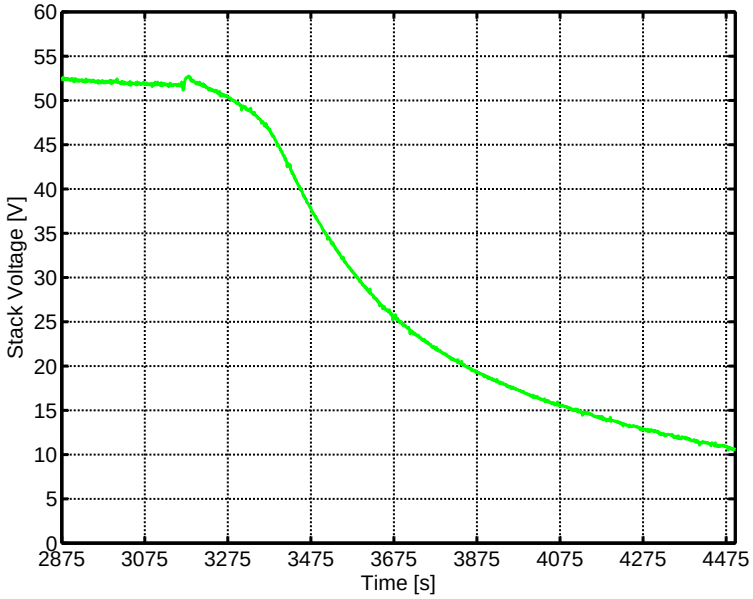

Figure 6.18: Fuel cell stack voltage and current during shut-down procedure.

Small amounts of hydrogen will still be present in the system during this shut down period, even if the stack hydrogen supply is shut off and the purge valve is opened. The method shown in figure 6.17, uses the removal of hydrogen by drawing a small current, to lower the fuel cell stack voltage, which is a known degrading factor in HTPEM fuel cells. The method of cooling the fuel cell down before shutting the system off is assumed

better for the system because no starvation of either anode or cathode is occurring. It is key to avoid high potentials in the stack and to avoid hydrogen starvation, and although the method of figure 6.18 is better, care must be taken, to ensure that not too high potentials are reached in the beginning of the process. A small bleeding resistance should be connected to drag the voltage down to a reasonable voltage level.

6.2.5 Error state

The error state can be accessed by most of the other states, and usually occurs to protect the system from significant degradation. The error state is triggered when the temperature rises above 190 ^{o}C to avoid permanent damage to the fuel cell polymer membrane. The error state is also reached if a current load is drawn with a corresponding average cell voltage lower than 0.3V. The system is in this case also shut down because of expected damage. The error state include complete shutdown of the system and in some cases with required reset to avoid further damage. During heating, purge and shutdown a time limit is set as to how long time these individual states are active. If e.g. heating is too slow, the heating element might require maintenance or could be damaged.

6.2.6 Discussion

One of the disadvantages of storing hydrogen in gaseous form are clearly that much volume is required. Nevertheless, the operation of fuel cell systems has proven very efficient and usable as power sources in the two presented electrical vehicles. One of the primary disadvantages when operating at high temperatures is the start-up time when a constant standby temperature is not available, but even onboard vehicles, this start-up time can be minimized further using efficient convective heating.

The power system integrated in the Hywet had the primary task of testing the direct connection of the HTPEM fuel cell stack to the Li-ion battery pack. The tests successfully show that this strategy can be used to charge the batteries efficiently while driving with some hybrid capabilities. The disadvantage is that the current delivered from the fuel cells cannot be controlled because of the absence of power electronics and is passively controlled by the battery pack voltage and SOC. The balance between the battery pack size, and the fuel cell stack power for the Hywet has not been optimized, and requires detailed information on typical driving cycles for such vehicles.

The complete energy available in the batteries of the GMR truck is approximately 2 kWh, and the fuel cell stack uses about 10% of this energy for heating the fuel cell system to operational temperature. Depending on real operating conditions, the battery pack size could be adjusted if more battery power is needed. Or the optimization presented in Paper A.8 could take into account this additional heating energy. When using a methanol based system it might be possible to use combusted methanol directly for system heating as described in section 5.4. Using this new power train in the GMR truck greatly decreases the total weight of the truck by removing the initial 174 kg battery pack using below half of this weight for the new power system. The runtime of the system is much dependent on the particular load cycle of the system and the hydrogen storage which is limited because of volume. Using the presented heat exchanger methanol reformer based solution is expected to greatly extend the runtime of the system.

———————

7

Conclusions

In the work presented here, the use of PBI-based HTPEM fuel cells for traction power generation in mobile applications was examined. The HTPEM fuel cell technology is a very reliable and efficient way of converting the chemical energy available in hydrogen, as well as in any given hydrocarbon based fuel, into electricity. The systems designed using these fuel cells benefit greatly from the advantages that this technology offers. The significant scientific contributions achieved in this work are summarized in the following.

7.1 Hydrogen based high temperature PEM fuel cells

Successful tests of stack designs using cathode air cooling showed stable operation with very small parasitic losses resulting in a very simple system design. Using cathode air cooling also greatly simplifies the stack design by removing the requirement for additional cooling channels in the bipolar plates of the stack. Minimizing the pressure losses in the stack is important for this cooling strategy to be successful and with a minimum of parasitic losses. One of the challenges encountered during the experiments with the HTPEM fuel cell stacks were that due to the high cathode air flow, a temperature difference from top to bottom and from the front to the end of the stack was identified. These temperature gradients were significantly reduced in the later versions of the fuel cell stacks by Serenergy. This work has shown that using cathode air cooling of HTPEM fuel cell stacks is a simple, robust and efficient way of converting hydrogen to electrical power and heat. Using a PI+feedforward temperature controller for

controlling the stack temperature yields stable system performance with good dynamic response to load changes. Another of the challenges encountered using the HTPEM fuel cells were due to the high temperatures required for operation. The fact that liquid water in the fuel cell membranes should be avoided requires a starting temperature of $\approx 100^{o}$C before a load can be applied. Reducing start-up time for these fuel cell stacks is of significant importance if they are to be used in applications requiring fast start-up. This work has demonstrated a reduction in start-up time from 57 min to around 6 min using electrically heated cathode air. With this reduction HTPEM fuel cells are also feasible in applications with only limited battery power available.

This work has presented the use of electrochemical impedance spectroscopy as a method for characterizing HTPEM fuel cell impedance. The use of this method for fuel cell diagnostics with single cells or fuel cell stacks is an important tool when conducting lifetime experiments, or online diagnosis. In systems with fuel cell anode impurities such as CO, EIS could be used to identify fuel cell performance and serve as an important control system input.

7.2 Methanol reformer based high temperature PEM fuel cell systems

The high temperatures of operation gives the HTPEM fuel cells good tolerances to impurities in the anode gas, enabling the use of reformer systems, such that liquid hydrocarbons can be used instead of hydrogen. In this way, the complications involved with hydrogen storage can be avoided. This work has demonstrated the use of a catalytically coated heat exchanger reformer for steam reforming methanol. Experiments and simulations have indicated that efficiencies comparable to pure H_2 systems can be expected if a proper heat exchanger network can be established using a reformer that produces low CO content reformate gas at SC close to 1. This is due to the relatively high temperatures of the HTPEM fuel cells which enable the possibility of using cathode exhaust heat to power the evaporation and operation of the reformer system efficiently. An important conclusion in the area of reformer system control is the significance of the precise estimation of the feedforward signal to the methanol and water mixture due

to η being sensitive to λ_{H_2}. Even small errors in this value can result in poor system efficiency and waste of fuel.

7.3 Fuel cell system applications

During power generation with fuel cells, many benefits can be gained through coupling with other electrical energy buffers. Simpler, more efficient and less expensive systems can be developed by the use of batteries or super capacitors together with fuel cells. Using such a configuration, the fuel cells do not need to generate peak powers, and can e.g. be used as onboard battery chargers extending the driving range of electrical vehicles. Combining different electrical energy storages can also benefit the lifetime of each of the components. A sharing of the power production will lower the depth-o-discharge for the batteries, and minimize the current fluctuations of the fuel cells, both affecting the lifetime of each of the components. During this work is was demonstrated that direct connection of a fuel cell stack network, and a Li-ion battery pack for traction control could be implemented without the use of power electronics. The battery charging is passively controlled by the battery impedance, if the two systems are properly dimensioned. Part of this research focused on characterizing fuel cells using electrochemical impedance spectroscopy. This method has shown promising results in the field of diagnosing fuel cell behaviour, and the developed hardware and software can be used in many other fields of research, including online identification of battery state-of-charge and state-of-health.

In the time frame of this work, the maturity of the presented fuel cell technology has evolved from interesting single cell research to potentially viable fuel cell power modules able to power many different applications using renewable energy.

8

Future work

Within all the areas presented in this dissertation, more knowledge is required in order to increase the efficiency, performance and understanding of how fuel cell systems work. On single cell as well as stack level, many challenges still exist in understanding the precise mechanisms of degradation in high temperature PEM fuel cells and how they are affected by different types of operating conditions including the use of reformate gas. When using reformer based systems the addition of CO in the anode gas affects the performance of the fuel cells. Using EIS techniques (such as described in A.2) could help to uncover not only the steady-state performance of the fuel cells, but also the changes in the fuel cell electrical characteristics. Exploring the impedance characteristics online of fuel cells running on hydrogen with a CO content could lead to model based predictions of the anode CO content by load current super positioning techniques. These predictions could in turn be used as control input states to improve the overall reformer system performance. More detailed information of the CO impact on life time is also required to determine if the performance increase on fuel cell stack voltage at higher temperatures makes it a benefit to increase the general stack temperature. The long term effects of different types of fuel cell heating and how the fuel cells react to being kept at a high standby temperature without producing electrical power is important to identify. Designing reformer systems with efficiencies comparable to pure hydrogen fed fuel cell systems is a possibility, but only of steam reforming at low temperature and steam-to-carbon ratio is achievable exploiting the high quality HTPEM fuel cell cathode exhaust air.

This work has in-depth treated some of the technical aspects of designing and controlling HTPEM fuel cell systems. If fuel cells are to be a part of a future energy system it is important that besides being technically viable, they also posses the socioeconomic benefits that make them a good choice for producing renewable energy.

Bibliography

[1] P. Aguiar, D. Chadwick, and L. Kershenbaum. **Modelling of an indirect internal reforming solid oxide fuel cell**. *Chemical Engineering Science*, **57**:1665–1677, 2002. 18

[2] R. K. Ahluwalia and X. Wang. **Effect of CO and CO_2 impurities on performance of direct hydrogen polymer-electrolyte fuel cells**. *Journal of Power Sources 180*, **180**:122–131, 2008. 49

[3] L. Alejo, R. Lago, M.A. Pena, and J.L.G. Fierro. **Partial oxidation of methanol to produce hydrogen over CuŨZn-based catalysts**. *Applied Catalysis A: General*, **162**:281–297, 1997. 51

[4] Leanne Ashworth and Ian Natanael Menjón Remón. *Optimization of a Methanol Reformer for a Hybrid Hydrogen Vehicle*. Master's thesis, Aalborg University, 2008. xx, 82

[5] BASF. **Celtec MEAs - Membrane Electrode Assemblies for High Temperature PEM Fuel Cells** [online]. 2008. Available from: `http://www.basf-fuelcell.com/en/projects/celtec-mea/celtec-p-1000-mea.html` [cited 17 February 2009]. xvii, 17

[6] BASF. **LT-MEA - Membrane electrode assembly for low temperature PEM fuel cells** [online]. 2008. Available from: `http://www.etek-inc.com/pdfs/MEA12E_v2.pdf` [cited 01 October 2008]. xvii, 13

[7] BASF. **LT-MEA - Membrane Electrode Assembly for Low Temperature PEM Fuel Cells** [online]. 2008. Available from: `http://www.etek-inc.com/pdfs/MEA12D_12T.pdf` [cited 01 October 2008]. xvii, 15

[8] Olga A. Baturina, Yannick Garsany, Thomas J. Zega, Rhonda M. Stroud, Terence Schull, and Karen E. Swider-Lyons. **Oxygen Reduction Reaction on Platinum/Tantalum Oxide Electrocatalysts for PEM Fuel Cells**. *Journal of the Electrochemical Society*, **155**:B1314–B1321, 2008. 11

[9] W. R. Baumgartner, P. Parz, S. D. Fraser, E. Wallnöfer, and V. Hacker. **Polarization study of a PEMFC with four reference electrodes at hydrogen starvation conditions**. *Journal of Power Sources*, **182**:413–421, 2008. 99

[10] Krishan Kumar Bhatia and Chao-Yang Wang. **Transient carbon monoxide poisoning of a polymer electrolyte fuel cell operating on diluted hydrogen feed**. *Electrochemica Acta*, **49**:2333–2341, 2004. 49

[11] Ulf Bossel. **Does a Hydrogen Economy Make Sense?** *Proceedings of the IEEE*, **94**, 2006. 30, 49

[12] Cabot Fuel Cells Group. **Total MEA Solutions for DMFC Product Developers** [online]. 2006. Available from: `http://www.fuelcellmarkets.com/cabot/news_and_information/3,1,6270,1,13971.html` [cited 01 October 2008]. xvii, 15

[13] Chundi Cao and Keith L. Hohn. **Study of reaction intermediates of methanol decomposition and catalytic partial oxidation on Pt/Al2O3**. *Applied Catalysis A: General*, **354**:26–32, 2009. 51

[14] L. Carrette, K. A. Friedrich, and U. Stimming. **Fuel cells: Principles, types, fuels, and applications**. *Journal of Chemical Physics and Physical Chemistry*, **1**:162–193, 2000. 24, 30

[15] N. Christiansen, H. Holm-Larsen, J. Hansen, S. Linderoth, P. Larsen, P. Hendriksen, and M. Mogensen. **Solid Oxide Fuel Cell Development at Topsoe Fuel Cell A/S and Risø**. *Oral presentation at Fuel Cell Seminar*, 2006. xvii, 18

[16] H. S. Chu, C. P. Wang, W. C. Liao, and W. M. Yan. **Transient behavior of CO poisoning of the anode catalyst layer of a PEM fuel cell**. *Journal of Power Sources*, **159**:1071–1077, 2006. 49

[17] P.J. Dauenhauer, J.R. Salge, and L.D. Schmidt. **Renewable hydrogen by autothermal steam reforming of volatile carbohydrates**. *Journal of Catalysis*, **244**:238–247, 2006. 51

BIBLIOGRAPHY

[18] DuPont Fuel Cells. **DuPont Fuel Cells** [online]. 2008. Available from: http://www2.dupont.com/Fuel_Cells/en_US/assets/downloads/dfc502.pdf [cited 01 October 2008]. xvii, 15

[19] DuPont Fuel Cells. **Membrane electrode assemblies MEA3 and MEA5** [online]. 2008. Available from: http://www2.dupont.com/Fuel_Cells/en_US/assets/downloads/dfc501.pdf [cited 01 October 2008]. xvii, 13

[20] B. Emonts, J. Bøgild Hansen, S. LIJgsgaard Jørgensen, B. Höhlein, and R. Peters. **Compact methanol reformer test for fuel-cell powered light-duty vehicles**. *Journal of Power Sources*, **71**:288–293, 1998. 51

[21] B. Emonts, J. Bøgild Hansen, H. Schmidt, T. Grube, B. Höhlein, R. Peters, and A. Tschauder. **Fuel cell drive system with hydrogen generation in test**. *Journal of Power Sources*, **86**:228–236, 2000. 51

[22] I. Eswaramoorthi and A. K. Dalai. **A comparative study on the performance of mesoporous SBA-15 supported Pd-Zn catalysts in partial oxidation and steam reforming of methanol for hydrogen production**. *Internation Journal of Hydrogen*, **34**:2580–2590, 2009. 51

[23] J. W. Fergus. **Metallic interconnects for solid oxide fuel cells**. *Materials Science and Engineering A-Structural Materials Properties Microstructres and Processing*, **397**:271–283, 2005. 19

[24] J. W. Fergus. **Properties of high-temperature PEFC Celtec5-P1000 MEAs in start/stop operation mode**. *Journal of Power Sources*, **176**:428–434, 2008. 22

[25] N. Fouquet, C. Doulet, C. Nouillant, G. Dauphin-Tanguy, and B. Ould-Bouamama. **Model based PEM fuel cell state-of-health monitoring via ac impedance measurements**. *Journal of Power Sources*, **159**:905–913, 2006. 14

[26] Gore. **GORE^{TM} PRIMEA® SERIES 56 MEAs** [online]. 2008. Available from: http://www.gore.com/MungoBlobs/primea_56_mea_datasheet.pdf [cited 01 October 2008]. xvii, 13

[27] Gore. **GORE^{TM} PRIMEA® SERIES 57 MEAs** [online]. 2008. Available from: http://www.gore.com/MungoBlobs/primea_57_mea_datasheet.pdf [cited 01 October 2008]. xvii, 13

[28] A. Hajimiragha, C. Canizares, M. Fowler, M. Geidl, and G. Andersson. **Optimal Energy Flow of Integrated Energy Systems with Hydrogen Economy Considerations**. *iREP Symposium- Bulk Power System Dynamics and Control*, 2007. 49

[29] A. Hauch, S. D. Ebbesen, S. H. Jensen, and M. Mogensen. **High temperature water electrolysis in solid oxide cells**. *International Journal of Hydrogen Energy*, **33**, 2008. 49

[30] G. Hübner. **High-temperature PEM Fuel Cells.** *Presentation at the 2nd International Workshop on Functional Materials for Mobile Hydrogen Storage.*, 2007. xvii, 17

[31] IPCC. **Working Group III Report Mitigation of Climate Change**. Technical report, IPCC, 2007. 7, 85

[32] S. H. Jensen, P. H. Larsen, and M. Mogensen. **Hydrogen and synthetic fuel production from renewable energy sources**. *International Journal of Hydrogen Energy*, **32**, 2007. 49

[33] Lars Christian Riis Johansen and Jakob Rabjerg Vang. **Modelling of a Hybrid SOFC-GT-ST Combined-Cycle Power Plant**. *Project report, 6th semester Fluids and Combustion Engineering*, 2008. xvii, 18

[34] Anders R. Korsgaard, Rasmus Refshauge, Mads P. Nielsen, Mads Bang, and Søren K. Kær. **Experimental Characterization and Modeling of commercial PBI-based MEA Performance**. *Journal of Power Sources*, **162**:239–245, 2006. 21, 37, 55

[35] J.R. Lattner and M. P. Harold. **Comparison of methanol-based fuel processors for PEM fuel cell systems**. *Applied Catalysis B: Environmental*, **56**:149–169, 2005. 51

[36] B. Linnhoff and A.R. Eastwood. **Overall site optimisation by Pinch Technology**. *Journal of Chemical Engineering Research and Design*, **75**:S138–S144, 1997. 72

[37] Srdjan M. Lukic, Jian Cao, Ramesh C. Bansal, Fernando Rodriguez, and Ali Emadi. **Energy Storage Systems for Automotive Applications**. *IEEE Transactions on Industrial Electronics*, **55**, 2008. 49

[38] K. Mitsuda and T. Murahashi. **Air and fuel starvation of phosphoric acid fuel cells: A study using a single cell with multi-reference electrodes**. *Journal of Applied Electrochemistry*, **21**:524–530, 1991. 99

[39] W. Mérida, D.A. Harrington, J.M. Le Canut, and G. McLean. **Characterisation of proton exchange membrane fuel cell (PEMFC) failures via electrochemical impedance spectroscopy**. *Journal of Power Sources*, **161**:264–273, 2006. 14

[40] Vijayadurga Nallathambi, Jong-Won Lee, Swaminatha P. Kumaraguru, Gang Wu, and Branko N. Popov. **Development of high performance carbon composite catalyst for oxygen reduction reaction in PEM Proton Exchange Membrane fuel cells**. *Journal of Power Sources*, **183**:34–42, 2008. 11

[41] K.C. Neyerlin, Ratndeep Srivastava, Chengfei Yu, and Peter Strasser. **Electrochemical activity and stability of dealloyed Pt-Cu and Pt-Cu-Co electrocatalysts for the oxygen reduction reaction (ORR)**. *Journal of Power Sources*, **186**:261–267, 2008. 11

[42] Steen Kristensen Niels Christiansen and Helge Holm-Larsen. **Status of the SOFC Development at Haldor Topsoe/Risoe**. *Oral presentation at Presented at SOFC-VIII*, 2003. xvii, 18

[43] Mads Pagh Nielsen. *Modeling of Proton Exchange Membrane Fuel Cell Systems*. PhD thesis, Aalborg University, January 2005. 11

[44] Ryan O'Hayre, Suk-Won Cha, Whitney Colella, and Fritz B. Prinz. *Fuel cell Fundamentals*. Wiley, 2006. 29, 30

[45] Poly Fuel. **Innovations Update** [online]. 2008. Available from: `http://www.polyfuel.com/cut-version/index.html` [cited 01 October 2008]. xvii, 13

[46] Poly Fuel. **Innovations Update** [online]. 2008. Available from: `http://www.polyfuel.com/cut-version/index.html` [cited 01 October 2008]. xvii, 15

[47] Erich Ramschak, Volker Peinecke, Peter Prenninger, Thomas Schaffer, Wolfgang Baumgartner, and Viktor Hacker. **Online stack monitoring tool for dynamically and stationary operated fuel cell systems**. *Fuel Cells Bulletin*, pages 12–15, 2006. 14

[48] Erich Ramschak, Volker Peinecke, Peter Prenninger, Thomas Schaffer, and Viktor Hacker. **Detection of fuel cell critical status by stack voltage analysis**. *Journal of Power Sources*, **157**:837–840, 2006. 14

[49] A. Reiche, K. Foli, O. Gronwald, S. Haufe, S. Kiel, U. Maehr, D. Melzner, F. Walter, and S. Weisshaar. **Sartorius HT-PEM Fuel Cell Technology**. *Proceedings of the Fuel Cell Seminar 2006*, pages 300–303, 2006. xvii, 17

[50] Thomas J. Schmidt and Jochen Baurmeister. **Properties of high-temperature PEFC Celtec-P 1000 MEAs in start/stop operation mode**. *Journal of Power Sources*, **176**:428–434, 2008. 99

[51] Chunshan Song. **Fuel processing for low-temperature and high-temperature fuel cells: Challenges, and opportunities for sustainable development in the 21st century**. *Catalysis today*, **77**:17–49, 2002. 18

[52] Danish Power Systems. **Dansih Power Systems - High Temperature PEM Fuel Cells**. *Information Leaflet*, September 2008. xvii, 17

[53] DTU Transport. **Transportvaneundersøgelsen 2008**, 2008. xvii, 8

[54] Martyn V. Twigg and Michael S. Spencer. **Deactivation of copper metal catalysts for methanol decomposition, methanol steam reforming and methanol synthesis**. *Topics in Catalysis*, **22**:191–203, 2003. 50

[55] W. Z. Zhu and S. C. Deevi. **Development of interconnect materials for solid oxide fuel cells**. *Materials Science and Engineering A-Structural Materials Properties Microstructres and Processing*, **348**:227–243, 2003. 19